



A Bayesian Approach for Inverse Problems in Synthetic Aperture Radar Imaging

Sha Zhu

► To cite this version:

Sha Zhu. A Bayesian Approach for Inverse Problems in Synthetic Aperture Radar Imaging. Other [cond-mat.other]. Université Paris Sud - Paris XI, 2012. English. NNT: 2012PA112264 . tel-00844748

HAL Id: tel-00844748

<https://theses.hal.science/tel-00844748>

Submitted on 15 Jul 2013

HAL is a multi-disciplinary open access archive for the deposit and dissemination of scientific research documents, whether they are published or not. The documents may come from teaching and research institutions in France or abroad, or from public or private research centers.

L'archive ouverte pluridisciplinaire **HAL**, est destinée au dépôt et à la diffusion de documents scientifiques de niveau recherche, publiés ou non, émanant des établissements d'enseignement et de recherche français ou étrangers, des laboratoires publics ou privés.

THÈSE

Présentée pour obtenir

LE GRADE DE DOCTEUR EN SCIENCES
DE L'UNIVERSITÉ PARIS-SUD XI

Spécialité: Traitement du signal et de l'image

École doctorale << Sciences et Technologies de l'Information, des
Télécommunications et des Systèmes >>

par

Sha ZHU

A Bayesian Approach for Inverse Problems in Synthetic Aperture Radar Imaging

Soutenue le 23 Oct. 2012 devant la Commission d'examen:

Mm.	Hong SUN	(Rapporteur)
M.	Emmanuel TROUVE	(Rapporteur)
M.	Ken SAUER	(Rapporteur)
M.	Ali MOHAMMAD-DJAFARI	(Directeur de thèse)
Mm.	Florence TUPIN	(Examinateur)
M.	Franck DAOUT	(Examinateur)



Thèse préparée au
Laboratoire des signaux et systèmes
UMR8506: Univ Paris-Sud – CNRS – SUPELEC
3, rue Joliot curie
91192, GIF SUR YVETTE, France

UNE APPROCHE BAYÉSIENNE POUR LES PROBLÈMES INVERSES EN IMAGERIE RADAR À SYNTHÈSE D'OUVERTURE

Résumé

L'imagerie Radar à Synthèse d'Ouverture (RSO) est une technique bien connue dans les domaines de télédétection, de surveillance aérienne, de géologie et de cartographie. Obtenir des images de haute résolution malgré la présence de bruit, tout en prenant en compte les caractéristiques des cibles dans la scène observée, les différents incertitudes de mesure et les erreurs résultantes de la modélisation, devient un axe de recherche très important.

Les méthodes classiques, souvent fondées sur i) la modélisation simplifiée de la scène ; ii) la linéarisation de la modélisation directe (relations mathématiques liant les signaux reçus, les signaux transmis et les cibles) simplifiée ; et iii) l'utilisation de méthodes d'inversion simplifiées comme la Transformée de Fourier Inverse (TFI) rapide, produisent des images avec une résolution spatiale faible, peu robustes au bruit et peu quantifiables (effets des lobes secondaires et bruit du speckle).

Dans cette thèse, nous proposons d'utiliser une approche bayésienne pour l'inversion. Elle permettrait de surmonter les inconvénients mentionnés des méthodes classiques, afin d'obtenir des images stables de haute résolution ainsi qu'une estimation plus précise des paramètres liés à la reconnaissance de cibles se trouvant dans la scène observée.

L'approche proposée est destinée aux problèmes inverses de l'imagerie RSO mono-, bi-, et multi- statique ainsi que l'imagerie des cibles à micromouvement. Les *a priori* appropriées de modélisation permettant d'améliorer les caractéristiques des cibles pour des scènes de diverses natures seront présentées. Des méthodes d'estimation rapides et efficaces utilisant des *a priori* simples ou hiérarchiques seront développées. Le problème de l'estimation des hyperparamètres sera également traité dans le cadre bayésien. Les résultats relatifs aux données synthétiques, expérimentales et réelles démontrent l'efficacité de l'approche proposée.

Mots-clés : inférence bayésienne, problèmes inverses, imagerie RSO, estimation de paramètres, micromouvement.

Abstract

Synthetic Aperture Radar (SAR) imaging is a well-known technique in the domain of remote sensing, aerospace surveillance, geography and mapping. To obtain images of high resolution under noise, taking into account of the characteristics of targets in the observed scene, the different uncertainties of measure and the modeling errors becomes very important.

Conventional imaging methods are based on i) over-simplified scene models, ii) a simplified linear forward modeling (mathematical relations between the transmitted signals, the received signals and the targets) and iii) using a very simplified Inverse Fast Fourier Transform (IFFT) to do the inversion, resulting in low resolution and noisy images with unsuppressed speckles and high side lobe artifacts.

In this thesis, we propose to use a Bayesian approach to SAR imaging, which overcomes many drawbacks of classical methods and brings higher resolution, more stable images and more accurate parameter estimation for target recognition.

The proposed unifying approach is used for inverse problems in Mono-, Bi- and Multi-static SAR imaging, as well as for micromotion target imaging. Appropriate priors for modeling different target scenes in terms of target features enhancement during imaging are proposed. Fast and effective estimation methods with simple and hierarchical priors are developed. The problem of hyperparameter estimation is also handled in this Bayesian approach framework. Results on both synthetic and real data demonstrate the effectiveness of the proposed approach.

Keywords : Bayesian inference, inverse problems, SAR imaging, parameter estimation, micromotion.

Acknowledgements

Life is like a journey that you have to remind yourself to go forward all the time. The courage is important, as well as the direction.

The accomplishment in this thesis were achieved by the help and support of many individuals.

First of all I would like to express my sincere gratitude to my advisor, Dr. Ali Mohammad-Djafari, for his continuous guidance, suggestions, patience and friendship during the course of my work. Not only in the scientific research but also in a life-permanent struggle, does he set an example of how to be a scientist for me. Many years ago, as a foreign student who came to France for study, he overcame a lot of difficulties and put much effort into his work. The way in which he keeps a critical thinking, sustained efforts and the passion for research touched me a lot. I am deeply grateful of his help in the completion of this thesis.

I would like to thank Dr. Hong Sun, Dr. Ken Sauer, Dr. Emmanuel Trouvé, Dr. Florence Tupin and Dr. Franck Daout for their advice and their willingness to be in my thesis committee.

I would like to thank my colleagues at GPI and L2S for having useful related discussions.

Thanks to Dr. Thomas Rodet. As the person in charge of GPI, from public resources to the barbecue, from technical discussions to useful suggestions, he is very conscientious and always ready to help everyone. Thanks to him for his kind help.

Thanks to my dear colleagues as well as friends at GPI: Yuling Zheng, the first Chinese girl that I got to know at GPI, thank her for the "sweet sandwich" during my writing; Caifang Cai, a kind Shanxi girl; Long Chen, a hard-working and easy going man; Leila Gharsalli, an active girl who always smiles; Mircea Dumitru who always shares his chocolate with others. Several good ideas came from our discussion.

Thanks a lot to the previous colleagues at GPI: Dr. Doriano Pougaza, my best African friend who helped me a lot, Dr. Hacheme Ayasso who is humorous and smart, never hesitates to answer my questions, Dr. Diarra Fall and Dr Isabelle Smith as the graduated PhD girls from GPI, set a good example for me as young women scientists. Thanks to Dr. Nicolas Gac who gave me much sincere help during the first days when I came to France. I would also like to thank the intern Felipe Wilches-Bernal for sharing ideas. Many thanks are given to Benoit Pencrech for his kind help on the French abstract.

Thanks to my colleagues at L2S: Dr. Li Song, Dr. Nabil Mohammed El Korso, Dr. Alessio Franci, Dr. Le minh Duong and Dr. Lana Iwaza for their useful advice.

Thanks to the secretary of L2S, Maryvonne Giron whom I troubled the most. From housing to doctor appointments, from the 'titre de séjour' to the French course, she was always so kind and so patient to me. I still remember that the day she brought the

cakes made by herself to us foreign students after the French course. In my mind, she is a truly elegant French lady.

Thanks to Mme. Veronique Veque, the director of doctoral school of University of Paris-Sud 11, and Mme. ludivine vagneur for their kind help.

I would also like to thank China Scholarship Council, for supporting my research abroad. I would like to thank the continuing support from NUDT. Thanks are given to Dr. Xuesong Wang, the director of the education department of Graduate school, Xiaoyuan Liu, the director of the degree department of Graduate school, Dr. Chaojing Tang and Dr. Xiang Li, the dean and the vice dean of School of Electronic Science and Engineering, Dr. Junjie Mao and Dr Hongqiang Wang for their guidance and help. Thanks are also given to Libin Yang, Yihua Hou, Wenwu Zhao and Dan Wu for their useful advice.

I would like to thank De Ben who is the Academician of China Engineering Academy and Dr. Genxing Xu who comes from the Institute of China Aerospace and Industry Group for their yeas of attention and help.

I would like to thank the teachers and the colleagues at Institute of Space Electronic Information (ISEI), NUDT. Thanks to Dr. Yuliang Qin who gives me many useful advice. Thanks to Bo Peng and Wuge Su who helped me a lot on administrative documents when I was abroad. Thanks to my good friend Dr. Yiping Chen who always stand by my side. Many thanks are given to Dr. Bin Deng, not only for his self-giving contribution of technical support but also for sharing the spirit of overcoming difficulties.

I would like to thank Dr. Weiwei Guo for always being open to answer any question at any time, let it be day or night. Many thanks are given to Dr. Lin Xue who helps me a lot on LaTex and many other details.

I would like to thank the Ph.Ds: Dr. Dun Li, Dr. Liqian Chen, Dr. Jun Zhu, Dr. Xiaobin Yin, Dr. Ming Xu, Dr. Kunliang Yao, Jijin Wang, Dr. Yang Xiang and Cong Zeng for their kind help.

I would like to thank my good friends I met in France: Ying Lou, Qiao Zhou, Yibin Lin, Jing Li, Qun Deng and Ruijiao Wang. The time we shared together made the pursuing way not be lonely. Though it may be short in one's life, it is treasurable to share the positives with each other.

I would like to thank the couples Wangqi Chen who treat me like their daughter. All the love and help from them give me the warmth as to be at home while I am far away from the family.

Not enough thanks are given to my parents, from my birth to becoming a grownup, each of my forward step can't proceed without their support. Thanks to my sister. From seventeen years old I left home for study, which leave me hardly any time to care about the family. She has done more than enough for the family. Thanks to my cousin. The confidence and the courage from him encourage me to be brave and optimistic for any challenge. Thanks for the love all of you have given to me. The family is my permanent harbor.

"Pas à pas, on va loin." From the thesis, I learned how to overcome the weakness, the fear, and learned to be brave, to be independent.

Finally, this thesis is dedicated to my mom, for all her deep love.

Sha ZHU

Juin 30, 2012 at Orsay, France

Contents

1	Introduction	21
1.1	Problem Motivation	21
1.1.1	Inverse problems and main characteristics	21
1.1.2	General factors of Synthetic Aperture Radar	23
1.1.3	SAR principle	25
1.1.4	Link to inverse problems	27
1.2	State of the Art	28
1.2.1	A historical overview of inverse problems	28
1.2.2	An overview of conventional SAR imaging algorithms	28
1.2.3	An overview of improving SAR resolution techniques	29
1.2.4	Challenges for SAR imaging	31
1.3	Bayesian Inference for SAR Imaging	32
1.3.1	Bayesian inference	32
1.3.2	Advantages of Bayesian inference for SAR imaging	33
1.3.3	Main steps of Bayesian inference for SAR imaging	34
1.4	Organization and Main Contributions of the Thesis	34
1.4.1	Organization	34
1.4.2	Main contributions	36
1.5	Publications	37
I	Forward Modeling and Inversion	39
2	Forward Modeling: from Scene to Data	41
2.1	Introduction	41
2.2	SAR Target Modeling	42

2.2.1	Assumptions on radar scattering	42
2.2.2	Target scene modeling	43
2.3	SAR Echo Modeling	44
2.3.1	Radar echo generation	44
2.3.2	SAR echo modeling	46
2.3.3	Projection-slice theorem	48
2.4	Mono-Static SAR	50
2.5	Bi-, Multi-Static SAR	52
2.6	SAR Imaging as Fourier Synthesis (FS)	54
2.7	General Forward Modeling	54
2.8	Conclusions	55
3	Inversion: from Data to Scene	57
3.1	Introduction	57
3.2	Classical Inversion Methods	58
3.2.1	Analytical methods	59
3.2.2	Regularization methods	59
3.3	Bayesian Approach	61
3.3.1	Bayesian estimation	61
3.3.2	Prior modeling	62
3.3.3	Hyperparameters estimation	65
3.3.4	Summary of Bayesian computation	67
3.4	Inference with Different Priors	68
3.4.1	Simple priors with MAP estimation	68
3.4.2	Gaussian prior with hyperparameters estimation	70
3.4.3	Sparse Gaussian prior with hyperparameters estimation	71
3.4.4	Total Variation (TV) prior and hierachial Bayesian estimation	72
3.5	Conclusions	75
II	Applications to Different SAR Imaging Systems	77
4	Bayesian Approach for Mono- and Bi-static SAR Imaging	79
4.1	Introduction	79

4.2	Simple Priors with MAP Estimation	80
4.2.1	Results with synthetic data	81
4.2.2	Results with real data	84
4.2.3	Analysis and discussions	85
4.3	JMAP for Hyperparameters Estimation	87
4.3.1	Results with synthetic data	88
4.3.2	Results with real data	88
4.3.3	Analysis and discussions	90
4.4	TV Prior and Hierarchical Bayesian Estimation	91
4.4.1	Results with synthetic data	91
4.4.2	Results with real data	92
4.4.3	Analysis and discussions	93
4.5	Conclusions	93
5	Bayesian Approach for Multi-static SAR Imaging	97
5.1	Introduction	97
5.2	Distributed Satellite Multi-Static SAR	98
5.3	Multi-Static SAR Imaging as a Data Fusion Problem	99
5.3.1	Different data fusion schemes	99
5.3.2	Bayesian data fusion	100
5.4	Experiments and Analysis	102
5.4.1	Results with synthetic data	102
5.4.2	Results with experimental data	104
5.5	Conclusions	106
III	Application to SAR Micromotion Target Imaging	109
6	Bayesian Approach for SAR Micro-Motion Target Imaging	111
6.1	Introduction	111
6.2	Micromotion Effect on SAR Imaging	112
6.2.1	Definition of micromotion	112
6.2.2	Effects on SAR imaging	112
6.3	Conventional Methods for SAR Micromotion Target Imaging	113

6.3.1	Conventional imaging methods	113
6.3.2	Compressive Sensing (CS) methods	114
6.3.3	Comprehensive analysis	115
6.4	Forward Modeling	115
6.5	Bayesian Inversion	119
6.5.1	Sparse signal representation and deterministic optimization	119
6.5.2	Bayesian sparse reconstruction	120
6.6	Simulation Results	125
6.6.1	Sampling pattern	125
6.6.2	Reconstruction when no micromotion	125
6.6.3	Reconstruction when micromotion is present	126
6.6.4	Reconstruction with micromotion and non-micromotion targets .	126
6.6.5	Reconstruction with MF method	126
6.6.6	Reconstruction with closely located micromotion targets	127
6.6.7	Analysis and discussions	127
6.7	Conclusions	128
7	Conclusions and perspectives	137
7.1	Conclusions	137
7.2	Perspectives	139
7.2.1	Forward modeling and inversion developing perspectives	139
7.2.2	Application perspectives	140
A	ann	143
References		145

List of Figures

1.1	Forward problem	22
1.2	Inverse problem	22
1.3	Forward model.	23
1.4	Inverse and estimation of the forward model output.	23
1.5	SAR principle.	25
1.6	Strip and Spot SAR.	27
2.1	SAR target models	44
2.2	Geometry of radar.	45
2.3	Ground plane geometry of SpotSAR.	47
2.4	Mono-static SAR geometry	50
2.5	Mono-static SAR signal support.	51
2.6	Bi-static and Multi-static SAR geometry	52
2.7	Bi-static and Multi-static SAR signal support.	53
2.8	Fourier Synthesis formulation of SAR imaging.	54
3.1	MAP computation.	67
3.2	Joint MAP computation.	67
3.3	Marginalization computation.	68
3.4	VBA computation.	68
4.1	Graphic model of forward modeling and Bayesian inversion.	80
4.2	Two simulated targets and generated complex data sets	82
4.3	Reconstructed results on simulated complex data	83
4.4	The original target of MSTAR	85
4.5	The magnitude of phase history data displaying in reverse video	85
4.6	Reconstructed results on MSTAR data	86

4.7	Different reconstruction errors with parameters λ and β in prior SGG	87
4.8	Different reconstruction errors with the parameter λ in prior SC	88
4.9	Jointly estimate the target and the hyperparameters.	88
4.10	Marginalization with hyperparameters.	89
4.11	Synthetic data	89
4.12	Bayesian reconstructed results with different priors	90
4.13	Jointly estimate the target and the hyperparameters with TV prior.	91
4.14	Synthetic data	93
4.15	Reconstruction results of the targets	94
4.16	Frequency magnitude of Isleta lake: a) Lake 1; b) Lake 2.	94
4.17	Real data reconstruction	95
5.1	Reconstruction results of Target 1	102
5.2	Fusion results of Target 1	103
5.3	Reconstruction results of Target 2	103
5.4	Fusion results of Target 2	104
5.5	Real data imaging geometry.	105
5.6	Results of fusion on real data	107
6.1	Micromotion effect on SAR imaging (time-frequency plane).	113
6.2	Parameter quantitative (super)cube.	114
6.3	Joint estimation and imaging frame.	116
6.4	Micromotion target imaging geometry	117
6.5	Sampling pattern in wavenumber space	125
6.6	Reconstruction results when no micromotion	129
6.7	Reconstruction results when micromotion is present	130
6.8	Reconstruction of a scene with micromotion and stationary targets	131
6.9	Reconstruction results with different methods with micromotion	132
6.10	Reconstruction of two close targets when micromotion is present	133
6.11	Reconstruction RMS of scattering coefficient and position	134
6.12	Reconstruction RMS of micromotion frequency and micromotion range	135
7.1	Bayesian SAR-ATR.	141
7.2	Jointly SAR MMTI.	142

List of Tables

4.1	Statistical results of reconstructed relative distance error	83
4.2	MSTAR public targets	84
4.3	Statistical results of MSTAR data	86
4.4	Statistical results on the two synthetic targets with Bayesian methods . .	89
4.5	Relative distance error of Reconstructed results for MSTAR data	90
4.6	Relative distance error of reconstruction on synthetic complex data . . .	92
4.7	Relative distance error of reconstruction on real data	92
5.1	System main measurement parameters	98
5.2	Comparison of reconstruction performances of three fusion methods . .	104
5.3	Experimental measurement parameters	105

Notations

<i>Symbol</i>	<i>Definition</i>
\mathcal{H}	forward operator
\mathcal{D}	derivative operator
$E\{\cdot\}$	expectation
$(\cdot)^{-1}$	inverse
$tr(\cdot)$	trace
∇	gradient
$\ln(\cdot)$	logarithm
$(\cdot)^T$	transpose
\star	convolution
$diag(\cdot)$	diagonal values of a matrix
$\ \cdot\ _2$	l_2 norm of a vector or a matrix
$\ \cdot\ _p$	l_p norm of a vector or a matrix
\exp	exponential
$(\cdot)^H$	conjugate transpose
$p(A)$	probability of an element A
i.i.d	independent and identical distribution
\propto	proportional to
$\Gamma(\cdot)$	Gamma function
\mathbb{R}	the set of real values
\mathbb{C}	the set of complex value
$\mathbb{R}^{M \times N}$	real matrix space with dimension $M \times N$
$\mathbb{C}^{M \times N}$	complex matrix space with dimension $M \times N$
\mathbf{f}	target vector
\mathbf{g}	data vector
N	number of elements in vector \mathbf{f}
M	number of elements in vector \mathbf{g}
\mathbf{H}	forward model
\mathbf{I}	identity matrix
ϵ	errors (modeling errors and noise)
$\hat{\mathbf{f}}$	estimate of \mathbf{f}
$\hat{\mathbf{g}}$	estimate of \mathbf{g}
$\Delta \mathbf{f}$	changes of \mathbf{f}
$\Delta \mathbf{g}$	changes of \mathbf{g}

B	bandwidth of transmitted pulses
c	wave propagation velocity
L_a	antenna length in azimuth direction
V_a	velocity of SAR platform
θ_{in}	injection angle
ρ_r	range resolution
ρ_a	azimuth resolution
L	radar flight range $(-L, L)$
$s(t)$	transmitted signal
$g(t)$	received signal
t	slow time (platform movement/azimuth direction)
t'	fast time (wave propagation/range direction)
τ	time delay
θ	azimuth angle
σ	radar cross section
ν	frequency
ν_c	carrier frequency
ω	angular frequency
R	distance between radar and target
R_c	vertical distance of the sensor path to the origin of the target
α_c	chirp ratio of transmitted signal
Ω	integration area of reflected signals
A'	scale factor accounting for propagation attenuation
u_p	radar line of sight
$\delta(\cdot)$	δ function
$r_\theta(u_p)$	Radon transform of $f(x, y)$ along the radar line of light θ
$g(t, \theta)$	received signal at angle θ
$S(\omega)$	spectra of the transmitted signals
$G(\omega, \theta)$	spectra of the received signals at angle θ
$\mathbf{r} = (x, y)^T$	space position vector
$\mathbf{k} = (k_x, k_y)$	wavenumber vector
θ_{tr}	angle of radar line of light for transmitter
θ_{cr}	angle of radar line of light for receiver
$\tau_{tc}(x, y, \theta_{tc})$	time delay between transmitter and target
$\tau_{cr}(x, y, \theta_{cr})$	time delay between target and receiver
$G(\omega, \theta_{tc}, \theta_{cr})$	the spectra of the received signals at transmitted angle θ_{tc} and received angle θ_{cr}
ϑ	parameter vector to be estimated, containing target position, amplitude of micromotion, rotation frequency, <i>etc.</i>
f_m	micromotion frequency
r_m	micromotion range
φ	micromotion phase

Abbreviations

<i>Acronym</i>	<i>Definition</i>
2D	Two dimensions space
3D	Three dimensions space
ATR	Auto Target Recognition
BCS	Bayesian Compressive Sensing
BPA	Back Projection Algorithm
BTW	Bayesian Total Variation
BWE	Band Width Extrapolation
CoSaMP	Compressive Sampling Matching Pursuit
CS	Compressive Sensing
CSA	Chirp Scaling Algorithm
CT	Computed Tomography
DFT	Discrete Fourier Transform
EM	Expectation Maximization
FFT	Fast Fourier Transform
FS	Fourier Synthesis
FT	Fourier Transform
GGM	Generalized Gauss Markov
GM	Gauss Markov
GMTI	Ground Moving Target Indication
GTD	Geometric Theory Diffraction
HRRP	High Range Resolution Profile
IG	Inverse Gamma
IFFT	Inverse Fourier Transform
ISAR	Inverse SAR
JMAP	Joint MAP
LFM	Linear Frequency Modulated
LOS	Line Of Sight
LS	Least Square
MAP	Maximum A Posteriori
MF	Matched Filtering
MIMO	Multiple Inputs Multiple Outputs
ML	Maximum Likelihood

MMTI	MicroMotion Target Indication
MRF	Markov Random Field
MSTAR	Moving and Stationary Target Acquisition and Recognition
QR	Quadratic Regularization
PDF	Probability Density Function
PFA	Polar Format Algorithm
PM	Posterior Mean
PRF	Pulse Repeat Frequency
Radar	RAdio Detection And Ranging
RCM	Range Cell Migration
RCMC	Range Cell Migration Correction
RCS	Radar Cross Section
RDA	Range Doppler Algorithm
RIP	Restricted Isometry Property
RMS	Root Mean Square
RVP	Residual Video Phase
SAR	Synthetic Aperture Radar
SBL	Sparse Bayesian Learning
SC	Separable Cauchy
SEM	Stochastic Expectation Maximization
SFM	Sinusoidal Frequency Modulated
SGG	Separable Generalized Gaussian
SNR	Signal Noise Ratio
SpotSAR	Spotlight SAR
StripSAR	Stripmap SAR
SVD	Singular Value Decomposition
SVM	Support Vector Machine
TV	Total Variation
VBA	Variational Bayesian Approximation



Introduction

1.1 Problem Motivation

1.1.1 Inverse problems and main characteristics

The way to observe the world, in most cases, is from reasons to results, i.e., from sources to observation. In mathematics, this kind of problem is named "*Forward problem*" and the relation between the observations and the sources is called "*Forward modeling*". If we denote the source as f and the observable quantity as g , then we can write:

$$g = \mathcal{H}f \quad (1.1)$$

where \mathcal{H} represents the *Forward operator*.

Note by \mathcal{F} the space of all possible $f \in \mathcal{F}$ and $g \in \mathcal{G}$, in such a way that \mathcal{G} is the image of the operator \mathcal{H} . Then we can discuss in details about *Forward problems* and *Inverse problems* and their corresponding difficulties via the notions of *well-posedness* and *ill-posedness* of a problem.

According to the definitions of well-posed mathematical problems proposed by French Mathematician J. Hadamard [Had23], a problem is called well-posed if the following three conditions are satisfied: existence, uniqueness and stability.

Forward problems in physics, by construction, are well posed except the case of chaotic or unstable systems. As illustrated in Figure 1.1, for a non-chaotic and stable system, the solution forcibly:

- exists ($\forall f \in \mathcal{F}, \exists g = \mathcal{H}f.$),
- is unique ($\forall f \in \mathcal{F}, \exists$ only one $g = \mathcal{H}f.$)
- and stable ($\forall f_1$ and f_2 such that $\|\Delta f\|_2^2 = \|f_2 - f_1\|_2^2 < \epsilon, \exists g_1 = \mathcal{H}f_1, g_2 = \mathcal{H}f_2$, such that $\|\Delta g\|_2^2 = \|g_2 - g_1\|_2^2 < \varsigma$, and when $\epsilon \rightarrow 0$, then $\varsigma \rightarrow 0$).

1.1.1 - Inverse problems and main characteristics

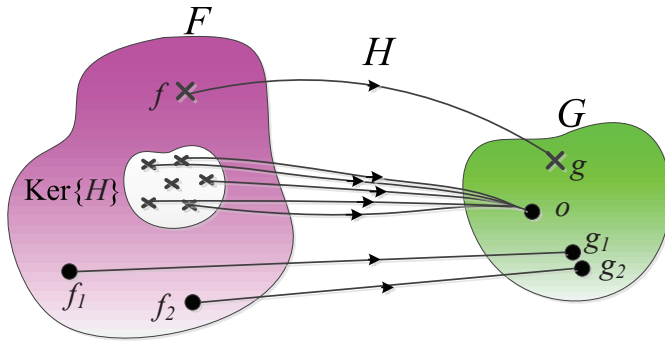


Figure 1.1: Forward problem: compute the model response $g \in \mathcal{G}$ (data) given a physical Forward model \mathcal{H} . Forward problems are in general well-posed.

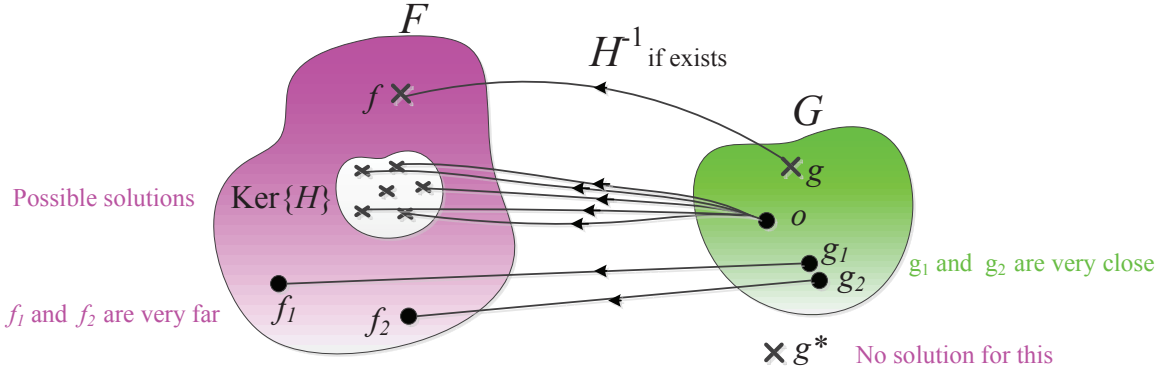


Figure 1.2: Inverse problem: infer about the physical model from the data. When the forward operator \mathcal{H} is given, the inverse problem is to find a solution for a given data g . Inverse problems are in general ill-posed.

However, Inverse problems, in general, are ill-posed [LC91, MD09a, Idi08, Wan07]. As illustrated in Figure 1.2, we can see that:

- The given data g may not belong to the range of the forward operator, so a solution for this data may not exist: in Figure 1.2, data g^* has not a solution;
- The solution may not be unique: all the $f \in \text{Ker}\{\mathcal{H}\}$ have the same data point 0. So,
 - if g_1 has a solution f_1 , all $f = f_1 + \text{ker}\{\mathcal{H}\}$ are also solutions;
 - if $\text{Ker}\{\mathcal{H}\} = 0$, then the solution is unique;
- The solution may not be stable in the sense that the inverse operator when exists may not be continuous: two very close data g_1 and g_2 may result in two very far solutions f_1 and f_2 .

To further explain this, we take a general imaging system as an example. We represent the errors (including measurement noise and modeling errors) as ϵ which usually comes from inner thermal noise and environmental noise [Sko70], then we establish a forward and an inverse model, respectively:

- **Forward problem:** from a given target scene \mathbf{f} , the forward model \mathbf{H} and the errors $\boldsymbol{\epsilon}$, we get the echo data \mathbf{g} , as illustrated in Figure 1.3. For a linear time invariant system, this becomes a typical convolution problem;

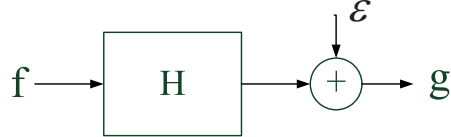


Figure 1.3: Forward model.

- **Inverse problem:** from observed data \mathbf{g} and the forward model \mathbf{H} (unknown or partly known), we get an estimate $\hat{\mathbf{f}}$ of the target scene \mathbf{f} , as illustrated in Figure 1.4:

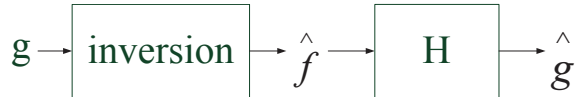


Figure 1.4: Inverse and estimation of the forward model output.

When $\hat{\mathbf{f}}$ is computed, we can also estimate $\hat{\mathbf{g}} = \mathbf{H}\hat{\mathbf{f}}$.

When the problem is ill-posed, a strict inverse operator \mathbf{H}^{-1} may not exist or when exists may not be unique or when exists and is unique, it may be too sensitive to small changes in the data $\Delta\mathbf{g}$ (errors or noise).

In that case $\frac{\|\Delta\mathbf{g}\|_2^2}{\|\mathbf{g}\|_2^2}$ and $\frac{\|\Delta\mathbf{f}\|_2^2}{\|\mathbf{f}\|_2^2}$ are related by the condition number $\text{cond}(\mathbf{H})$ of the operator \mathbf{H} . If the operator \mathbf{H} is ill-posed (or ill-conditioned in the finite dimensional case), then $\text{cond}(\mathbf{H})$ may be large and small changes in the data may result in huge changes in the solution. Using the notation of this figure, $\|\Delta\mathbf{g}\|_2^2 = \|\mathbf{g} - \hat{\mathbf{g}}\|_2^2$ may be very small but $\|\Delta\mathbf{f}\|_2^2 = \|\mathbf{f} - \hat{\mathbf{f}}\|_2^2$ may be very large.

1.1.2 General factors of Synthetic Aperture Radar

Radar is acronym for RAdio Detection And Ranging, which is an active microwave imaging system using electromagnetic waves to determine the range, altitude, direction, or speed of interested targets. For its capability of observation and detection under long-distance, whole orientation, all weather and all day conditions, radar plays a very important role in military ground space surveillance and earth observation.

In 1951, Wiley firstly found that by making use of the Doppler shift of received echo signals, the resolution of side-looking radar was improved [Sko01]. This significant discovery led to the birth of Synthetic Aperture Radar (SAR) [Kov76]. The most noticeable advantage of SAR is the capability of generating high resolution images, in both two directions of *range* (the direction of wave propagation) and *cross-range* (or named *azimuth*, the direction of sensor flight path). Because SAR imageries contain fine

1.1.2 - General factors of Synthetic Aperture Radar

structures of the target scene and provide abundant information of underlying features of interest, high resolution SAR images are vital to the performances of Auto Target Recognition (ATR) [TCYS12, LDQL11, HZF⁺11, DFW⁺10, LLZ10, ZXT05].

Generally speaking, the frequency of radar transmitted pulses, the beam pattern of radar antenna, the geometry of SAR system and the relative motion between radar and target compose the most important factors of SAR [Whi05]. By selecting different frequency band of radar, radar wave propagation and reflection characteristics of target will be changed; By controlling the direction of antenna beam, the illumination area as well as the integration angle of imaging will be different; By constituting different location positions of radar transmitter and receiver(s), not only the orientation of target scattering but also the imaging area will be changed; Finally, the relative motion between target and sensor affects the accuracy of quadratic phase compensation and thus brings difficulties in the case of its complicated form.

SAR was early designed as Mono-static, where radar receiver and transmitter are collocated. However, as a high power transmitter is easily to be detected by counter, Bi- and Multi-static SAR systems become a developing trend [Sul04, WG91]. Especially with recent development of space-borne techniques, satellite distributed SAR presents important potentials: it takes advantage of the passive multi radar in observation, broadening the observation range, improving its resolution and decreasing the probability of detection and recognition.

The relative motion between target and sensor is another concerned issue. For most stationary scenes, the motion of the sensor platform is known thus it can be compensated completely. Nevertheless, for moving targets, especially for non-corporative targets with complex motion, the imaging process becomes intractable. Thus, SAR Ground Moving Target Indication (SAR-GMTI) attracts great research interests. An expected radar can undertake the compound task to monitor a ground area, indicate and track moving targets and finally produce high resolution imageries of moving targets for classification. However, unlike maneuvering artificial targets, the micromotion (such as rotation, vibration, sinusoidal motion, *etc.*) target imaging becomes extremely difficult.

Many researches have been conducted to improve the resolution of SAR in both hardware development and data processing techniques. The items and the subjects we present are between the most important parts of the research on radar and SAR imaging in many French, European, American and other international research institutions, such as ONERA in France, European Aerospace Agency and NASA in USA.

In military field, SAR has been widely applied in air traffic control, nautical radars to locate landmarks and other ships, aircraft anti-collision systems, ocean-surveillance systems, outer-space surveillance systems, meteorological precipitation monitoring, altimetry and flight-control systems, target-locating systems and ground-penetrating radar geological observations.

In civil field, SAR is also considered as a mature technique. It is widely used for remote sensing for environmental earth observation, climate prediction and interferometrical analysis. So from the social point of view, any real methodological and technological progress will have great impact for environmental as well as for economical cost reduction aspects in environmental observation and surveys.

1.1.3 SAR principle

A typical process of radar scattering can be described as: radar mounted on a platform (airplane or satellite) sends electromagnetic waves to ground targets and collects radar pulses with a receiving antenna. The received signals are called radar echoes, which contain abundant information about the target scattering characteristics, the spatial position, etc.

Resolution and synthetic aperture technique

The spatial resolution is defined as the least distance for discriminating two close targets, which in SAR imagery can be divided into two directions: range resolution and azimuth resolution. Generally they are defined as the width of pulse response at half-power points for a point target of two directions, respectively.

SAR users attempt to obtain high resolution images. As real aperture radar, on range direction SAR obtain High Range Resolution Profile (HRRP) by transmitting high frequency pulses and followed by pulse compression process; However, on azimuth direction, SAR is greatly different from conventional radar: it obtains a high azimuth resolution by sending coherently pulses and accumulating them along its flight path. By using quadratic phase compensation, the amplitudes and phases of backscattering echoes become coherent (called full phase coherent), which are received by antenna coherently. In this way, an equivalent large antenna (synthetic aperture) is formed, as illustrated in Figure 1.5.

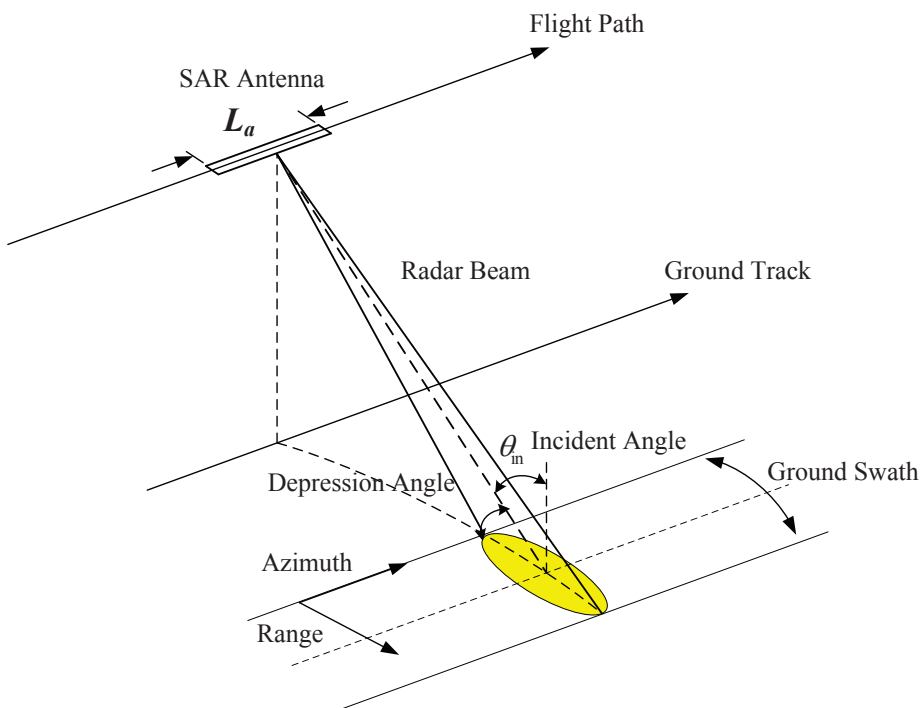


Figure 1.5: SAR principle.

1.1.3 - SAR principle

- Range resolution

The range resolution of SAR (after matched filtering) is [CM06].

$$\rho_r = \frac{c}{2B \sin \theta_{in}} \quad (1.2)$$

where B is the bandwidth of transmitted pulses, c is the velocity of propagation of wave and θ_{in} is the incident angle of radar waves. The complementary angle of θ_{in} is named as the depression angle. Normally, under far field condition, where the distance between radar and target is very far, the depression angle can be omitted. In this case, the range resolution can be approximated as $\rho_r = \frac{c}{2B}$.

- Azimuth resolution

The theoretical azimuth resolution of SAR is

$$\rho_a = \frac{L_a}{2} \quad (1.3)$$

where L_a is the length of antenna in azimuth direction. Thus the azimuth resolution doesn't change with the distance of radar and the target.

As we can see, by increasing the bandwidth of the transmitted signal or the accumulated angle, SAR resolution can be improved. However, this way is limited by the hardware complexity and real observation conditions. Therefore, how to improve SAR resolution with limited bandwidth and angle becomes very important.

SAR working mode

In the previous analysis, we have seen that SAR uses the relative movement between radar antenna and target to form a huge synthetic aperture. Along the flight path, at each point of observation, radar beam formed in the direction of the antenna, emanates an area on the ground and collects the reflected signals. Along the direction of the movement of radar platform, there comes an illuminating strip on the ground which is called the ground swath.

Depending on different shapes of the ground swath, SAR system can be mainly divided into two distinct working modes: Stripmap and Spotlight [Sul04]¹ as illustrated in Figure 1.6:

1. In stripmap mode SAR (StripSAR), the squint angle between the beam direction and the flight path (assuming as a line) keeps the same. A stripmap on the ground which is parallel to the flight path can be observed continuously. StripSAR is mainly used for large area imaging, which doesn't require a very high resolution.
2. In spotlight mode SAR (SpotSAR), however, at each observation point of the synthetic aperture, transmitter antenna is adjusted to the same region so that the antenna is steered to illuminate a single spot of terrain continuously. Comparing to StripSAR, SpotSAR has a longer illumination time towards the target scene and obtain an increased azimuth resolution.

In this thesis, we consider SpotSAR for its capability of high resolution.

1. There also exists another mode of ScanSAR which is not included in our discussion.

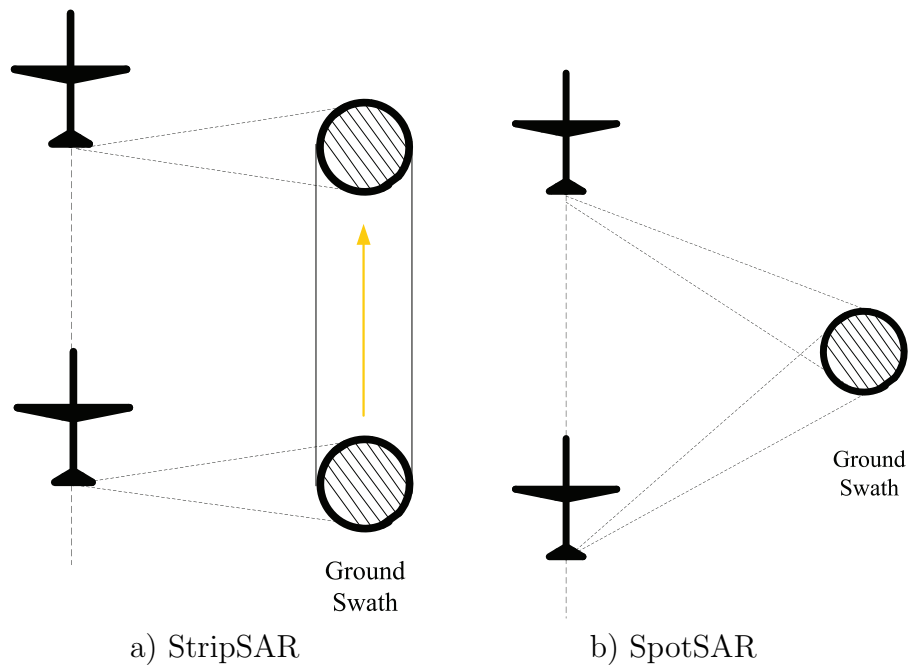


Figure 1.6: Strip and Spot SAR.

SAR geometry

When radar transmitter and receiver are located in the same place, this geometry is named as Mono-static.

Instead, when radar transmitter and the receiver are located separately, this geometry is named as Bi-static. When there are more than one receivers and all the distances between antennas are pretty larger than themselves dimensions, this is called Multi-static. Obviously, a Multi-static radar can be decomposed into a set of several (the number equals that of receivers) Bi-static transmitter-receiver pairs.

1.1.4 Link to inverse problems

As we have discussed above, the forward model of the SAR system is then to generate echo signal \mathbf{g} for the target with scattering coefficients \mathbf{f} based on the forward operator \mathbf{H} of the system under some observation noise ϵ as shown in Figure 1.3. \mathbf{g} , \mathbf{f} and \mathbf{H} are all complex. Then, the problem of SAR imaging is to recover the scattering coefficients \mathbf{f} of the target from the echo \mathbf{g} , which is usually an ill-posed inverse problem. This work concerns such an inverse problem of SAR imaging to recover the scattering coefficients \mathbf{f} from the partial noisy observation \mathbf{g} under a Bayesian framework.

1.2 State of the Art

1.2.1 A historical overview of inverse problems

Inverse problems arise from indirect observations of interests, which were firstly studied in mathematics and now have been widely applied for earth physics, life science, finance science and computer science [MD09a].

The historical overview of inverse problems can be mainly divided into three stages:

1. 1902-1960. Hadamard firstly proposed the notions of *well-posedness* and *ill-posedness* [Had23]. In this stage, for the reason lacking of efficient tools of inversion and proper applications, research was mainly focusing on theoretical level of mathematics.
2. 1960s-1980s. Propelled by the urgent requirements of applications in engineering fields as graphics, remote sensing, medical science, inverse problems started being studied broadly. The typical applications such as Computed Tomography (CT) for medical imaging, parameters estimation in remote sensing and signal reconstruction in optics were developed. Particularly the regularization theory proposed by Tikhonov marked a breakthrough in theory [TAJ77]. From then on, regularization methods became being treated as the main tool for inverse problems.
3. 1980s-now. Regularization methods and their corresponding optimization computing algorithms were widely used. Research in recent thirty years mainly focused on solutions to discrete ill-posed problems and all the optimization methods such as gradient methods [FM99, BC95, Wu01], conjugate gradient methods [GN92], singular value decomposition (SVD) methods [Cha82], support vector machine (SVM) methods [VGS96, SYCS10], etc. Bayesian methods recently are more highlighted [MDZDF10, MD12, FRB⁺03, ASB03, XXZ⁺11, HHM12, FN05, LCW04, TB03, MD03, SLM02, QD01, Lut90, SSD99]. A link between Maximum A Posteriori (MAP) estimation and the regularization methods helped the introduction of the Bayesian methods to be well accepted in applied mathematics and engineering communities. At this period, it combines the knowledge of computing science, applied mathematics and statistics, being considered as one of the most exciting cross-disciplinaries.

1.2.2 An overview of conventional SAR imaging algorithms

SAR echo generation can be represented by firstly the product of the target scattering coefficients (reflectivity) and antenna pattern in range direction, and then the convolution with two pulse response functions. The objective of SAR imaging is to reconstruct the target scattering coefficients from echo data. SAR echoes can be considered as the output of a two dimensional linear system. The input of the system is target reflectivity.

There have been a large number of algorithms proposed for SAR imaging. These algorithms process either in the time domain, *i.e.*, Polar Format Algorithms (PFA) and Back-Projection Algorithm (BPA), or in the frequency domain, *i.e.*, Range-Doppler

algorithm (RDA) and Chirp-Scaling Algorithm (CSA).

RDA [BXW05, Bam92] and CSA [CGM95b, CW05, RRB⁺94] involve only the Fast Fourier Transform (FFT) and complex multiplication. Thus they have advantages of fast processing, high efficiency and easiness for implementation in the frequency domain. However, FFT-based methods lead to a limited resolution which is decided by the bandwidth of transmitter and the integration angle. In corresponding to Fourier's point of view, SAR imaging system is a band-pass filter and the system response function is assigned to be zero when out of the cut-off frequency. The comparatively large approximation processing in frequency domain decreases the accuracy of imaging and results in serious side lobe artifacts [PEPC10].

In order to overcome the drawbacks of performing FFT directly, PFA was developed [CGM95b]. PFA can be considered as an application of the projection-slice theorem and normally used in SpotSAR. It demodulates the received echoes with reference to the relative reference center (in general is the center of the scene), then saves the demodulated data in the frequency domain in the polar coordinate format, followed by the 2-D non-uniform interpolation processing and finally performs the 2D Inverse FFT (IFFT) on the interpolation results to get the focused SAR image. PFA well solves the problem of spectrum aliasing. However, it has two drawbacks: first of all, 2D interpolation processing leads to the comparatively complex implementation, large computation and low efficiency; secondly, the assumption of plane wave limits its use only for far distance and small area imaging.

Another important projection method is BPA [DFW⁺10, Yeg99, MR96, MML99, BB00, UHS03, CHS06]. BPA has no limitations on integration angle or flight path, so it can be used in Bi- and Multi-static SAR imaging [HBCW01].

1.2.3 An overview of improving SAR resolution techniques

The recognition performance is mainly determined by the quality of information provided in radar images.

However, during the process of image acquisition, due to the effects of the motion blur (motion of targets), the noise introduced by imaging process and the spectrum overlap of the image caused by the sub-sampling, the resolution of the resulting SAR images is decreased. In addition, the SAR images suffer from so called speckle noise lying in most of the coherent imaging systems. In particular, the received echo is affected by the random phase fluctuation within the resolution cell, which also introduce the observation noise.

Based on SAR principle, SAR resolution can be improved by the increased bandwidth or synthetic aperture. However, this way is limited by the hardware cost and the real condition. In response to the contradictions, signal processing technique becomes an alternative way.

There are mainly two categories of methods to improve SAR resolution [SK10c]:

1. Methods by compensating non-ideal factors to reach theoretical resolution

1.2.3 - An overview of improving SAR resolution techniques

A nature thinking to reach the theoretical value of resolution is to compensate non coherent signals to realize the coherent integration at different scattering points. The non coherent signals are due to all kinds of non-ideal factors which include complex relative motion [SK10c, SK10a, XWB05], phase center drift of antennas [MMJ07, XPX04, JK08], system random noise, inhomogeneous propagating medium [Bel08, JZ07, DS08] and other noises.

All these methods are trying to recover image's spectrum to the cut-off frequency corresponding to the diffraction limit frequency. However, these methods cause information loss beyond the cut-off frequency. The effects as low resolution, side lobe artifacts and speckles of SAR images are inevitable.

2. Methods by spectral estimation, bandwidth extrapolation and regularization to surpass theoretical resolution

It is essential a parameters estimation problem for SAR imaging that aims to estimate scattering coefficients of targets. There are in general two categories of parameter estimations approaches: parametric and non-parametric. After necessary pre-processing, non-parametric methods treat the SAR imaging as to estimate the power spectral density of signal. Classical SAR imaging methods fall into the family of the non-parametric method. Comparing to non-parametric methods, parametric methods parameterize the imaging model and try to estimate these model parameters which usually provide higher resolution.

Spectral estimation method

Spectral estimation method is one of the most conventional superresolution methods [ZXQ⁺10]. Parametric spectral estimation method normally bring high accuracy. However, there are two drawbacks: i) The errors of judging may affect the result seriously as the performance depends on the matching degree. However, it is difficult to judge the order of the model; ii) Large computation and the difficulty to search in global also limit its application [PEPC10].

Band Width Extrapolation (BWE) method

BWE method is another important method which does not assume the parametric model of radar target echo, instead, they use the observed data to infer/estimate non-observed frequency band or aperture, realizing virtual bandwidth and/or aperture extension. Comparing to spectral estimation method, BWE method is non-parametric thus achieves better robustness. However, there exists the limitation of the extrapolated bandwidth and/or aperture, which is normally considered as two times of the original and high SNR is also needed.

Regularization method

Regularization method originates from the solution for inverse problems. As SAR imaging problem can be formulated as an inverse problem which is ill-posed [CB09, Shk04b, Shk04a, Shk10a], the prior knowledge is required to regularize the results [Sko08, Ric05, JwE⁺96, Sou99].

Regularization methods often use a linear parameter estimation model, or dif-

ferential equations with variational constraints. The quadratic function of the unknown quantities leads to Tikhonov regularization [TAJ77, TA63], which finally involves a computationally straightforward optimization problem. However, useful features in the resulting imagery such as edges are badly suppressed. To address these drawbacks, [ÇK01, Çet01, SCMS09] proposed a non-quadratic regularization method to SAR imaging in terms of improving resolution. With the proposed method, target features can be enhanced including point features (such as positions of point scatters) and region features (such as shapes of targets). However, how to determine regularized parameters is still an open problem. An efficient way to get the optimal and automatically estimated model parameters is herein needed.

Compressive Sensing (CS) method

Sparse signal representation and CS are emerging techniques for improving SAR resolution [Shk04b, Shk04a, RT07, VV09, BMK10b]. The sparsity in SAR images or in the frequency domain are explored to get the sparse representation of the signal. The computation load of parameter estimation can be herein significantly decreased [Don92, DH01, Don06b, Don06a, DET06, CRT06b, CRT06a, CRT08]. In addition, by using CS for SAR imaging, the resolution can be improved with less data [OC12, WLJW11, SCMS11, ZXQ⁺10, TALDM10, Shk10a, Shk10b, VcFW08, YYSH09]. However, all these methods depend on the accuracy of the model and require high SNR.

Over current research, by exploiting appropriate prior models as well as utilizing prior information has become a new develop trend to improve SAR resolution. A novel approach is needed for combining the information of observed data and the prior knowledge of the target scene and the noise, to bring a distinct solution to SAR imaging.

1.2.4 Challenges for SAR imaging

Taking an overview of the current research on SAR imaging, we can see that the technology has been advanced significantly but the problem still has not been solved radically.

Conventional SAR imaging methods are usually based on:

1. Point scattering model as target scene modeling;
2. Simplified linear forward model linking the received signal to the target reflectivity and the transmitted radar signal;
3. The use of a very simplified way for inversion such as Inverse Fast Fourier Transform (IFFT).

These three drawbacks result in low resolution, noisy, unstable and not quantitatively useable images, with unsuppressed speckles and high side lobe artifacts.

In practice, complicated target scenes, low SNR (ratio between signal power and noise power), complex relative motion between radar and target and non-ideal sensing

1.3.1 - Bayesian inference

ways, making the existed SAR imaging methods be seriously challenged.

1. Complicated target scene

Besides point targets, more complicated target scenes include extended targets, multi targets, or multi target features should be considered. Complicated target scenes might be continuous mountains, large populated areas, or shores and lakes, which not only make imaging very difficult but also make feature extraction and target recognition even harder.

2. Low SNR in practice

In practice, the long distance between SAR and the target results in a low SNR of observed signals. For example, echoes of the satellite-borne SAR targets are usually submerged in background clutters, which leads to the decrease of the image resolution or even blur.

3. Complex relative motion between radar and target

SAR uses relative motion between target-radar based on coherent integration to obtain high resolution in azimuth dimension. However, the complex relative motion between them impedes the coherent integration.

4. Non-ideal sensing ways

Conventional imaging methods are based on an ideal sensing way, which do uniform sampling in spatial-, time- and frequency-domains. However, in terms of realizing certain objective (for example to decrease the data sampling rate and the data volume), the non-ideal sensing way becomes a new trend of radar sensing. The most representative ways include sparse spatial frequency sampling, random sampling, CS, etc.

Hence, challenges to conventional SAR imaging methods demand for new solutions. It is necessary to study the SAR imaging problem with a distinct inversion framework i) to fully exploit and use the prior information of target scene; ii) to establish the appropriate physical model as well as the mathematical model and iii) to design the inversion as well as the corresponding fast computation algorithms, so as to obtain a satisfying solution.

1.3 Bayesian Inference for SAR Imaging

1.3.1 Bayesian inference

Comparing to the deterministic regularization methods which give only regularized solutions but do not handle the error and uncertainties, the Bayesian inference is a natural approach to handle the inverse problems by providing not only a regularized solution but also its remaining uncertainties by taking into account of the uncertainties and errors due to the measurement system and additional noise [MD06a, MD09a, PEPC10, FBR⁺⁰⁰].

The basic idea of Bayesian approach is to combine the information in a probabilistic way, which comes from the forward model \mathbf{H} , the observed data through the likelihood $p(\mathbf{g}|\mathbf{f})$ and the prior knowledge through the prior probability law $p(\mathbf{f})$. The Bayesian rule then combines these two terms to obtain the posterior law $p(\mathbf{f}|\mathbf{g})$ from which we can infer the unknown \mathbf{f} .

Thus by defining uncertainties by probability criteria, it provides a more efficient tool to automatically obtain the optimal model parameter and makes the estimation problem to be solved more reasonably. By jointly using Bayesian and regularization techniques for incorporating the prior knowledge, the resolution can be effectively improved [FBS02, DeG98, PEPC10, GBM94, GBM94].

1.3.2 Advantages of Bayesian inference for SAR imaging

Generally speaking, under the Bayesian inference framework, the problem of SAR imaging can benefit in the following three aspects:

- Accounting for the uncertainties in the forward model through the likelihood $p(\mathbf{g}|\mathbf{f})$;
- Accounting for prior knowledge about the unknown scene \mathbf{f} through $p(\mathbf{f})$;
- Combining the information contents of $p(\mathbf{g}|\mathbf{f})$ and $p(\mathbf{f})$ through the Bayes rule.

Bayesian methods based on appropriate prior modeling, can effectively compensate for the lack of complete information in the data about the unknowns, which usually gives a satisfactory solution [MD03, SLM02, VV09].

1. Regularization method can get a stable solution of the inverse problem through regularization constraints, but the difficulty in determining the regularization parameter affects the inversion performance. Interpreting the regularization methods as the MAP estimation can give more tools for the determination of the regularization terms and parameters. Bayesian framework provides the flexibility for different priors, starting from simple separable Gaussian models to Markovian and to the very sophisticated hierarchical models. Through appropriate prior modeling, high-resolution SAR images of the target and meanwhile the enhancement of the multiple features of target features can be achieved.
2. Radar target scattering in high frequencies can be well approximated as a sum of several individual scatterers, which provides an important basis for using sparse signal representation. Compared with traditional CS SAR imaging methods, the advantages of the Bayesian CS (BCS) approach is, being able to model noise and error, so a more sparse representation of the target can be obtained. BCS approach can also be used for moving target imaging, realizing the joint estimation of motion and scattering parameters.

[MD12] proposed a Bayesian approach with prior laws enforcing sparsity for inverse problems and source separation, with emphasis on sparsity analysis. In [ZMDW⁺12], we proposed a signal representation approach for micromotion target imaging based on a Bayesian framework. Our proposed research, to a certain

1.4.1 - Organization

degree, has some in common with finding solutions to inverse problems by employing CS in imaging. Sparse recovery algorithm, the core of CS, can be viewed as a solution to the ill-posed CS problem by using sparse prior information. However, the objective of our proposed research is to establish a unifying framework for exploiting various prior information including sparse priors.

3. The conventional SAR imaging method is sensitive to noise. The Bayesian approach can not only estimate the unknown target, but also jointly estimate the noise. Thus it has the characteristic of being not sensitive to model noise. Therefore, it is stable in conditions of low SNR compared to conventional imaging methods, suppressing the noise and background clutter while imaging.

[Jin12] exploited a heavy-tailed t distribution for data noise modeling, with a certain degree of robustness. [XXZ⁺11] studied the Bayesian estimation problem for Inverse SAR (ISAR) imaging. [AA10] proposed two Bayesian multiscale approaches in terms of suppressing speckles during SAR imaging. A generalized autoregressive (conditional heteroscedasticity) model was developed.

In summary, comparing with the limitations of existing SAR imaging theory and technical bottlenecks, Bayesian approach provides a fundamentally different way to address the new challenges.

1.3.3 Main steps of Bayesian inference for SAR imaging

To solve the problem of SAR imaging, the main steps of Bayesian approach include: the forward modeling, the prior modeling, obtaining the posterior expression and an estimation criterion, and finally proposing appropriate Bayesian computation algorithms.

Thus, how to establish the forward model for different situations, how to assign appropriate priors for target scenes and how to implement Bayesian computation, become very important for Bayesian approach. These issues are going to be addressed in this thesis.

1.4 Organization and Main Contributions of the Thesis

1.4.1 Organization

This thesis is organized as following:

Part I, including Chapter 2 and Chapter 3, presents the different forward modeling problems as well as the classical and proposed inversion methods.

In Chapter 2 we establish the forward model of SAR imaging. Firstly, based on some assumptions of radar scattering, we present target modeling. Then, we derive SAR echo model based on a tomographic SpotSAR model. For different geometries of Mono-, Bi-

and Multi- static SAR, a general linear inverse problem focusing on Fourier Synthesis (FS) is presented.

In Chapter 3, we study the Bayesian approach to inverse problems, with emphasis on assigning prior models and hyperparameter estimation. Firstly, we study two classes of priors for modeling the unknown complex target reflectivity scene: separable priors and Markovian priors, in corresponding to point targets and homogeneous extended targets with edges, respectively. Then we consider the hierarchical models with hidden variables. For practical reasons we also need to consider the estimation of the hyperparameters. In summary we consider different criteria and different corresponding approximations and computational algorithms, such as MAP, Joint MAP (JMAP), Marginalization and Variational Bayesian Approximation (VBA) methods.

Part II, including chapter 4 and chapter 5, presents the proposed approach for inverse problems in different SAR imaging systems.

In Chapter 4, we consider Mono- and Bi-static SAR imaging and present the inversion results with proposed Bayesian methods. In particular, two typical SAR target scenes of separable point targets and homogeneous extended targets, are assigned with appropriate priors studied in Chapter 3. We analyze the effect of different priors on SAR image reconstruction performance. Then, we apply our proposed estimation methods to different data sets. Numerical simulation and experimental results demonstrate the efficiency of the proposed method.

In Chapter 5, we consider Multi-static SAR imaging where we have more than one data sets. We study the problem with application in distributed satellite SAR. In order to cope with the reconstruction problem with multi data sets of multi-frequencies and multi-static, we propose three different fusion schemes. Through comparison, the proposed Bayesian joint fusion and reconstruction method has the best performance, realizing inversion based on multi data sets from the same observed target scene. Comparing to classical data-level fusion methods, the proposed Bayesian fusion method takes the advantage of incorporating the prior information of the original target.

Part III as Chapter 6, addresses the problem of SAR micromotion target imaging.

In chapter 6, we consider the problem of micromotion target imaging. Instead of dealing with the tough issue of the ambiguity of radar, we formulate the problem as a parameter estimation problem. CS technique is used to find the most sparse representation of the unknown target. We propose an efficient Bayesian approach with sparsity-enforcing priors. A VBA approach is proposed for the hierarchical estimation of the unknowns, the hidden variables and the hyperparameters of the problem.

Finally, in Chapter 7, we draw conclusions of our work and point out the perspectives.

1.4.2 - Main contributions

1.4.2 Main contributions

In this thesis, we try to overcome the drawbacks of conventional SAR imaging methods by:

1. More various target reflectivity modeling;
2. More realistic forward modeling counting for uncertainties;
3. More efficient inversion methods based on regularization and the Bayesian inference approach.

The combination of these three ingredients result in high-resolution, more stable to noise and more precise images as well as more accurate parameter estimation. The final aim is to improve the performance for various tasks of SAR-ATR and SAR-GMTI. The contributions of this thesis mainly include:

1. We systematically elaborated a mathematical forward model of SAR imaging with different geometries and target motions.
 - a) We analyzed the characteristics of two typical radar target scenes.
 - b) We derived the SAR echo model for Mono-, Bi- and Multi-static SAR.
 - c) We established a unifying Fourier Synthesis model for these three geometries.
 - d) We established a micromotion model for SAR targets experiencing rotation, where the SAR imaging problem becomes a nonlinear problem and conventional imaging method fails.
2. We proposed a Bayesian approach for different SAR imaging problems.
 - a) We proposed the following priors: Three simple priors of Separable Generalized Gaussian (SGG), Separable Cauchy (SC) and Generalized Gauss-Markov (GGM); Priors with hyperparameters and hierarchical models: Generalized Gaussian prior, Sparse Gaussian prior, Total Variation (TV) prior and *Student-t* prior. We also analyzed the effects of different priors on inversion.
 - b) We developed different algorithmic solutions for different estimators, including MAP, JMAP, Marginalization and VBA.
 - c) We studied the problem of data fusion arising in Multi-static SAR and proposed a Bayesian joint fusion and inversion method with comparison to other two different fusion methods.
 - d) We firstly addressed the problem of micromotion target imaging by proposing a Bayesian CS (BCS) method for micromotion target imaging and parameter estimation.
3. We demonstrated the performance of the proposed approach through experiments on synthetic, experimental and real data. With comparison to conventional SAR imaging methods and regularization methods, the results demonstrated the effectiveness and feasibility of the proposed Bayesian approach.

1.5 Publications

Journal:

1. **Sha Zhu**, Ali Mohammad-Djafari, Hongqiang Wang, Bin Deng, Xiang Li, Junjie Mao. Parameter estimation for SAR micromotion based on sparse signal representation, EURASIP (Europe Advance on Signal Processing): special issue on Sparse Signal Representation, 2012:13, doi: 10.1186/1687-6180-2012-13)
2. Bin Deng, Hongqiang Wang, Yuliang Qin, **Sha Zhu**, and Xiang Li. Rotating Parabolic-Reflector Antenna Target in SAR Data: Model, Characteristics, and Parameter Estimation, International Journal of Antennas and Propagation, Vol. 2013, Article ID 583865, 13 pages, 2013. doi:10.1155/2013/583865
3. **Sha Zhu**, Yanpeng Li, Xiang Li, JunJie Mao. Parameter estimation of superimposed chirps with single degree of freedom based on sparse signal representation, Chinese Journal of Modern Radar, Vol.30 No.4, April 2008, 59-63 (In Chinese)
4. **Sha Zhu**, Hongqiang Wang, Xiang Li, JunJie Mao. Analyses of constellation area navigation capacity and key-satellite, Chinese Space Science Technology, Vol.28, No.5, June 2008,20-24 (In Chinese)
5. Yuliang Qin, **Sha Zhu**, Hongqiangwang, Xiang Li. Characteristics and potential applications of sub-millimeter seeker, Chinese Journal of Modern Defense Technology, Vol.36, No.6 December 2008, 144-148 (In Chinese)

Proceedings:

6. **Sha Zhu**, Ali Mohammad-Djafari, Hongqiang Wang, Xiang Li. A novel hierarchical Bayesian estimation approach for SAR imaging, In AIP Conference Proceedings of 31th International Workshop on Bayesian Inference and Maximum Entropy Methods in Science and Engineering (Maxent2011), Waterloo, Canada, 2012, Vol. 1443, p. 222-229 (EI index, Access No 12696474)
7. **Sha Zhu**, Ali Mohammad-Djafari, Xiang Li, Junjie Mao. Inverse problems arise in different Synthetic Aperture Radar imaging systems and a general Bayesian approach for them, in proceedings of IS & T/SPIE Electronic Imaging: Computational Imaging Inverse Problems (SPIE2011), U.S.A, Jan. 20-23, 2011, Vol.7873, No. 6, p. 787306(14pp). (EI index, Access No 11893142)
8. **Sha Zhu**, Ali Mohammad-Djafari. A Bayesian approach to Fourier Synthesis inverse problem with application in SAR imaging, In AIP Conference Proceedings of 30th International Workshop on Bayesian Inference and Maximum Entropy Methods in Science and Engineering (Maxent2010), Chamonix, France. March 14, 2011, Vol. 1305, p. 258-265 (EI index, Access No 11873321, Doi: 10.1063/1.3573625)
9. Ali Mohammad-Djafari, **Sha Zhu**, Franck Daout, Philippe Fargette. Fusion of multistatic synthetic aperture radar data to obtain a super-resolution imaging, Journal of Physics: Conference Series 8th International Workshop on Information Optics (WIO2009), Jul. 20-24, 2009, Paris, France. Vol. 206, No.1, p. 012022(3 pp.) (EI index, Access No 11367953)

1.4.2 - Main contributions

10. **Sha Zhu**, Peng You, Hongqiang Wang, Xiang Li, Ali Mohammad-Djafari. Recognition-oriented Bayesian SAR imaging, 3rd IEEE International Asia-Pacific Conference on Synthetic Aperture Radar (ApSAR2011), 26-30 Sept. 2011, Seoul, South Korea, 4 pp. (EI index, Access No 12390631)
11. **Sha Zhu**, Hongqiang Wang, Xiang Li. A new method for parameter estimation of multi-component LFM signal based on sparse signal representation, in proceedings of IEEE International Conference on Information and Automation (ICIA2008), Jun. 15-19, 2008, Zhangjiajie, China, p. 15-19 (EI index, Access No 10179064)

Part I

Forward Modeling and Inversion

2

Forward Modeling: from Scene to Data

2.1 Introduction

The objective of this chapter is to present the forward modeling of SAR imaging.

SAR observation system relies on emitting electromagnetic waves to a target and measuring its response. To solve the problem of SAR imaging, first of all we need to establish the forward model linking the target and received signals.

Firstly, we present the target scene modeling. Several assumptions on radar scattering center theory are presented. Then, we give a brief presentation of SAR target scene model.

Then, we focus on the echo modeling, where we start from the simple case of radar echo signal generation towards point target scene. In the following, we derive SAR echo modeling, with several factors considered: the geometry of transmitter-object-receiver, the form of radar transmitted pulses, antenna beam pattern and characteristics of radar target scattering.

In SpotSAR within a small observing angle, SAR imaging can be explained by the tomographic model. Based on the projection-slice theorem, we establish the forward model of echo generation.

Finally, we conclude our model as a very general case and get the relation of forward modeling under a linear assumption.

The chapter is organized as following: in Section 2.2, target modeling is presented, with several assumptions of radar scattering given in Section 2.3. Then, radar echo modeling and SAR echo modeling are derived. Based on SpotSAR model, the observation model for three different geometries: Mono- (Section 2.4), Bi- and Multi-static SAR (Section 2.5) are established. The problem of Fourier Synthesis (FS) is presented in Section 2.6 and the general model is presented in Section 2.7.

2.2.1 - Assumptions on radar scattering

2.2 SAR Target Modeling

Radar is closely related to radar target characteristics [HYX05]. The final aim of radar is to obtain the information of targets, which include not only the motion and trajectory information, but also the geometric shape and physical parameters.

The coherent characteristic makes the differences of SAR image structure and data processing method compared to optical imaging [CW05]. In order to achieve a better performance of the image reconstruction, an explicit model of target scene should be set on SAR imaging principle.

2.2.1 Assumptions on radar scattering

Definition 1. *Radar Cross Section (RCS) is a physical characterization of radar target scattering ability against the irradiation of electromagnetic wave. Based on the point of view of electromagnetic scattering theory [BSU87, Kno85], the electromagnetic scattering energy of radar target can be expressed as the product of the equivalent area of the target and the incident power density, which is based on the assumptions of the irradiation of plane electromagnetic wave and the isotropic target scattering.*

It is difficult to strictly analyze and calculate the pulse response of the target, which needs more knowledge about the electromagnetic theory which does not belong to the range of our study in this thesis. Our work is mainly based on the Optical Geometric Theory Diffraction (GTD) theory and the backscattering theory. For simplicity, we make the following assumptions:

1. Far field condition

Assume the far field condition, where the distance of target is far enough (infinite). With far field condition, the incident wave is approximately to be the plane wave, then RCS is independent to the distance.

2. Backscattering model

Based on GTD, when target size is larger than wavelength of incident wave, the backscattering of the target can be considered as composed by several separate scattering centers. Thus the pulse response of the target (the reflectivity distribution function) is approximately modeled by the scattering model.

3. Neglecting the multi-path scattering and shielding effect between scatterers

Each scatter center is assumed to be separately of scattering and the effect of multi-scattering and shielding effect is neglected.

4. Within a small radar viewing angle, the location and the amplitude of scattering centers remain invariant to some extent.

Strictly speaking, the scattering characteristic of the target is related to the direction of radar sight. For example, there is a strong back specular reflection when the plate fuselage is vertical to the radar Line Of Sight (LOS), while at the other

angles of small deviation angle the specular reflection turns to a different direction and will not be received by the radar. which is slowly changed with the variation of the angle and is also related to the radar wavelength. B.Bhanu depicts the invariance of scatterer location and magnitude for MSTAR images [IBG98].

These four assumptions form the basis of our analysis. In this thesis, we consider the ideal scattering center model, i.e., the location and the complex amplitude of RCS is not changed with the frequency or azimuth angle, while the phase is linearly dependent on frequency and is sine (cosine) on azimuth angular.

2.2.2 Target scene modeling

SAR imaging scene is the area of the illumination on the ground scatterers by the radar beam. Considering that a SAR system illuminates a scene which is composed by the background and targets, herein, the received echo including the part from targets which is called as “radar echo signal”, as well as the part from background which is called as “clutter signal”. As a result, the obtained SAR image is also made of background and interested targets.

We may distinguish between “background”, “physical target” and “equivalent scattering target” and for each case we may give appropriate models. However, we more often have the knowledge of a whole scene. In this thesis, we only consider the target scene with zero background to concentrate on the recovery of scattering coefficients. focus on scene modeling instead of discriminating each part. The probabilistic characteristic of scene models may need a statistical chart.

Physical target model

Based on electromagnetic theory, according to the relative size of the radar target to the wavelength of radar transmitted wave as well as the resolutions of SAR systems, radar targets can be divided into two types: point targets and extended targets.

A single point target is a target having small dimensions compared to the angular and range resolution of the radar. Point target refers to the target which is composed of a single dominant (or a small number of) isolated scattering point(s).

Extended target refers to the target which is a collection of a large number of scattering points. It is normally presented by the weak scattering homogeneous area.

Scattering centers model

According radar scattering theory, at high frequencies, the total electromagnetic scattering of the radar target can be considered as the scattering from several separate scattering centers. The equivalent scattering centers contain much physical structure information of the target.

An increasing research interest is focused on the sparsity of SAR target, which lie in two aspects: in one hand, image itself with the majority data representing clutter,

2.3.1 - Radar echo generation

shadow, which is approximately dealt as zero when comparing with targets; in the other, parameters of parametric model representing unknown target or data in transform domain, are comparatively larger at target's edges and other signatures than those in corresponding to clutter and shadow regions, thus parameters representing interested regions have sparsity.

In this thesis, we mainly consider two kinds of target scenes, illustrated in Figure 2.1.

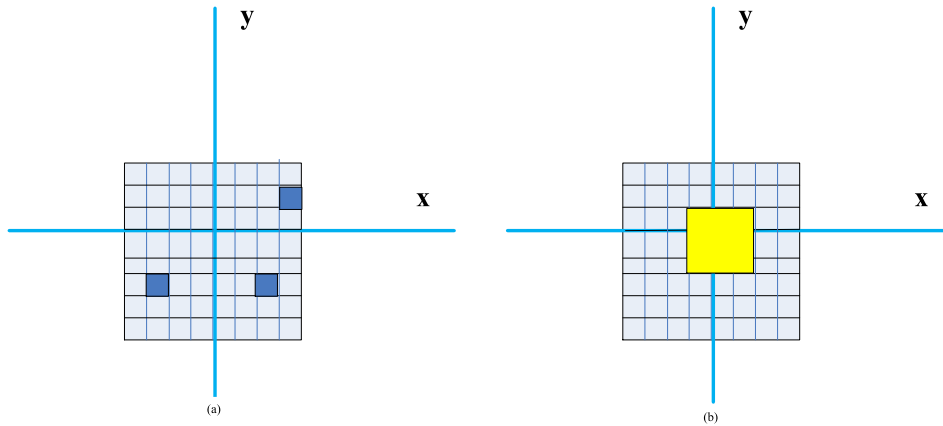


Figure 2.1: SAR target models: (a) Point targets where the point sources are isolated very far from each other; (b) Extended targets where the point sources are close to be grouped in compact regions but localized through different resolution cells.

2.3 SAR Echo Modeling

2.3.1 Radar echo generation

As we have discussed, RCS is used to describe the scattering function of target, which reflect the interaction between the scene, the transmitted signal and the received signal. We denote RCS by σ , the value of which depends on the frequency of the radar transmitter, the direction of the transmitted and the received antenna(s) and the physical scattering characteristics of the target, including the material, the shape, the roughness, *etc.* SAR imaging process from SAR echo is essentially to estimate target scattering coefficients.

We begin with the relationship in the time domain. Assume the transmitted signal is $s(t)$ and the received signal is $g(t)$. In real physical problems, both the knowns and unknowns are continuous. However, for the first step of the analysis, we start from a very simple case with a scene effectively composed by several point scatterers.

When radar illuminates the interested region in the target scene, for each scatterer, we receive the reflected signal. Thus, the total received signals should be the sum of the reflected signals from all the effective scatterers. For each scatterer, we have:

$$g(t) = \sigma \cdot s(t - \tau) \quad (2.1)$$

where τ denotes the time delay, given by

$$\tau = \frac{2R}{c} \quad (2.2)$$

where R is the distance of the radar transmitter (receiver) and the scatterer, and c is the propagation velocity of wave.

Assume there are N scatterers in the observed region of the target scene and the interaction function RCS of i th scatterer in the observed scene is denoted by σ_i , $i = 1, \dots, N$, herein the received signal can be given by

$$g(t) = \sum_{i=1}^N \sigma_i s(t - \tau_i) = \sum_{i=1}^N \sigma_i s(t - \frac{2R_i}{c}) \quad (2.3)$$

where σ_i is the scattering coefficients of the i^{th} scatterer which are usually complex. As illustrated in Figure 2.2, considering the 2D cartesian coordinates (x, y) , sensor locates at the position (x_r, y_r) , and scatterers locate at the position (x_m, y_n) with RCS denoted by σ_{mn} , $m = 1, \dots, l_x$, $n = 1, \dots, l_y$

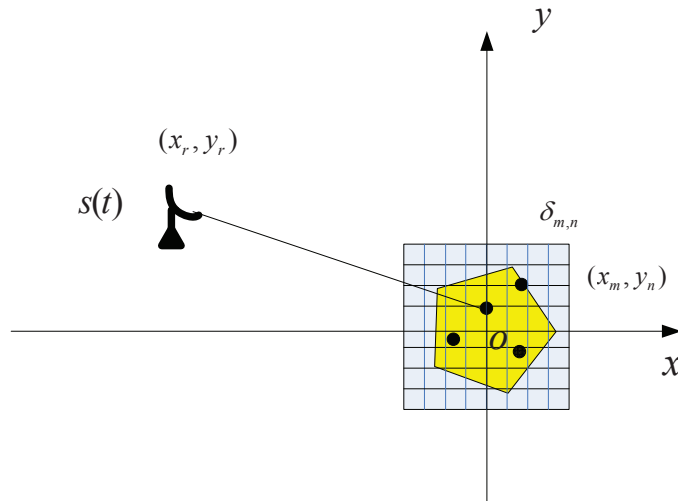


Figure 2.2: Geometry of radar.

we have

$$g(t) = \sum_{n=1}^{l_y} \sum_{m=1}^{l_x} \sigma_{mn} s(t - \tau_{mn}) = \sum_{n=1}^{l_y} \sum_{m=1}^{l_x} \sigma_{mn} s(t - \frac{2}{c} \sqrt{(x_r - x_m)^2 + (y_r - y_n)^2}) \quad (2.4)$$

where σ_{mn} is non-zero when there is a scatterer at the position (x_m, y_n) or zero when there is none of the scatterers.

In real practice, the target is composed by the continuous regions instead of the discrete scatterers. Herein the integration should take place of the sum operation:

$$g(t) = \iint f(x, y) s(t - \tau(x, y)) dx dy \quad (2.5)$$

2.3.2 - SAR echo modeling

the function $f(x, y)$ can be physically interpreted as the electromagnetic reluctivities due to all scattering centers in the scene, denoting the unknown function to be estimated. $g(t)$ is the sum of all the reflected signals, named as "echo", denoting the known data that has been observed. Until now, the problem becomes: with the observed echo data $g(t)$, trying to reconstruct the reflectivities of the original target $f(x, y)$.

2.3.2 SAR echo modeling

We consider a SpotSAR geometry [CGM⁺95a, Fit88, JwE⁺96, MJOJ83]. In such a geometry of data collection, the $x-y$ coordinate is centered on the footprint of the target illuminated by a radar beam from a moving radar. The radar beam, as operating in spotlight mode, is continuously pointed at the ground patch with a constant depression angle.

Here the radar return yields a projectional view of the target provided that the phase front of the radio waves have no significant curvature, i.e., satisfying the far field condition. For simplicity, the depression angle is omitted. In this way, we get the ground plane geometry of SpotSAR [Fit88, CGM⁺95a, CGM⁺95a, MJOJ83, Sou92].

As illustrated in Figure 2.3, in a cartesian coordinate (x, y) , the origin is set as the center of the target. Radar traverses the flight path from the range of $-L$ to L with different positions over dimension y . For each position of the radar, there forms a viewing (azimuth) angle θ between radar light direction u_p and the axis x .

Without loss of generality, we adopt the classical assumption of "Stop-and-Go": the sensor and scattering target are assumed to be stationary during the time interval during which the pulse watches over the target [FL99]. For a pulsed system, assume that the pulses are transmitted at times t' . This time scale along the range direction is called "fast time"; in the opposite, the timescale t on which the antenna moves along azimuth direction is called "slow time", because the range timescale, corresponding to the velocity of sensor, normally moves much slower than azimuth timescale, corresponding to the velocity of wave propagation. Thus, with "Stop-and-Go" assumption, radar is provided to stop over each pulse interval.

In such a way, the reflectivity function $f(x, y)$ can be physically interpreted as the scattering filed at (x, y) due to an illumination from radar at a given observing angle θ . Thus, along the given range direction at angle θ , for each point scatterers with positions denoted by u_p , we get the echo observation model.

$$g(t, \theta) = \iint f(x, y) s(t - \tau(x, y, \theta)) dx dy \quad (2.6)$$

where $\tau(x, y, \theta)$ denotes the time delay of different positions of radar transmitter.

Let the radar transmit a linear frequency modulated pulse signal which is commonly used in SAR,

$$s(t) = \begin{cases} \exp^{j(\nu_c t + \alpha_c t^2)}, & |t| \leq \frac{T}{2} \\ 0, & \text{otherwise} \end{cases} \quad (2.7)$$

where ν_c is the carrier frequency, α_c is the chirp ratio. For the point at $u_p = (x, y)$, the

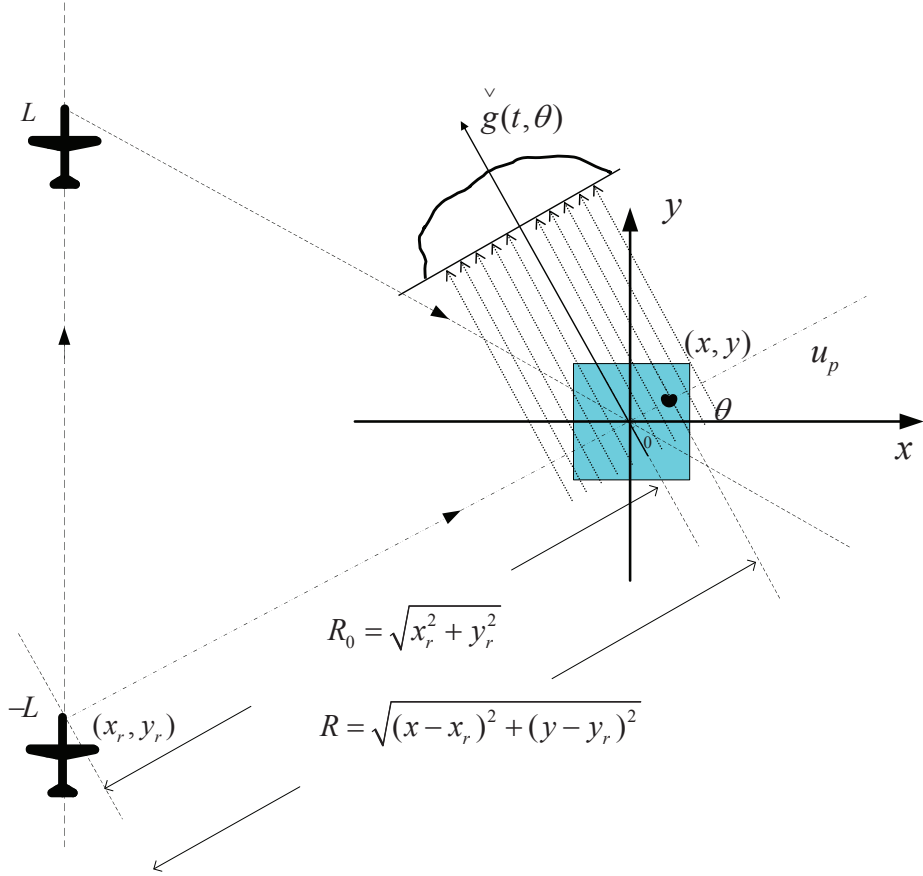


Figure 2.3: Ground plane geometry of SpotSAR.

return signal is

$$g_1(t, x, y) = A' \cdot f(x, y)s(t - \tau) \quad (2.8)$$

where A' is a scale factor accounting for propagation attenuation and other effects and

$$\tau = \frac{2R}{c}, \quad R = \sqrt{(x - x_r)^2 + (y - y_r)^2} \quad (2.9)$$

where R is the distance between radar and the target. τ is the round travel time (time delay), (x_r, y_r) is the position of the radar at time t . Conditioned on the far field so that the size of target is not too large, one can use Fresnel approximation to write

$$R \approx R_0 + x \cos \theta + y \sin \theta + \frac{\sqrt{x^2 + y^2}}{2R_0} \quad (2.10)$$

where θ is the angle of radar line of light (azimuth angle), $\cos \theta = \frac{x_r}{R_0}$, $\sin \theta = \frac{y_r}{R_0}$ and $R_0 = \sqrt{x_r^2 + y_r^2}$. On the condition of far field, $R_0 \gg \sqrt{x^2 + y^2}$, R can further be approximated by

$$R \approx R_0 + x \cos \theta + y \sin \theta \quad (2.11)$$

Then, the received signal from the entire target can be modeled as integral

$$g(t, \theta) = A' \iint_{\Omega} f(x, y)s(t - \frac{2R_0}{c} - \frac{2(x \cos \theta + y \sin \theta)}{c}) dx dy \quad (2.12)$$

2.3.3 - Projection-slice theorem

where Ω is the integration area of reflected signals. The first step of Dechirp is pulse compression with respect to fast time t' or to mix with the reference signal which is delayed in phase and quadrature versions of transmitted FM chirp,

$$\exp\{-j(\nu_c(t - \tau_0) + \alpha_c(t - \tau_0)^2)\}$$

where the $\tau_0 = \frac{2R_0}{c}$ and it gives

$$\begin{aligned} \tilde{g}(t, \theta) &= \iint f(x, y) \exp\left\{j\nu_c(2t - \frac{2(x \cos \theta + y \sin \theta)}{c} - 2\tau_0)\right\} \\ &\quad \cdot \exp\left\{\alpha_c\left((t - \tau_0)^2 + (t - \tau_0 - \frac{2(x \cos \theta + y \sin \theta)}{c})^2\right)\right\} \\ &\quad \cdot \exp\left\{j\left[\frac{4\alpha_c(x \cos \theta + y \sin \theta)^2}{c^2} - \frac{2(x \cos \theta + y \sin \theta)}{c}(\nu_c + 2\alpha_c(t - \tau_0))\right]\right\} dx dy \end{aligned} \quad (2.13)$$

The first term is centered on the carrier frequency ν_c and the second term is not, so a signal after low-pass filtering and mixing with the reference signal, becomes

$$\begin{aligned} \tilde{g}(t, \theta) &= \iint f(x, y) \exp\left\{j\frac{4\alpha_c(x \cos \theta + y \sin \theta)^2}{c^2}\right\} \\ &\quad \cdot \exp\left\{-j\frac{2(x \cos \theta + y \sin \theta)}{c}(\nu_c + 2\alpha_c(t - \tau_0))\right\} dx dy \end{aligned} \quad (2.14)$$

the quadratic phase term can be removed through some operations, *e.g.*, interpolation or motion compensation which is not discussed here and gives the following approximation

$$\check{g}(t, \theta) = \iint f(x, y) \exp\left\{-j\frac{2(\nu_c + 2\alpha_c(t - \tau_0))}{c}(x \cos \theta + y \sin \theta)\right\} dx dy \quad (2.15)$$

It can be seen that the processed signal $\check{g}(\theta, t)$ is the Fourier transform of a projection of target along a direction θ with the spatial frequency $k = \frac{2(\nu_c + 2\alpha_c(t - \tau_0))}{c}$, $\frac{-T}{2} + \frac{2(R+L)}{c} \leq t \leq \frac{-T}{2} + \frac{2(R-L)}{c}$.

2.3.3 Projection-slice theorem

Munson [MJOJ83] pointed out that in SpotSAR mode, the reconstruction methods were fundamentally similar to that of Computed Tomography (CT) reconstruction. The returned signal at a moment in time is proportional to the sum of all reflections along contours equidistant from the antennas.

The approximation of echo signal Equation (2.15) after some preprocessing operations can be also expressed as

$$\check{g}(t, \theta) = \int_{u_p} \iint_{x,y} f(x, y) \delta(u_p - x \cos \theta - y \sin \theta) \exp\left\{-j\frac{2k}{c}u_p\right\} dx dy du_p \quad (2.16)$$

where $\delta(\cdot)$ is the δ function and let

$$r_\theta(u_p) = \iint_{\Omega} f(x, y) \delta(u_p - x \cos \theta - y \sin \theta) dx dy \quad (2.17)$$

$g(t, \theta)$ is then

$$\check{g}(t, \theta) = \int_{-L}^L r_\theta(u_p) s\left(t - \frac{2R_0}{c} - \frac{2u_p}{c}\right) du_p \quad (2.18)$$

where $r_\theta(u_p)$ is actually the Radon transform of $f(x, y)$ along the radar line of light θ .

Let

$$F(X, Y) = \iint f(x, y) \exp\{-j(xX + yY)\} dx dy \quad (2.19)$$

and the inverse Fourier transform is given by

$$f(x, y) = \frac{1}{4\pi^2} \iint F(X, Y) \exp\{j(xX + yY)\} dX dY \quad (2.20)$$

The projection of $f(x, y)$ at angle θ is formally given by

$$r_\theta(u_p) = \iint f(x, y) \delta(u_p - x \cos \theta - y \sin \theta) dx dy \quad (2.21)$$

The 1D Fourier transform of $r_\theta(u_p)$ with respect to u_p is given by

$$R_\theta(U_p) = \int r_\theta(u_p) \exp\{-ju_p U_p\} du_p \quad (2.22)$$

Thus, the projection-slice theorem can be stated by

$$R_\theta(U_p) = F(U_p \cos \theta, U_p \sin \theta) \quad (2.23)$$

Thus, Equation (2.15) is

$$\check{g}(t, \theta) = R_\theta(U_p) \quad (2.24)$$

From the Equation (2.23) and Equation (2.24), Equation (2.24) can be written in the wavenumber-domain as

$$G(k, \theta) = \iint f(x, y) \exp\{-j(k_x x + k_y y)\} dx dy \quad (2.25)$$

where $k_x = U_p \cos \theta$ and $k_y = U_p \sin \theta$.

These relations are described in Figure 2.3, from which we find that the received data is corresponding to the straight line segment with the angle θ . Actually for the whole integration angle, we get the signal support in the wavenumber domain. We can then recognize a FT equation between the spectrum of the received signal and the 2D FT of the scene in Equation (2.25).

In above, we derived the echo observation model for SpotSAR in terms of Fourier projection slice theorem. However, there are obvious differences between tomographic imaging and SpotSAR [MJOJ83]: for example, in spotSAR, the line integral involved in the projection is taken perpendicular to the direction in which the radio waves travel; and the most striking differences is that SpotSAR data are necessarily narrow-band.

Actually, the transform domain data (signal support) is related to the bandwidth of the radar as well as the observation (azimuth) angle, and is also related to the different geometries of SAR. In the following, we will try to establish a general forward model for different geometries: Mono-, Bi- and Multi-static, and then analyze the different presentation of signal support in the Fourier domain.

2.3.3 - Projection-slice theorem

2.4 Mono-Static SAR

As discussed above, in the Mono-static SAR, we define:

- $\mathbf{r} = (x, y)^T$ a space coordinate (x, y) with $r = |\mathbf{r}| = \sqrt{x^2 + y^2}$;
- $\mathbf{k} = (k_x, k_y)$ the corresponding Fourier space coordinates of space coordinates (x, y) : $k = |\mathbf{k}| = \sqrt{k_x^2 + k_y^2}$;
- ν the frequency;
- θ the azimuth angle and R its distance between radar and the target;
- $g(t, \theta)$ the received signal in time domain;
- $G(\omega, \theta)$ the spectra of received signals in frequency domain.

The Mono-static SAR geometry is illustrated in Figure 2.4, with the origin still placed in the center of the target. The figure is similar to the one in the previous section. However, we redo this without the projection part to be more focused on its geometry and try to analyze the corresponding Fourier domain data support.

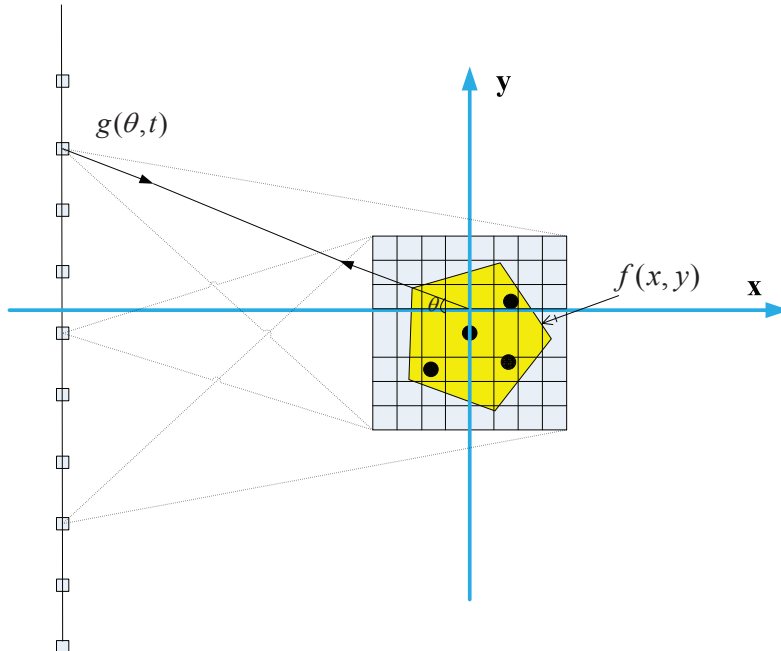


Figure 2.4: Mono-static SAR geometry: Transmitter and Receiver are collocated.

In the time domain, following the same procedures of radar echo generation, we have

$$g(t, \theta) = \iint f(x, y) s(t - \tau(x, y, \theta)) dx dy \quad (2.26)$$

then we have the spectra of the received signals

$$G(\omega, \theta) = S(\omega) \iint f(x, y) \exp\{-j\omega\tau(x, y, \theta)\} dx dy \quad (2.27)$$

where $S(\omega)$ represents the spectra of the transmitted signals. We represent received signals in the wavenumber domain (phase history domain), we have the time delay

$$\tau(x, y, \theta) = \frac{2R}{c} = \frac{2}{\omega} R \times k \quad (2.28)$$

Use the vectors defined above, it can also be written as

$$\tau(x, y, \theta) = \frac{2}{\omega} \mathbf{r}^T \mathbf{k} = \frac{2}{\omega} (k_x x + k_y y) \quad (2.29)$$

The spectra of the received signals

$$G(\omega, \theta) = S(\omega) \iint f(x, y) \exp \{-j2(k_x x + k_y y)\} dx dy \quad (2.30)$$

Assume $S(\omega)$ to be constant in a bandwidth $\Delta\omega$ so can be omitted, we obtain Equation (2.25).

Till now, we get the relation between the spectra of the received signal and Fourier Transform of the target. To further examine this, we observe it in the wavenumber domain. The received data

$$k_x x + k_y y = r(k_x \cos \theta + k_y \sin \theta) = k(x \cos \theta + y \sin \theta) \quad (2.31)$$

as illustrated in Figure 2.5, is corresponding to the straight line segment with the azimuth angle θ . Then for the whole integration angle, we get the signal support in the wavenumber domain.

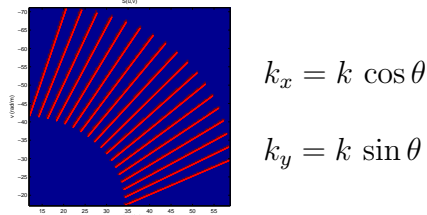


Figure 2.5: Mono-static SAR signal support.

As we can see, for Mono-static SAR, in the typical Fourier domain sampling, the transform domain data in a SAR system are restricted to lie in a small annulus segment. The sample in the radial dimension is proportional to the signal bandwidth, the inner and outer edges that are determined by the frequency content of the transmitted chirp; while the samples in the angle dimension is proportional to the coherent angle, or to say, the pulse numbers of the coherent processing interval.

In all, in the Fourier domain, radial band is limited by the finite bandwidth of the transmitted pulse and the angular band is limited by the finite viewing angle of the radar. The support of the signal in the Fourier domain, affects the image's resolution.

If we can get a greater diversity in either frequency or the angular, or both, we can try to get a higher resolution. A perfect case is to get the support for the high frequency in the whole band and the whole angle.

2.3.3 - Projection-slice theorem

2.5 Bi-, Multi-Static SAR

Now, we consider Bi-static SAR geometry model [Sou92, Sou91], where radar transmitter and receiver are located separately. With the same assumptions in Mono-static case, as illustrated in Figure 2.6, the location of radar transmitter location is fixed, while the receiver moves around a circular trajectory of radius r , assuming that compensations have been done, at this time the geometry can be viewed as an ideal turntable model [BXW05]. In the spatial two-dimension coordinate plane, we parameterize the position of radar transmitter by angle θ_{tc} , denoting the angle of radar line of light for transmitter. Similarly, we have θ_{cr} denoting the angle of the receiver position.

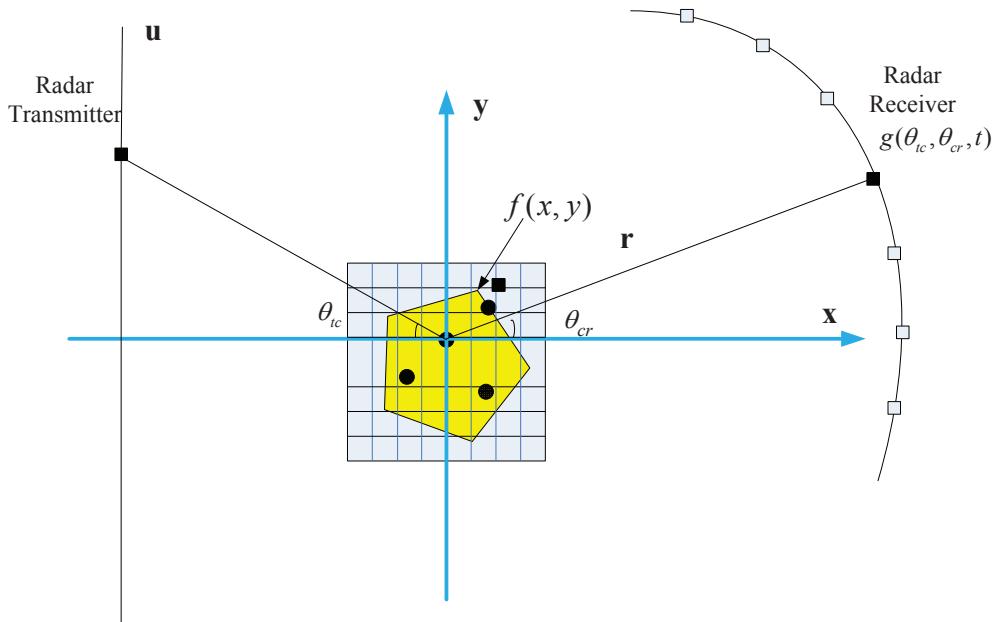


Figure 2.6: Bi- and Multi-static SAR geometry: Transmitter and Receiver(s) are separately located.

If we change the positions of receiver(s) along the circular trajectory, for each position of the receiver, the geometry turns into the Bi-static case; if there are more than one receivers, the geometry turns into the Multi-static case.

Again, the relation between the transmitted signal $s(t)$ and the received signal $g(t)$ reflected from target $f(x, y)$ can be written as

$$g(t, \theta_{tc}, \theta_{cr}) = \iint f(x, y) s(t - \tau_{tc}(x, y, \theta_{tc}) - \tau_{cr}(x, y, \theta_{cr})) dx dy \quad (2.32)$$

where $\tau_{tc}(x, y, \theta_{tc})$ represents the time delay between the transmitted signal and the target and $\tau_{cr}(x, y, \theta_{cr})$ represents the time delay between the target and the received signal.

The wavenumber vector of the transmitter and the receiver are given as [Fel09]:

$$\mathbf{k}_{tc} = \begin{pmatrix} k \cos \theta_{tc} \\ k \sin \theta_{tc} \end{pmatrix} \quad \mathbf{k}_{cr} = \begin{pmatrix} k \cos \theta_{cr} \\ k \sin \theta_{cr} \end{pmatrix} \quad (2.33)$$

If we follow the same form of the position vector of a scatter point $\mathbf{r} = (x, y)^T$, we can write the delay for the transmitter and the receiver, respectively:

$$\tau_{tc}(x, y, \theta_{tc}) = \frac{1}{\omega} \mathbf{r}^T \mathbf{k}_{tc} = \frac{k}{\omega} (\cos \theta_{tc} x + \sin \theta_{tc} y) \quad (2.34)$$

$$\tau_{cr}(x, y, \theta_{cr}) = \frac{1}{\omega} \mathbf{r}^T \mathbf{k}_{cr} = \frac{k}{\omega} (\cos \theta_{cr} x + \sin \theta_{cr} y) \quad (2.35)$$

The total delay becomes:

$$\tau_{tc} + \tau_{cr} = \frac{k}{\omega} \{(\cos \theta_{tc} + \cos \theta_{cr}) x + (\sin \theta_{tc} + \sin \theta_{cr}) y\} \quad (2.36)$$

and get

$$\mathbf{k} = \begin{bmatrix} k_x \\ k_y \end{bmatrix} = \begin{bmatrix} k(\cos \theta_{tc} + \cos \theta_{cr}) \\ k(\sin \theta_{tc} + \sin \theta_{cr}) \end{bmatrix}, \quad |\mathbf{k}| = k = \frac{\omega}{c} \quad (2.37)$$

We can then follow the same process to get the spectra of the received signal, but this time, the relation between (k_x, k_y) and $(\theta_{tc}, \theta_{cr})$ becomes different.

As illustrated in Figure 2.7, for each sampling of radar received signal at a spatial position of the angle θ_{cr} , the received signal over the target, corresponds to a sample point in the wavenumber domain (k_x, k_y) ; when position of the radar receiver changes, the position of the received data in the wavenumber domain accordingly changes. For the angle accumulation over the whole coherent processing interval, we get a new signal support.

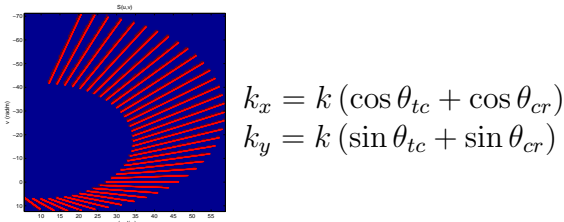


Figure 2.7: Bi-static and Multi-static SAR signal support.

In summary, in all three cases, the spectrum of each received signal $G(\omega, \theta)$ at a given angle θ in the Mono-static case and $G(\omega, \theta_{tc}, \theta_{cr})$ at a given angle of transmitter-receiver $(\theta_{tc}, \theta_{cr})$ in the Bi-static and Multi-static cases, give some information in the Fourier domain (k_x, k_y) on a segment of a straight line. The length of the segment line depends on the bandwidth of the transmitted signal and its orientation on the geometry of transmitter-object-receiver. Thus structure and topology of those points form the support of the signal in the Fourier domain, which depend on the bandwidth of the transmitted signal and the relative positions of transmitter-receiver respected to the target, and the resolution is affected by the relative position between the transmitters and receivers.

2.3.3 - Projection-slice theorem

2.6 SAR Imaging as Fourier Synthesis (FS)

Mathematically speaking, after some simplification [CB09], the problem of SAR imaging becomes the Fourier Synthesis (FS) [ZMD10, MD03] which consists of estimating an unknown target $f(x, y)$ from the partial and truncated information of its Fourier Transform (FT) $F(k_x, k_y)$. To focus our discussion on a general inversion method we present the relation between the FT of the observed signals and the 2D spatial FT of the scene by the following:

$$G(k_x, k_y) = M(k_x, k_y)F(k_x, k_y) + \epsilon(k_x, k_y) \quad (2.38)$$

where

$$F(k_x, k_y) = \iint f(x, y) \exp -j(k_x x + k_y y) \, dx \, dy. \quad (2.39)$$

where $\epsilon(k_x, k_y)$ is the observation noise from measure process, $k = \sqrt{k_x^2 + k_y^2} = 2\pi/\nu$ is the wave number, in the wavenumber domain, $F(k_x, k_y)$ is the FT of $f(x, y)$, $G(k_x, k_y)$ is of the FT the observed data and $M(k_x, k_y)$ is a binary valued function which is equal to one on the points where we have the data and zero elsewhere. In fact $M(k_x, k_y)$ is related to the radar frequency and measurement system geometries, illustrated in Figure 2.8.

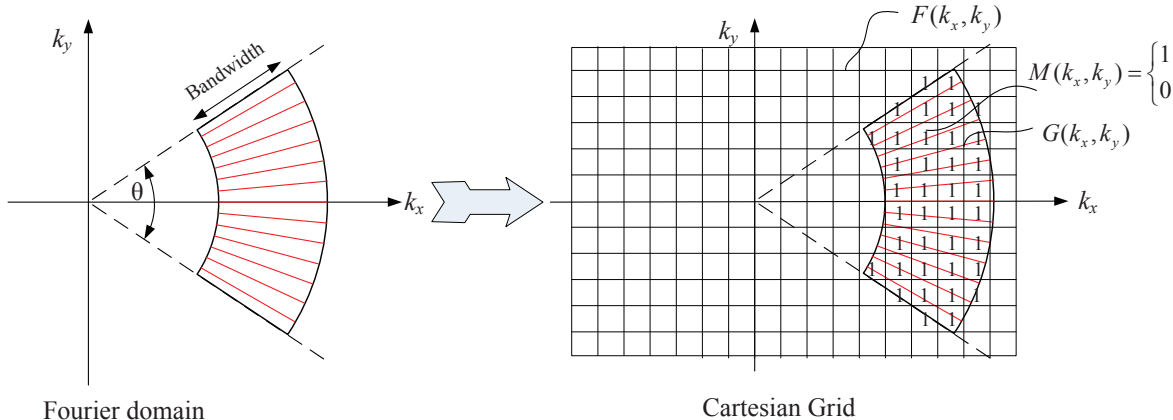


Figure 2.8: Fourier Synthesis formulation of SAR imaging.

2.7 General Forward Modeling

Real received signals are discrete version of the continuous signal $g(t, \theta_{tc}, \theta_{cr})$. $G(\omega, \theta_{tc}, \theta_{cr})$ is then computed using Discrete Fourier Transform (DFT) giving values of $F(k_x, k_y)$ and then $G(k_x, k_y)$ on a finite number of points in the Fourier domain. Arrange all these values in a vector \mathbf{g} . Discretize the space of the scene into pixels and arrange all the pixel values in a vector \mathbf{f} . Then, knowing that the relation between \mathbf{g} and \mathbf{f} is a DFT which is a linear operation, we can describe it through a matrix \mathbf{H} (DFT matrix).

Then, we can write

$$\mathbf{g} = \mathbf{H} \mathbf{f} + \boldsymbol{\epsilon} \quad (2.40)$$

where $\boldsymbol{\epsilon}$ represents additive observation noise [Sko70, Weh87, ÇKCn03]. The relation between 2D spectra $G(k_x, k_y)$ of the demodulated received signals and the 2D scattering coefficients of the unknown target $f(x, y)$ is a limited support of FT.

2.8 Conclusions

In this chapter, we first established forward models of SAR imaging. Several assumptions on radar scattering center theory were made. Based on these assumptions, radar echo modeling was derived. According to the projection-slice theorem, a tomographic SpotSAR model was discussed. In the following, the mathematical forward models were established for different SAR geometries. Thus, the SAR imaging is then an ill-posed inversion problem to estimate reflectivities from partial observation of the scattering field. Solving this kind of problem, we need to incorporate prior information to obtain an accurate estimation.

3

Inversion: from Data to Scene

3.1 Introduction

The objective of this chapter is to develop a Bayesian estimation approach based on the forward model which is established in Chapter 2.

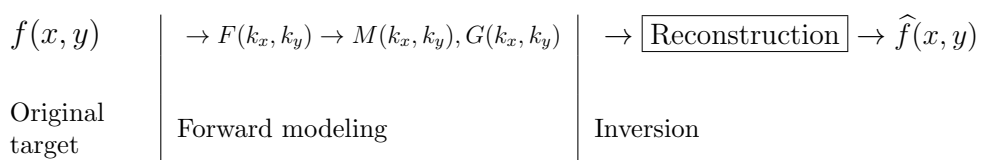
Upon the validity of the forward model, the inverse problem becomes to reconstruct the original target \mathbf{f} using the observed data \mathbf{g} . When this inversion is done, we can also compute $\widehat{\mathbf{g}} = \mathbf{H}\widehat{\mathbf{f}}$ which can be compared to the observed data and the difference $\|\Delta\mathbf{g}\|_2^2 = \|\mathbf{g} - \widehat{\mathbf{g}}\|_2^2$ can give us an indication about the goodness of the inversion. However, we must be careful that $\|\Delta\mathbf{g}\|_2^2$ is a necessary measure to the goodness of the inversion but not sufficient. In fact small value of $\|\Delta\mathbf{g}\|_2^2$ may not necessarily result in small value of $\|\Delta\mathbf{f}\|_2^2 = \|\mathbf{f} - \widehat{\mathbf{f}}\|_2^2$ due to the ill-posedness of the problem.

In 2D, we denote the data \mathbf{g} as $G(k_x, k_y)$ and $M(k_x, k_y)$, the estimation of the original target \mathbf{f} as $\widehat{f}(x, y)$ and $\widehat{G}(k_x, k_y)$ as the prediction of the data in the Fourier domain particularly on those points where we do not have any data.

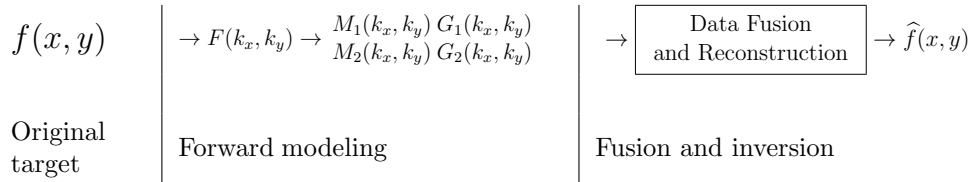
$$G(k_x, k_y), M(k_x, k_y) \longrightarrow \boxed{\text{Inversion}} \longrightarrow \widehat{f}(x, y) \longrightarrow \widehat{G}(k_x, k_y)$$

For different geometries of SAR, the mathematical model for forward modeling and inversion can be illustrated as the following:

- Mono-, or Bi-static SAR



- Multi-static SAR



For the simplest case as Mono- or Bi-static, the objective is to find an optimal reconstruction (will be studied in Chapter 4); while for a more complicated case as multi-static, the objective becomes data fusion for obtaining super-resolution images (will be studied in Chapter 5). In this chapter, we focus on the Bayesian approach.

The chapter is organized as follows:

Firstly, in Section 3.2, we give a brief introduction of the classical inversion methods for SAR imaging. Then, aiming at pushing further their limitations, we propose the Bayesian inference methods in Section 3.3. We present a detailed description of the Bayesian approach with different target prior modeling: simple and hierarchical priors. We also consider the hyperparameters estimation using either joint MAP (JMAP), the marginalization and the variational Bayesian approximation (VBA).

For the inference, in Section 3.4, first of all, we propose separable priors for scenes consisting of point sources and then Markovian priors for scenes consisting of homogeneous regions. For Gaussian prior and Sparse Gaussian prior, we consider the hyperparameters estimation in a marginalization framework. For Total Variation (TV) Markovian prior, we propose a hierarchical Bayesian estimation method.

3.2 Classical Inversion Methods

There are many inversion methods for inverse problems [Ger74, Jon86, CK01, MD06b, MD06a, MDDF09], such as analytical methods, parametric methods as least square and generalized inversion and regularization methods. For our case where the problem is to estimate an image from the partial knowledge of its Fourier domain, the oldest and also the simplest one is the Gerchberg-Papoulis iterative method [Ger74, Pap75, MBM08, PK08] which imposes some constraint on the solution (band limited) in an iterative way. However, when the data are too incomplete, the results depend strongly on the type of constraints (prior knowledge of the band and positivity). Even if, this method may work in some cases, in general, we may need to include more prior information on the solution to obtain a satisfactory result.

3.2.1 Analytical methods

One simple classical method for SAR imaging is to use the Inverse Fast Fourier Transform (IFFT) [Bri88, CS00]. The inversion is given as:

$$\hat{f}(x, y) = \text{IFFT}\{G(k_x, k_y)M(k_x, k_y)\} \quad (3.1)$$

the equation above turns to be

$$\hat{f}(x, y) = \text{IFFT}\{G(k_x, k_y)\} \quad (3.2)$$

if we could obtain $M(k_x, k_y) = 1$ in the full wavenumber domain on a cartesian grid.

Unfortunately, due to the limitation of the bandwidth and the integration angle, the Fourier domain is never complete and the inversion becomes an ill-posed problem. The classical IFFT methods assume all the unobserved data (the values of $G(k_x, k_y)$ on those points where $M(k_x, k_y) = 0$) to be zero. Through zero-filling extrapolation and interpolation to a rectangular Cartesian grid, FFT-based methods propose a classical solution.

As can been seen, the solution to the problem of $\mathbf{g} = \mathbf{H}\mathbf{f} + \boldsymbol{\epsilon}$ depends on the properties of the forward model \mathbf{H} . Indeed, in the forward model \mathbf{H} is an approximate 2D Fourier transform, denoting by \mathbf{H}^t the conjugate transpose of \mathbf{H} . The IFFT method is equivalent to:

$$\hat{\mathbf{f}} \approx \mathbf{H}^t \mathbf{g} \quad (3.3)$$

In the general case of a linear operation, the Least Square (LS) solution is given by

$$\hat{\mathbf{f}} = \arg \min_{\mathbf{f}} \|\mathbf{g} - \mathbf{H}\mathbf{f}\|_2^2 = (\mathbf{H}^t \mathbf{H})^{-1} \mathbf{H}^t \mathbf{g} \quad (3.4)$$

if $\mathbf{H}^t \mathbf{H}$ is invertible. In the complete data Fourier Synthesis case (column exponential basis of the system response function are orthogonal), the matrix \mathbf{H} is the FT matrix and we have $\mathbf{H}^t \mathbf{H} = \mathbf{I}$. This explains that the solution $\hat{\mathbf{f}} = \mathbf{H}^t \mathbf{g}$ would be exact for that case, but for the incomplete data situation $\mathbf{H}^t \mathbf{H} \neq \mathbf{I}$.

3.2.2 Regularization methods

Besides the analytical method [DJ02], regularization theory has been playing a very important role for solving inverse problems in SAR imaging [CK01]. Regularization method is based on the prior information of the unknown object, trying to “restore” the original information as much as possible.

One of the most successful regularization methods consists in minimizing of a compound criterion as [MD06b]:

$$\hat{\mathbf{f}} = \arg \min_{\mathbf{f}} \{J(\mathbf{f})\} \quad (3.5)$$

with

$$J(\mathbf{f}) = \Delta_1(\mathbf{g}, \mathbf{H}\mathbf{f}) + \lambda \Delta_2(\mathbf{f}, \mathbf{f}_0) \quad (3.6)$$

where Δ_1 and Δ_2 are two distances. Δ_1 is a measure of adequacy of the data \mathbf{g} to the output of the forward model $\mathbf{H}\mathbf{f}$, for example for LS $\Delta_1 = \|\mathbf{g} - \mathbf{H}\mathbf{f}\|_2^2$. Δ_2 is a

3.2.2 - Regularization methods

criterion to be chosen to translate some prior knowledge or to enforce some properties of the desired solution, for example the smoothness $\Delta_2 = \|\mathbf{D}\mathbf{f}\|_2^2$ where \mathbf{D} is a derivative operator.

Other choices are possible for both parts Δ_1 and Δ_2 . λ is a regularization parameter which has to be chosen in such a way to obtain a good balance between the two terms. \mathbf{f}_0 is the default solution.

A classical case is when Δ_1 and Δ_2 are both quadratic:

$$J(\mathbf{f}) = \|\mathbf{g} - \mathbf{H}\mathbf{f}\|_2^2 + \lambda\|\mathbf{f} - \mathbf{f}_0\|_2^2 \quad (3.7)$$

where we can have an analytic expression for the solution

$$\widehat{\mathbf{f}} = \mathbf{f}_0 + (\mathbf{H}^t \mathbf{H} + \lambda \mathbf{I})^{-1} \mathbf{H}^t (\mathbf{g} - \mathbf{H}\mathbf{f}_0) \quad (3.8)$$

When $\mathbf{f}_0 = 0$, then we have $\widehat{\mathbf{f}} = (\mathbf{H}^t \mathbf{H} + \lambda \mathbf{I})^{-1} \mathbf{H}^t \mathbf{g}$; and when $\lambda = 0$, we obtain the LS solution $\widehat{\mathbf{f}} = (\mathbf{H}^t \mathbf{H})^{-1} \mathbf{H}^t \mathbf{g}$ of Equation (3.4).

The main advantage of the regularized solution when $\lambda > 0$ is that $\mathbf{H}^t \mathbf{H} + \lambda \mathbf{I}$ will be always better conditioned than $\mathbf{H}^t \mathbf{H}$ and thus the regularized solution will be more stable.

There are many other distances and in particular l_1 for example

$$J(\mathbf{f}) = \|\mathbf{g} - \mathbf{H}\mathbf{f}\|_2^2 + \lambda\|\mathbf{f}\|_1 \quad (3.9)$$

but unfortunately in these cases there is no more analytic expression for the solution.

However, even in the case of quadratic criterion where we have analytical expression, in practical applications a gradient based algorithm is used to obtain the solution. The main steps of such a algorithm is given below:

1. $\mathbf{f}^{(0)} = 0$,
2. $\mathbf{f}^{(k+1)} = \mathbf{f}^{(k)} + \alpha^{(k)} \mathbf{d}^{(k)}$ until convergency,
where $\mathbf{d}^{(k)}$ may be any descent direction, for example the opposite of the gradient:
$$\mathbf{d}^{(k)} = 2\mathbf{H}^t(\mathbf{g} - \mathbf{H}\mathbf{f}^{(k)}) - 2\lambda\mathbf{f}^{(k)},$$
3. $\alpha^{(k)}$ is the step which can be constant or evaluated at each iteration.

There are many different methods to obtain satisfactory $\alpha^{(k)}$ which also insure the convergency of the algorithm [NW99, BT09, SMW05].

Regularization methods generally try to balance the fidelity to data and prior knowledge to obtain a stable solution. The main problems of regularization methods include: determination of the regularization parameter, the arguments of choosing two distances which are manually decided depending on personal experience and quantification of the uncertainties associated with the obtained solutions. In the next section, we will see these inadequacies can be overcome by the Bayesian estimation framework.

3.3 Bayesian Approach

3.3.1 Bayesian estimation

From an ideal point of view, the Bayesian framework is based on the forward model $\mathbf{g} = \mathbf{H}\mathbf{f} + \boldsymbol{\epsilon}$, where \mathbf{g} is the observed data. Due to not only the measurement noise but also the fact that the forward model is finitely exact and comprises uncertainty, we have to account for these uncertainties. This can be done through a probabilistic model $p(\mathbf{g}|\mathbf{f})$ which is also called the likelihood. The next step is to translate our incomplete prior knowledge on \mathbf{f} through a prior probability law $p(\mathbf{f})$.

From a methodological view, the Bayesian framework is based on the sum and product rule of the probability theory:

$$p(A, B) = p(A|B)p(B) = p(B|A)p(A) \quad (3.10)$$

So $p(A|B) = p(B|A)p(A)/p(B)$, where A is the assumption and B is the observed data under the assumption. If we assume that all the probability laws have probability densities, we have:

$$p(\mathbf{f}|\mathbf{g}) = p(\mathbf{g}|\mathbf{f})p(\mathbf{f})/p(\mathbf{g}) \quad (3.11)$$

where $p(\mathbf{g}) = \int p(\mathbf{g}|\mathbf{f})p(\mathbf{f}) d\mathbf{f}$

In classical statical methods, we only use $p(\mathbf{g}|\mathbf{f})$, for example the Maximum Likelihood (ML):

$$\widehat{\mathbf{f}}_{ML} = \arg \max_{\mathbf{f}} p(\mathbf{g}|\mathbf{f}) \quad (3.12)$$

In the Bayesian approach, the main step is the use of the prior $p(\mathbf{f})$ and the use of the posterior $p(\mathbf{f}|\mathbf{g})$. So it is important to assign $p(\mathbf{f})$ properly.

For this, we may make two important remarks [Fér06]:

- It is almost impossible that, in a real physical problem, we have no information about the observed target or the observation procedure.
- It is almost impossible that, in a real physical problem, the prior information of the target can be exactly represented by one certain probability distribution.

The first point shows that, in most problems, it is possible to decide for a family of prior laws for specific class of targets. The second point shows that we can not probably fix the parameters of this prior law *a priori*. However these parameters can be estimated either from a set of training targets or even *a posteriori* from the observed data.

The Bayesian estimation framework can be summarized as follows:

1. Prior modeling

Assign the prior probability distributions $p(\mathbf{g}|\mathbf{f})$ and $p(\mathbf{f})$ to translate our knowledge about the data \mathbf{g} given \mathbf{f} (forward model and the errors $\boldsymbol{\epsilon}$) and the unknown image \mathbf{f} .

2. Compute the posterior probability law

Once $p(\mathbf{g}|\mathbf{f})$ and $p(\mathbf{f})$ are assigned, we can use them through the Bayesian rule to find $p(\mathbf{f}|\mathbf{g})$

$$p(\mathbf{f}|\mathbf{g}) \propto p(\mathbf{g}|\mathbf{f})p(\mathbf{f}) \quad (3.13)$$

3.3.2 - Prior modeling

which contains all the information coming from the data via $p(\mathbf{g}|\mathbf{f})$ and from *a priori* $p(\mathbf{f})$.

3. Use this posterior probability law to infer the unknown \mathbf{f} .

To make the choice of the estimator, there are two simple options:

1. **Maximum A Posterior (MAP)**

For the Maximum A Posterior (MAP) estimation:

$$\begin{aligned}\hat{\mathbf{f}} &= \arg \max_{\mathbf{f}} \{p(\mathbf{f}|\mathbf{g})\} = \arg \min_{\mathbf{f}} \{J(\mathbf{f})\} \\ \text{where } J(\mathbf{f}) &= -\ln p(\mathbf{g}|\mathbf{f}) - \ln p(\mathbf{f})\end{aligned}\quad (3.14)$$

2. **Posterior Mean (PM)**

For the Posterior Mean (PM):

$$\hat{\mathbf{f}} = \int \mathbf{f} p(\mathbf{f}|\mathbf{g}) d\mathbf{f}. \quad (3.15)$$

The computation of the MAP solution needs an optimization algorithm and the PM solution needs an integration algorithm.

When the error term $\boldsymbol{\epsilon}$ is assumed to be centered, white, Gaussian with given variance σ_ϵ^2 :

$$p(\mathbf{g}|\mathbf{f}) \propto \exp \left\{ -\frac{1}{2\sigma_\epsilon^2} \|\mathbf{g} - \mathbf{H}\mathbf{f}\|_2^2 \right\} \quad (3.16)$$

From aforementioned analysis, we could see that within the Bayesian framework, three steps are very important:

1. Forward modeling of SAR imaging which describes the relation between the unknown scene \mathbf{f} and the measurement data \mathbf{g} via $p(\mathbf{g}|\mathbf{f})$ which is called likelihood;
2. Prior modeling $p(\mathbf{f})$ of the target scene depends on the way that we model the scene.
3. Computing the posterior $p(\mathbf{f}|\mathbf{g})$ and the choice of an estimator MAP or PM to obtain the reconstruction $\hat{\mathbf{f}}$.

In this thesis, we work on these three points, with the emphasis of prior modeling and computation. The objective of the former is to discover the effectiveness of different prior models of radar targets and the performances on Bayesian inversion, while the latter is to propose effective computation tools for complex prior models with hyperparameter estimation and hidden variables.

3.3.2 Prior modeling

As discussed above, the introduction of additional prior information or constraints on scattering coefficients \mathbf{f} could turn an ill-posed inverse problem to be regularized. Moreover, promising target prior modeling can not only suppress the noise thus reserve

target information, but also realize the local control on reconstruction, such as edge and/or texture preserving, which enhances the target features for recognition. Our work originated from this motivation, trying to find prior information taking account for different scattering characteristics and preserving desired features in imaging.

The key of the Bayesian inversion methods of SAR imaging is to design some prior distribution to model some prior information of scattering coefficients and to recover the scattering coefficients under the Bayesian principle. Sparsity and local continuity are considered as general characteristics in SAR imaging. In the following, we will model these prior information by choosing different probabilistic distributions.

1) Sparsity

Radar target at high frequencies can be treated as the composition of several scattering centers, which provides the possibility of SAR imaging via sparse prior representation. The back scattering of dominant scatterers is comparatively higher than others whose values are nearly zeros, i.e., the reflectivity field of the target $f(x, y)$ at few locations is of high value while at other majority locations is near zero. This means that the distribution of the values of $f(x, y)$ has a great peak near to zero while having heavy tails. The heavy tailed probability distributions can be used to describe radar target composed mainly by dominant scattering point reflectors.

2) Local continuity

For radar target scenes composed by extended reflectivity homogenous regions, the function $f(x, y)$ can be modeled by a piecewise smooth function. Markovian models provide appropriate tools for such a statistic description of an image. By using Markovian models and their variants, we impose smoothness on the magnitudes of the reconstructed complex-valued field reflectivities \mathbf{f} and preserve edge as well.

Based on the analysis of composition about two typical radar target scenes, here we propose three different prior models:

1) Separable Generalized Gaussian (SGG)

$$p(\mathbf{f}) \propto \exp \left\{ -\gamma \sum_j |f_j|^\beta \right\} \propto \exp \left\{ -\gamma \|\mathbf{f}\|_\beta^\beta \right\} \quad (3.17)$$

where $1 \leq \beta \leq 2$ and $|f_j|$ is the magnitude (or absolute value) of the complex value f_j , $\|\mathbf{f}\|_\beta^\beta = \sum_j |f_j|^\beta$. By using this prior, the MAP criterion to be optimized becomes

$$J(\mathbf{f}) = \frac{1}{\sigma_e^2} \|\mathbf{g} - \mathbf{Hf}\|_2^2 + \gamma \sum_j |f_j|^\beta \quad (3.18)$$

SGG family actually includes Laplace distribution when $\beta = 1$, Gaussian distribution when $\beta = 2$ and when $1 \leq \beta < 2$, it can be used for representing sparse signals or images. One can also use $0 < \beta \leq 1$ but in this case the criterion is no more convex.

Hence, this prior is appropriate to targets composed of point scatter models (such as the small size metallic reflectors). When there are amount of reflectors in the observed scene, β could be taken nearly to be 2; by contrast, when there are only few reflectors,

3.3.2 - Prior modeling

β should be adjusted closely to 1 but always > 1 to have a strict convex criterion.

2) Separable Cauchy (SC)

$$p(\mathbf{f}) \propto \prod_j \frac{\gamma}{\sqrt{1 + |f_j|^2}} \propto \exp \left\{ -\frac{\gamma}{2} \sum_j \ln(1 + |f_j|^2) \right\} \quad (3.19)$$

Employing this prior, we get:

$$J(\mathbf{f}) = \frac{1}{\sigma_\epsilon^2} \|\mathbf{g} - \mathbf{H}\mathbf{f}\|_2^2 + \gamma \sum_j \ln(1 + |f_j|^2) \quad (3.20)$$

Cauchy distribution has also been used for sparse signals, due to its longer tails than the Gaussian.

Thus this prior could also be used for point targets, in particular for modeling those reflectors of high amplitudes.

3) Generalized Gauss Markov (GGM)

$$p(\mathbf{f}) \propto \exp \left\{ -\gamma_1 \sum_j |f_j|^{\beta_1} - \gamma_2 \sum_j ||f_j| - |f_{j-1}||^{\beta_2} \right\} \quad (3.21)$$

where $1 \leq \beta_1, \beta_2 \leq 2$. By using this prior, we have:

$$J(\mathbf{f}) = \frac{1}{\sigma_\epsilon^2} \|\mathbf{g} - \mathbf{H}\mathbf{f}\|_2^2 + \gamma_1 \|\mathbf{f}\|_{\beta_1}^{\beta_1} + \gamma_2 \|\mathbf{D}|\mathbf{f}|^{\beta_2}\|_{\beta_2}^{\beta_2} \quad (3.22)$$

where $Q(\mathbf{f}) = \|\mathbf{g} - \mathbf{H}\mathbf{f}\|_2^2$ again represents the LS criterion, and $\mathbf{D} = \text{Toeplitz}([-1, 1])$ is the first order discrete derivative matrix which is a Toeplitz matrix. We may remark that $\gamma_1 = 0$ and $\beta_1, \beta_2 = 2$ result in the classical Tikhonov regularization term $\Omega(\mathbf{f}) = \|\mathbf{D}|\mathbf{f}|^2\|_2^2$.

Herein, this prior is proper to those targets having comparatively large sizes or composed by homogeneous regions.

4) Generalized Markov (GM)

$$p(\|\mathbf{f}\|) \propto \exp \left\{ -\gamma \sum_j \phi(|f_j| - |f_{j-1}|) \right\} \quad (3.23)$$

where $\phi(\cdot)$ is a positive function which represents the potential function of Markov field, which can be chosen, for example, between the following possibilities:

$$\phi(t) = \{t^2, |t|^\beta, \ln(1 - |t|^2)\} \quad (3.24)$$

and many other convex or non convex functions. With these priors, we obtain:

$$J(\mathbf{f}) = \frac{1}{\sigma_\epsilon^2} \|\mathbf{g} - \mathbf{H}\mathbf{f}\|_2^2 + \gamma \sum_j \phi(|f_j| - |f_{j-1}|). \quad (3.25)$$

This prior is proper to those targets having comparatively large sizes or composed by homogeneous regions.

3.3.3 Hyperparameters estimation

To obtain $p(\mathbf{f}|\mathbf{g})$, the probability laws $p(\mathbf{g}|\mathbf{f})$ and $p(\mathbf{f})$ are needed. But these probability laws depend on some parameters which may not be known *a priori*. We may want to estimate them too from the data. For this we may also assign a prior $p(\boldsymbol{\theta})$ to translate our prior knowledge about them and then obtain the expression of the joint posterior law:

$$p(\mathbf{f}, \boldsymbol{\theta} | \mathbf{g}) = \frac{p(\mathbf{g} | \mathbf{f}, \boldsymbol{\theta}_1) p(\mathbf{f} | \boldsymbol{\theta}_2) p(\boldsymbol{\theta})}{p(\mathbf{g})} \quad (3.26)$$

where $\boldsymbol{\theta} = (\boldsymbol{\theta}_1, \boldsymbol{\theta}_2)$ is the hyperparameters depending on different situations:

- $\boldsymbol{\theta}_1 = \sigma_\epsilon^2$ is the variance of the noise in Equation (3.16),
- $\boldsymbol{\theta}_2 = \gamma$ is for example the parameter of the prior in Equation (5.10), Equation (3.19) or Equation (3.23),
- $\boldsymbol{\theta}_2 = (\gamma_1, \gamma_2)$ in the prior in Equation (3.21).

The problem of hyperparameter estimation along with the estimation of the unknown \mathbf{f} is addressed by many researchers [IG93, Idi01, MD09b, MD09a]. Mainly three great families of methods exist:

1. Joint MAP

Given the expression of $p(\mathbf{f}, \boldsymbol{\theta} | \mathbf{g})$, we may try to define the Joint MAP (JMAP) solution:

$$\begin{aligned} (\hat{\mathbf{f}}, \hat{\boldsymbol{\theta}}) &= \arg \max_{(\mathbf{f}, \boldsymbol{\theta})} \{p(\mathbf{f}, \boldsymbol{\theta} | \mathbf{g})\} = \arg \min_{(\mathbf{f}, \boldsymbol{\theta})} \{-\ln p(\mathbf{f}, \boldsymbol{\theta} | \mathbf{g})\} \\ &= \arg \min_{(\mathbf{f}, \boldsymbol{\theta})} \{-\ln p(\mathbf{g} | \mathbf{f}, \boldsymbol{\theta}_1) - \ln p(\mathbf{f} | \boldsymbol{\theta}_2) - \ln p(\boldsymbol{\theta})\} \end{aligned} \quad (3.27)$$

The existence of a unique maximum and the unimodality of the $p(\mathbf{f}, \boldsymbol{\theta} | \mathbf{g})$ has to be verified by appropriate choice of the priors $p(\boldsymbol{\theta}_1)$ and $p(\boldsymbol{\theta}_2)$.

However, the joint optimization may not always be easy to realize. Then, in general, one can use an iterative alternate optimization algorithm as follows:

$$\left\{ \begin{array}{l} \hat{\mathbf{f}}^{(k+1)} = \arg \min_{\boldsymbol{\theta}} \{-\ln p(\mathbf{f}, \boldsymbol{\theta}^{(k)} | \mathbf{g})\} \\ \hat{\boldsymbol{\theta}}^{(k+1)} = \arg \min_{\boldsymbol{\theta}} \{-\ln p(\hat{\mathbf{f}}^{(k+1)}, \boldsymbol{\theta} | \mathbf{g})\} \end{array} \right. \quad (3.28)$$

Concerning the expression of $p(\boldsymbol{\theta}) = p(\boldsymbol{\theta}_1)p(\boldsymbol{\theta}_2)$, we use the conjugate priors when possible, for example Inverse Gamma for the variances σ_ϵ^2 .

2. Marginalization

3.3.3 - Hyperparameters estimation

Bayesian framework provides the possibility to compute the marginal posterior laws of $\boldsymbol{\theta}$ by first writing the expression of $p(\mathbf{f}, \boldsymbol{\theta}|\mathbf{g})$, then integrating \mathbf{f} to obtain $p(\boldsymbol{\theta}|\mathbf{g})$,

$$p(\boldsymbol{\theta}|\mathbf{g}) = \int p(\mathbf{f}, \boldsymbol{\theta}|\mathbf{g}) \, d\mathbf{f} \quad (3.29)$$

and then obtain $\hat{\boldsymbol{\theta}}$ first and use them for the computation of the linear parts \mathbf{f} using $p(\mathbf{f}|\mathbf{g}, \hat{\boldsymbol{\theta}})$. We may mention for example:

$$\hat{\boldsymbol{\theta}} = \arg \max_{\boldsymbol{\theta}} p(\boldsymbol{\theta}|\mathbf{g}) \longrightarrow \hat{\mathbf{f}} = \arg \max_{\mathbf{f}} p(\mathbf{f}|\mathbf{g}, \hat{\boldsymbol{\theta}}) \quad (3.30)$$

We may note that

$$p(\boldsymbol{\theta}|\mathbf{g}) \propto p(\mathbf{g}|\boldsymbol{\theta})p(\boldsymbol{\theta}), \quad (3.31)$$

where

$$p(\mathbf{g}|\boldsymbol{\theta}) = \int p(\mathbf{g}|\mathbf{f}, \boldsymbol{\theta}_1) p(\mathbf{f}|\boldsymbol{\theta}_2) \, d\mathbf{f} \quad (3.32)$$

and where $p(\mathbf{g}|\boldsymbol{\theta})$ is the classical likelihood or the evidence of the model. The classical ML method for estimating $\boldsymbol{\theta}$ is

$$\hat{\boldsymbol{\theta}}_{ML} = \arg \max_{\boldsymbol{\theta}} p(\mathbf{g}|\boldsymbol{\theta}). \quad (3.33)$$

The following scheme $\hat{\boldsymbol{\theta}}_{ML} = \arg \max_{\boldsymbol{\theta}} p(\mathbf{g}|\boldsymbol{\theta}) \longrightarrow \hat{\mathbf{f}} = \arg \max_{\mathbf{f}} p(\mathbf{f}|\mathbf{g}, \hat{\boldsymbol{\theta}}_{ML})$ is used classically and called *Type II likelihood method* [Bis06]. Unfortunately, getting an analytical expression for $p(\mathbf{g}|\boldsymbol{\theta})$ is not always possible. This fact has conducted many researchers to propose the algorithms such as Expectation Maximization (EM) or stochastic versions of it (SEM) to obtain the $\hat{\boldsymbol{\theta}}_{MV}$. The same kind of algorithms have also been used to obtain $\boldsymbol{\theta}$ in Equation (3.30).

3. Variational Bayesian Approximations (VBA)

We may do better than JMAP than using $p(\mathbf{f}, \boldsymbol{\theta}|\mathbf{g})$. However, the full Bayesian inference using this joint posterior law is usually intractable and an approximation method is required. Variational Bayesian Approximation (VBA) approximates this joint posterior law by a separable one $q(\mathbf{f}, \boldsymbol{\theta}|\mathbf{g}) = q_1(\mathbf{f})q_2(\boldsymbol{\theta})$ using the Kullback-Leibler divergence as the criterion and then use $q_1(\mathbf{f})$ and $q_2(\boldsymbol{\theta})$ to make inference about \mathbf{f} and $\boldsymbol{\theta}$, separately.

In our case, the joint posterior law of all the unknowns $p(\mathbf{f}, \boldsymbol{\theta})$ (the unknown target, hidden variables and hyperparameters) is approximated by a separable probability law via the variational Bayesian principle. It involves in finding a distribution $q(\mathbf{f}, \boldsymbol{\theta}) = q_1(\mathbf{f})q_2(\boldsymbol{\theta})$ which is computed flexibly but approximate to the true posterior distribution. It is achieved by minimizing the Kullback-Leibler divergence between the $q(\mathbf{f}, \boldsymbol{\theta})$ and the $p(\mathbf{f}, \boldsymbol{\theta}|\mathbf{g})$ [Bis06],

$$\text{KL}(q(\mathbf{f}, \boldsymbol{\theta})||p(\mathbf{f}, \boldsymbol{\theta}|\mathbf{g})) = \iint q(\mathbf{f}, \boldsymbol{\theta}) \log \frac{q(\mathbf{f}, \boldsymbol{\theta})}{p(\mathbf{f}, \boldsymbol{\theta}|\mathbf{g})} \, d\mathbf{f} \, d\boldsymbol{\theta} \quad (3.34)$$

It can be showed that

$$\text{KL}(q_1, q_2||p) = <\ln q_1>_{q_1} + <\ln q_2>_{q_2} - <\ln p>_{q_1} - <\ln p>_{q_2} \quad (3.35)$$

where $\langle \cdot \rangle_q$ means the expected value with respect to q .

Unfortunately, the solution can not be obtained in a direct way but can be obtained by an alternative optimization:

$$\begin{aligned} q_1 &\propto \exp(-\langle \ln p(\mathbf{f}, \boldsymbol{\theta} | \mathbf{g}) \rangle_{q_2}) \\ q_2 &\propto \exp(-\langle \ln p(\mathbf{f}, \boldsymbol{\theta} | \mathbf{g}) \rangle_{q_1}) \end{aligned} \quad (3.36)$$

The expressions and computations becomes much easier when $p(\mathbf{f}, \boldsymbol{\theta} | \mathbf{g})$ is chosen to be in an exponential family with conjugate priors [MD12].

In general then, we obtain an iterative algorithm, where at each iteration, the parameters of q_1 and q_2 are updated. Finally, when the final expressions of $q_1(\mathbf{f})$ and $q_2(\boldsymbol{\theta})$ are obtained, we can use them to obtain estimates for \mathbf{f} and $\boldsymbol{\theta}$.

3.3.4 Summary of Bayesian computation

For different prior models, we summarize the Bayesian computation as following:

1. Simple optimization of $p(\mathbf{f} | \boldsymbol{\theta}, \mathbf{g})$ for MAP when $\boldsymbol{\theta}$ is assumed to be known or has been determined before, is illustrated in Figure 3.1;

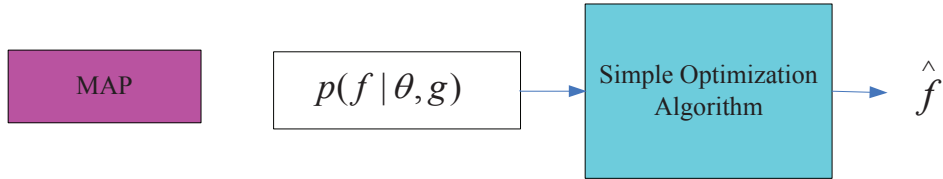


Figure 3.1: MAP computation.

2. Joint optimization of $p(\mathbf{f}, \boldsymbol{\theta} | \mathbf{g})$ for joint MAP when the estimation of hyperparameters are needed (unsupervised techniques), is illustrated in Figure 3.2;

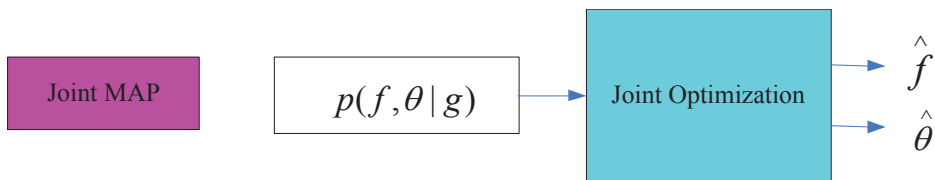


Figure 3.2: Joint MAP computation.

3. Marginalization of $p(\mathbf{f}, \boldsymbol{\theta} | \mathbf{g})$ with respect to \mathbf{f} to obtain $p(\boldsymbol{\theta} | \mathbf{g})$ and then its optimization to obtain $\hat{\boldsymbol{\theta}}$ and finally its utilization in the expression of $p(\mathbf{f}, \hat{\boldsymbol{\theta}} | \mathbf{g})$ or $p(\mathbf{f} | \hat{\boldsymbol{\theta}}, \mathbf{g})$ to obtain $\hat{\mathbf{f}}$, is illustrated in Figure 3.3;
4. Variational Bayesian approximation (VBA) of the joint $p(\mathbf{f}, \boldsymbol{\theta} | \mathbf{g})$ by a separable $q(\mathbf{f}, \boldsymbol{\theta} | \mathbf{g}) = q_1(\mathbf{f}) q_2(\boldsymbol{\theta})$, and then using them for estimation, is illustrated in Figure 3.4;

3.4.1 - Simple priors with MAP estimation

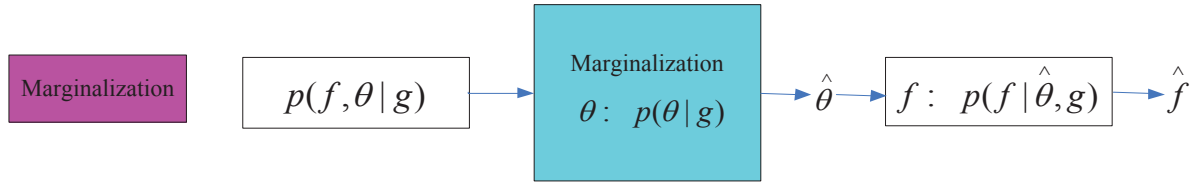


Figure 3.3: Marginalization computation.

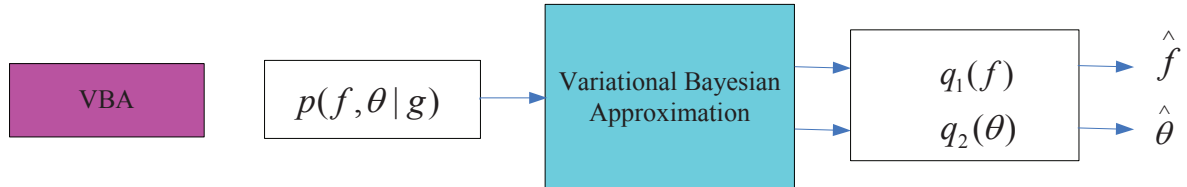


Figure 3.4: VBA computation.

3.4 Inference with Different Priors

3.4.1 Simple priors with MAP estimation

The Bayesian framework permits us a flexible framework by incorporating different priors. We firstly consider three prior models which are defined in section 3.3.2 and make a brief discussion of the estimation for each prior model.

1. Separable Generalized Gaussian (SGG)

$$p(\mathbf{f}) \propto \exp\left\{-\gamma \sum_j |f_j|^\beta\right\} \quad (3.37)$$

with $1 \leq \beta \leq 2$. $\beta = 2$ corresponds to the Gaussian model while $\beta = 1$ is the classic l_1 sparse model.

When considering Gaussian priors ($\beta = 2$), the posterior law becomes Gaussian too and all the estimators (MAP and PM) become the same and $\|\mathbf{f}\|_2^2 = \mathbf{f}^t \mathbf{f}$, where $(\cdot)^*$ is the conjugate transpose and $|f_j|^2 = f_j^* f_j$, f_j^* denotes the conjugate of complex value f_j . We can then have exact expression of the posterior:

$$p(\mathbf{f} | \mathbf{g}) = \mathcal{N}(\hat{\mathbf{f}}, \hat{\Sigma}) \quad (3.38)$$

where $\hat{\Sigma} = (\mathbf{H}^t \mathbf{H} + \lambda \mathbf{I})^{-1}$ with $\lambda = \gamma \sigma_\epsilon^2$
and where

$$\hat{\mathbf{f}} = \arg \max_{\mathbf{f}} p(\mathbf{f} | \mathbf{g}) = \arg \max_{\mathbf{f}} J(\mathbf{f}) \quad (3.39)$$

$$\hat{\mathbf{f}} = (\mathbf{H}^t \mathbf{H} + \lambda \mathbf{I})^{-1} \mathbf{H}^t \mathbf{g} = \frac{1}{\sigma_\epsilon^2} \hat{\Sigma} \mathbf{H}^t, \quad \text{with } \hat{\Sigma} = \sigma_\epsilon^2 (\mathbf{H}^t \mathbf{H} + \lambda \mathbf{I})^{-1} \quad (3.40)$$

If we can compute $\widehat{\Sigma}$, then we can use it as a measure of remaining uncertainty. For example, we can use the diagonal elements of $\widehat{\delta}_j = \widehat{\Sigma}_{jj}$ to put error based on the solution $\widehat{\mathbf{f}}$. However in practical application these computations may become too expensive.

When considering $0 < \beta \leq 1$, the term $\|\mathbf{f}\|_\beta^\beta$ is non continuous, the objective function with respect to \mathbf{f}

$$\begin{aligned} J(\mathbf{f}) &= \|\mathbf{g} - \mathbf{H}\mathbf{f}\|_2^2 + \lambda \sum_j |f_j|^\beta \\ &\approx \|\mathbf{g} - \mathbf{H}\mathbf{f}\|_2^2 + \lambda \sum_j (|f_j|^2 + \zeta)^{\beta/2} \end{aligned} \quad (3.41)$$

where the value of ζ is a small value, saying 10^{-10} . We adopt the gradient descent to optimize Equation (3.41) with respect to \mathbf{f} , the gradient is

$$\nabla J = 2\mathbf{H}^t \mathbf{H}\mathbf{f} - 2\mathbf{H}^t \mathbf{g} + \lambda\beta\Lambda(\mathbf{f})\mathbf{f} \quad (3.42)$$

where

$$\Lambda(\mathbf{f}) = \text{diag}[(|f_j|^2 + \zeta)^{\beta/2-1}] \quad (3.43)$$

The computation process is listed in Algorithm 1.

Algorithm 1 Reconstruction with Generalized Gaussian distribution

Input: \mathbf{g} , the maximum number iterations N_{iter}

Output: the reconstructed image $\widehat{\mathbf{f}}$, λ .

- 1: Initialize $\mathbf{f}^{(0)}$ by IFFT method
 - 2: **for** $k = 1$ to N_{iter} **do**
 - 3: $\widehat{\mathbf{f}}^{(k)} = \arg \min_{\mathbf{f}} J(\mathbf{f}, \Lambda(\mathbf{f}^{(k-1)}))$
 - 4: $\Lambda(\mathbf{f}^{(k)}) = \text{diag}[(|f_j^{k-1}|^2 + \zeta)^{\beta/2-1}]$
 - 5: **if** $\|\widehat{\mathbf{f}}^{(k)} - \widehat{\mathbf{f}}^{(k-1)}\|_2^2 / \|\widehat{\mathbf{f}}^{(k-1)}\|_2^2 \leq \varepsilon$ **then**
 - 6: Break;
 - 7: **end if**
 - 8: **end for**
-

2. Separable Cauchy (SC)

$$p(\mathbf{f}) \propto \prod_j \frac{\gamma}{\sqrt{1 + |f_j|^2}} \propto \exp\left\{-\frac{\gamma}{2} \sum_j \ln(1 + |f_j|^2)\right\} \quad (3.44)$$

For SC prior, there is no known exact expression for the posterior law. However the MAP solution can still be computed by appropriate optimization algorithm. In this case, we must be careful about the convergency of the gradient based optimization algorithms.

3.4.2 - Gaussian prior with hyperparameters estimation

3. Generalized Gauss-Markov (GGM)

$$p(\mathbf{f}) \propto \exp\left\{-\gamma_1 \sum_j |f_j|^{\beta_1} - \gamma_2 \sum_j ||f_j| - |f_{j-1}||^{\beta_2}\right\} \quad (3.45)$$

If $1 < \beta_1, \beta_2 \leq 2$, then the criterion is convex and we can again use gradient based methods. A special attention has to be paid to the values of γ_1 , γ_2 , β_1 and β_2 . Their proper choice is not an easy task. In general we fix $\beta_1 = \beta_2 = 1.1$, then γ_1 and γ_2 can be determined either by cross validation or in a Bayesian framework by assigning to them inverse Gamma priors.

3.4.2 Gaussian prior with hyperparameters estimation

We consider the case for exploring the hyperparameters estimation and begin with considering a simple Gaussian prior model. The case of linear models and Gaussian priors is interesting because many steps of the Bayesian computation can be done analytically.

$$p(\mathbf{f}|\sigma_f^2) = \mathcal{N}(\mathbf{f}|0, \sigma_f^2 \mathbf{I}) \quad (3.46)$$

which allows us easily computing the posterior probability $p(\mathbf{f}|\mathbf{g})$ and the evidence of model $p(\mathbf{g}|\boldsymbol{\theta})$. Combining with the Gaussian likelihood

$$p(\mathbf{g}|\mathbf{f}, \sigma_\epsilon^2) = \mathcal{N}(\mathbf{g}|\mathbf{H}\mathbf{f}, \sigma_\epsilon^2 \mathbf{I}) \quad (3.47)$$

gives the posterior probability of \mathbf{f}

$$p(\mathbf{f}|\mathbf{g}, \sigma_\epsilon^2, \sigma_f^2) = \mathcal{N}(\mathbf{f}|\hat{\boldsymbol{\mu}}_f, \hat{\Sigma}_f) \quad (3.48)$$

with

$$\hat{\boldsymbol{\mu}}_f = \sigma_\epsilon^{-2} \hat{\Sigma}_f \mathbf{H}^t \mathbf{g} \quad (3.49)$$

$$\hat{\Sigma}_f = (\sigma_\epsilon^{-2} \mathbf{I} + \sigma_\epsilon^{-2} \mathbf{H}^t \mathbf{H})^{-1} \quad (3.50)$$

It is noteworthy that $\sigma_\epsilon^2/\sigma_f^2$ can be interpreted as the regularization parameter λ in the regularization model Equation 3.7. But there is a big difference of Bayesian and regularization parameters: a fully Bayesian treatment of the model is capable of automatic determination of these parameters $\sigma_\epsilon^2, \sigma_f^2$. For this we can assign them Inverse Gamma priors and try to estimate them either jointly with \mathbf{f} or first estimate them using the ML and then use them for the inversion step.

The evidence of the model in such a simple case is

$$p(\mathbf{g}|\sigma_\epsilon^2, \sigma_f^2) = \left(\frac{1}{2\pi\sigma_\epsilon^2}\right)^{\frac{M}{2}} \left(\frac{1}{\sigma_f^2}\right)^{\frac{N}{2}} |\sigma_f^{-2} \mathbf{I} + \sigma_\epsilon^{-2} \mathbf{H}^t \mathbf{H}|^{-\frac{1}{2}} \exp\left\{-\frac{\|\mathbf{g} - \mathbf{H}\boldsymbol{\mu}_f\|_2^2}{2\sigma_\epsilon^2} - \frac{\|\boldsymbol{\mu}_f\|_2^2}{2\sigma_f^2}\right\} \quad (3.51)$$

Taking the logarithms of evidence of the model yields the log-marginal likelihood

$$\begin{aligned} \ln p(\mathbf{g}|\sigma_\epsilon^2, \sigma_f^2) &= -\frac{N}{2} \ln \sigma_f^2 - \frac{M}{2} \ln \sigma_\epsilon^2 \\ &\quad - \frac{1}{2\sigma_\epsilon^2} \|\mathbf{g} - \mathbf{H}\boldsymbol{\mu}_f\|_2^2 - \frac{1}{2\sigma_f^2} \boldsymbol{\mu}_f^t \boldsymbol{\mu}_f - \frac{1}{2} \ln |\sigma_f^{-2} \mathbf{I} + \sigma_\epsilon^{-2} \mathbf{H}^t \mathbf{H}| - \frac{N}{2} \ln(2\pi) \end{aligned} \quad (3.52)$$

Denoted by γ_i the N greatest eigenvalues of the matrix $\sigma_\epsilon^{-2} \mathbf{H}^t \mathbf{H}$, the Equation (3.52) can be well approximated by [Tip01, ZMDLM11]:

$$\begin{aligned}\ln p(\mathbf{g} | \sigma_\epsilon^2, \sigma_f^2) = & -\frac{N}{2} \ln \sigma_f^2 - \frac{M}{2} \ln \sigma_\epsilon^2 \\ & - \frac{1}{2\sigma_\epsilon^2} \|\mathbf{g} - \mathbf{H}\boldsymbol{\mu}_f\|_2^2 - \frac{1}{2\sigma_f^2} \boldsymbol{\mu}_f^t \boldsymbol{\mu}_f - \frac{1}{2} \sum_{i=1}^M \ln(\sigma_f^{-2} + \gamma_i) - \frac{N}{2} \ln(2\pi)\end{aligned}\quad (3.53)$$

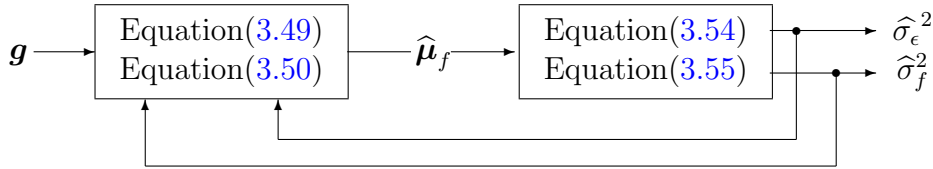
Setting the derivatives of the marginal likelihood with respect to $\sigma_\epsilon^2, \sigma_f^2$ to zeros gives

$$\sigma_\epsilon^2 = \frac{\|\mathbf{g} - \mathbf{H}\boldsymbol{\mu}_f\|_2^2}{N - \gamma} \quad (3.54)$$

$$\sigma_f^2 = \frac{\boldsymbol{\mu}_f^t \boldsymbol{\mu}_f}{\gamma} \quad (3.55)$$

with $\gamma = \sum_{i=1}^N \frac{\gamma_i}{\gamma_i + \sigma_f^{-2}}$. Note the estimations of $\sigma_\epsilon^2, \sigma_f^2$ depend on the estimation $\boldsymbol{\mu}_f$ of \mathbf{f} which itself depends on $\sigma_\epsilon^2, \sigma_f^2$. Herein we adopt an iterative procedural that estimates \mathbf{f} given by Equation 3.49 holding the $\sigma_\epsilon^2, \sigma_f^2$ fixed and then finds $\sigma_\epsilon^2, \sigma_f^2$ by fixing $\boldsymbol{\mu}_f$. This process is repeated until convergence.

This scheme is summarized as following:



The main computational cost in this approach is the computation of N greatest eigenvalues of the matrix $\sigma_\epsilon^2 \mathbf{H}^t \mathbf{H}$. For some particular case of the inverse problems we can use the structure of $\mathbf{H}^t \mathbf{H}$ to obtain this computation fast.

3.4.3 Sparse Gaussian prior with hyperparameters estimation

We also propose a sparse Gaussian prior as the one used usually in the Sparse Bayesian Learning (SBL) framework [Tip01], which is

$$p(\mathbf{f} | \Sigma) = \prod_{j=1}^N \mathcal{N}(f_j | 0, \sigma_j^2) \quad (3.56)$$

with $\Sigma = \text{diag}(\sigma_1^2, \dots, \sigma_M^2)$, which gives the possibility to account for some non-stationarity in the image by having different variances σ_j^2 for each pixel.

Similar to the derivation of the simple case of Gaussian prior, the posterior probability of \mathbf{f} is

$$p(\mathbf{f} | \mathbf{g}, \sigma_\epsilon^2, \Sigma) = \mathcal{N}(\mathbf{f} | \hat{\boldsymbol{\mu}}_f, \hat{\Sigma}_f) \quad (3.57)$$

3.4.4 - Total Variation (TV) prior and hierachial Bayesian estimation

with

$$\hat{\boldsymbol{\mu}}_f = \sigma_\epsilon^{-2} \hat{\boldsymbol{\Sigma}}_f \mathbf{H}^t \mathbf{g} \quad (3.58)$$

$$\hat{\boldsymbol{\Sigma}}_f = (\mathbf{A} + \sigma_\epsilon^{-2} \mathbf{H}^t \mathbf{H})^{-1} \quad (3.59)$$

with $\mathbf{A} = \boldsymbol{\Sigma}^{-1} = \text{diag}(\sigma_1^{-2}, \dots, \sigma_N^{-2})$. The evidence of the model is

$$p(\mathbf{g} | \sigma_\epsilon^2, \boldsymbol{\Sigma}) = (2\pi)^{-M/2} |\sigma_\epsilon^2 + \mathbf{H} \mathbf{A}^{-1} \mathbf{H}|^{-1/2} \exp\left\{-\frac{1}{2} \mathbf{g}^t (\sigma_\epsilon^2 + \mathbf{H} \mathbf{A}^{-1} \mathbf{H})^{-1} \mathbf{g}\right\} \quad (3.60)$$

Maximizing this evidence of the model gives the estimation of σ_ϵ^2 and $\boldsymbol{\Sigma}_i^2$

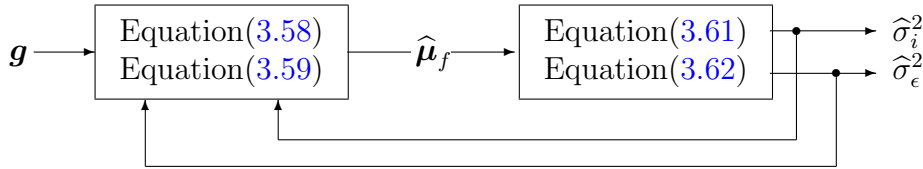
$$\sigma_i^2 = \frac{|\mu_i|^2}{\gamma_i}, i = 1, 2, \dots, N \quad (3.61)$$

$$\sigma_\epsilon^2 = \frac{\|\mathbf{g} - \mathbf{H} \hat{\boldsymbol{\mu}}_f\|_2^2}{N - \sum_i \gamma_i} \quad (3.62)$$

with

$$\gamma_i = 1 - (\hat{\boldsymbol{\Sigma}}_f^{-1})_{ii} / \sigma_i^2. \quad (3.63)$$

This scheme is summarized as following:



Here the main computational cost is also the computation of γ_i in Equation (3.63) which has to be done at each iteration.

3.4.4 Total Variation (TV) prior and hierachial Bayesian estimation

In this section, We consider a special case of Generalized Gauss Markov distribution with $\beta_1 = 0$ and $\beta_2 = 1$, which is so-called Total Variation (TV) prior. The Total-Variation-based method pioneered by Rudin *et al.* [ROF92] has been widely used in real-value image reconstruction and denoising, *etc.* [BMK08, CEPY05, DTR10] and achieved good performance. Intrinsically, TV is the l_1 norm of derivatives with replacement of l_2 norm and has been proved more appropriate for image reconstruction. It can preserve the edges while enhance the smoothness of the region. In the point of view of Markov Random Field (MRF), TV prior is a special case of the more general MRF. We extend the classic TV prior to the MRF model being not limited to the first-order derivatives.

In this section, we consider the Bayesian approach with TV prior. Again assuming the noise to be Gaussian, we have:

$$p(\mathbf{g} | \mathbf{f}, \beta) \propto \beta^{M/2} \exp\left(-\frac{\beta}{2} \|\mathbf{g} - \mathbf{H} \mathbf{f}\|_2^2\right) \quad (3.64)$$

Here, we consider a TV prior for \mathbf{f} for its capability of strengthening the smoothness of the region and preserve the edge. This prior has been widely used in the community of image processing and computer vision but not much attention in the community of SAR. Similar to [BMK08], the revised TV prior adapted to SAR image reconstruction:

$$p(\mathbf{f}) \propto \alpha^{N/2} \exp\left\{-\frac{\alpha}{2} \text{TV}(\mathbf{f})\right\} \quad (3.65)$$

where the TV prior is given by

$$\text{TV}(\mathbf{f}) = \sum_j \sqrt{\Delta_j^h(\mathbf{f}) + \Delta_j^v(\mathbf{f})} \quad (3.66)$$

where $\Delta_j^h(\mathbf{f})$, and $\Delta_j^v(\mathbf{f})$ are the horizontal and vertical first order differentiate operators, respectively.

$$\begin{aligned}\Delta_i^h(\mathbf{f}) &= ||f_i| - |f_{l_i}|| \\ \Delta_i^v(\mathbf{f}) &= ||f_i| - |f_{a_i}||\end{aligned}$$

We can further rewrite it as

$$\begin{aligned}p(\mathbf{f}) &\propto \alpha^{N/2} \exp\left(-\frac{\alpha}{2} \sum_i (|f_i| - |f_{j-1}|)^2\right) \\ &= \alpha^{N/2} \exp\left(-\frac{\alpha}{2} \|\mathbf{D}\mathbf{f}\|_2^2\right)\end{aligned} \quad (3.67)$$

where \mathbf{D} is a $N \times N$ high-pass filter matrix which are used to impose smoothness constraints on the image estimate. For TV prior with the first-order differentiation operator in 1D case, it is given by

$$\mathbf{D} = \begin{bmatrix} 1 & 0 & \dots & 0 \\ -1 & 1 & \dots & 0 \\ 0 & -1 & 1 & \dots \\ \vdots & \vdots & \ddots & \vdots \\ 0 & \dots & -1 & 1 \end{bmatrix} \quad (3.68)$$

We also take a conjugate prior on hyperparameters α, β as Gamma distribution, which are, respectively

$$p(\alpha|a_0, b_0) = \frac{b_0^{a_0}}{\Gamma(a_0)} \alpha^{a_0-1} \exp(-b_0\alpha) \quad (3.69)$$

$$p(\beta) = \frac{d_0^{c_0}}{\Gamma(c_0)} \beta^{c_0-1} \exp(-d_0\beta) \quad (3.70)$$

The posterior on $\{\mathbf{f}, \alpha, \beta\}$ is

$$p(\mathbf{f}, \alpha, \beta | \mathbf{g}) \propto p(\mathbf{g} | \mathbf{f}, \beta) p(\mathbf{f} | \alpha) p(\alpha) p(\beta) \quad (3.71)$$

We here concentrate on the JMAP estimation of $\{\mathbf{f}, \alpha, \beta\}$, i.e.,

$$\begin{aligned}\{\hat{\mathbf{f}}, \hat{\alpha}, \hat{\beta}\} &= \arg \max_{(\mathbf{f}, \alpha, \beta)} \{\ln p(\mathbf{f}, \alpha, \beta | \mathbf{g})\} \\ &= \arg \min_{(\mathbf{f}, \alpha, \beta)} \{J(\mathbf{f}, \alpha, \beta)\}\end{aligned} \quad (3.72)$$

3.4.4 - Total Variation (TV) prior and hierarchical Bayesian estimation

where the objective function

$$\begin{aligned} J(\mathbf{f}, \alpha, \beta) &= \frac{\beta}{2} \|\mathbf{g} - \mathbf{H}\mathbf{f}\|_2^2 + \frac{\alpha}{2} \|\mathbf{D}|\mathbf{f}|\|_2^2 \\ &\quad - \left(\frac{M}{2} + c_0 - 1 \right) \ln \beta + d_0 \beta \\ &\quad - \left(\frac{N}{2} + a_0 - 1 \right) \ln \alpha + b_0 \alpha \end{aligned} \quad (3.73)$$

We adopt a coordinate-descent method to optimize J that basically optimizes one of variables $\mathbf{f}, \alpha, \beta$ while fixing the others iteratively.

Optimize \mathbf{f} in complex domain

The radar scattering coefficients are usually complex. We rewrite Equation (3.65) as

$$\begin{aligned} p(\mathbf{f}) &\propto \alpha^{M/2} \exp\left(-\frac{\alpha}{2} \sum_i (|f_i| - |f_{i-1}|)\right) \\ &= \alpha^{M/2} \exp\left(-\frac{\alpha}{2} \|\mathbf{D}|\mathbf{f}|\|_2^2\right) \\ &= \alpha^{M/2} \exp\left(-\frac{\alpha}{2} \|\mathbf{D}\mathbf{S}\mathbf{f}\|_2^2\right) \end{aligned} \quad (3.74)$$

where

$$\mathbf{S} = \text{diag}([\exp(-js_1), \exp(-js_2), \dots, \exp(-js_N)]), \quad \mathbf{s} = [s_1, s_2, \dots, s_N] \quad (3.75)$$

and

$$s_j = \phi(f_j), \forall j \quad (3.76)$$

where $\phi(f_j)$ is the phase of f_j . However, $\hat{\mathbf{f}}^{(k)}$ in Step 3 is not immediately obtained since the regularization term $\|\mathbf{D}|\mathbf{f}|\|_2^2$ is non-differentiable and nonlinear, therefore we adopt a majority-minimization (MM) method to optimize. For brevity, the superscript k and the term irrelative to \mathbf{f} will be dropped off.

$$\hat{\mathbf{f}} = \arg \min_{\mathbf{f}} J(\mathbf{f}) = \arg \min_{\mathbf{f}} \|\mathbf{g} - \mathbf{H}\mathbf{f}\|_2^2 + \lambda \|\mathbf{D}\mathbf{S}\mathbf{f}\|_2^2 \quad (3.77)$$

where $\lambda = \alpha/\beta$.

Instead of optimizing $J(\mathbf{f})$ in Equation (3.77) directly, we iteratively minimize its so-called majority function $\tilde{J}(\mathbf{f}|\mathbf{f}^{(k)})$ such at [BMK08]

$$\begin{aligned} J(\mathbf{f}) &\leq \tilde{J}(\mathbf{f}|\mathbf{f}^{(k)}), \forall \mathbf{f} \\ J(\mathbf{f}^{(k)}) &= \tilde{J}(\mathbf{f}^{(k)}|\mathbf{f}^{(k)}) \end{aligned} \quad (3.78)$$

where $\mathbf{f}^{(k)}$ is the estimation at the iteration k . It can be easily shown that the function

$$\begin{aligned} \tilde{J}(\mathbf{f}|\mathbf{f}^{(k)}) &= \|\mathbf{g} - \mathbf{H}\mathbf{f}\|_2^2 \\ &\quad + \frac{\lambda}{2} \sum_j \left\{ \frac{\|[\mathbf{D}\mathbf{S}\mathbf{f}]_j\|_2^2}{2\|[\mathbf{D}|\mathbf{f}^{(k)}]\|_2^2} + \frac{1}{2} \|[\mathbf{D}|\mathbf{f}^{(k)}]\|_j^2 \right\} \end{aligned} \quad (3.79)$$

is the Majority function which satisfies the conditions Equation (3.78), where $[\mathbf{x}]_j$ denotes the j^{th} element of \mathbf{x} and

$$\tilde{J}(\mathbf{f}|\mathbf{f}^{(k)}) = \|\mathbf{g} - \mathbf{H}\mathbf{f}\|_2^2 + \frac{\lambda}{4}[\mathbf{D}\mathbf{S}\mathbf{f}]' \mathbf{W} [\mathbf{D}\mathbf{S}\mathbf{f}] \quad (3.80)$$

where

$$\mathbf{W} = \text{diag}(1/\|[\mathbf{D}\mathbf{f}^{(k)}]\]_j\|_2^2, j = 1, 2, \dots, N). \quad (3.81)$$

Equation (3.80) is an iterative weighted least square problem which can be solved by the conjugated gradient descent method avoiding the inverse operation of a large-scale matrix with the gradients

$$\nabla_{\mathbf{f}} \tilde{J}(\mathbf{f}|\mathbf{f}^{(k)}) = -2\mathbf{H}'(\mathbf{g} - \mathbf{H}\mathbf{f}) + \frac{\lambda}{2}[\mathbf{D}\mathbf{S}]' \mathbf{W} [\mathbf{D}\mathbf{S}\mathbf{f}] \quad (3.82)$$

Algorithm 2 Majorization-Minimization algorithm

Input: \mathbf{g} , λ , the maximum number iterations N_{iter}

Output: the reconstructed image \mathbf{f}

- 1: Initialize $\mathbf{f}^{(0)}$ by IFT method
 - 2: **for** $k = 1$ to N_{iter} **do**
 - 3: Compute $s_j = \phi(f_j)$;
 - 4: Minimize the equation 3.41 using gradient descent method
 - 5: **if** $\left\| |\hat{\mathbf{f}}^{(k)}| - |\hat{\mathbf{f}}^{(k-1)}| \right\|_2^2 / \|\hat{\mathbf{f}}^{(k-1)}\|_2^2 \leq \varepsilon$ **then**
 - 6: Break;
 - 7: **end if**
 - 8: **end for**
-

3.5 Conclusions

In this chapter, a Bayesian inference methodology for SAR imaging was proposed. The deficiencies of classical inversion methods were analyzed. The statical probability distribution functions for two kinds of typical SAR target scenes were presented. Simple priors as well as the hierarchical priors with hyperparameters were then appropriately proposed. Different estimation approaches as MAP, Joint MAP, the marginalization and VBA were presented. Then, proposed different priors and estimation methods were implemented respectively: firstly MAP estimation with three simple priors, then hyperparameters estimation of the marginalization with a simple Gaussian prior and a sparse Gaussian prior and finally a hierarchical Bayesian method with a generalized TV prior. A coordinate-descent optimization method was developed for TV estimation.

Part II

Applications to Different SAR Imaging Systems

4

Bayesian Approach for Mono- and Bi-static SAR Imaging

4.1 Introduction

The objective of this chapter is to apply the proposed Bayesian approach for Mono- and Bi-Static SAR imaging.

In the process of SAR imaging, there are many degradation factors leading to the decrease of the resolution of imaging system. Aiming at improving the resolution of SAR images, technologies on hardware data processing have been developed. Conventional Mono-static SpotSAR imaging can acquire high resolution for its long integration time. However, as the transmitter and the receiver are collocated, radar itself is easily being detected by counter. Recently, the emergence of Bi-static SAR [[GPSG10](#), [MM07](#)] provides a possibility to improve the resolution as well as to decrease the probability of detection, playing a very important role in space surveillance.

From the mathematical point of view, for Mono- or Bi-static SAR imaging, we need to handle the ill-posed problem by using one data set to reconstruct the unknown target scene. By applying probability distributions to different quantities, we can then use the framework of estimation in the Bayesian sense [[MD09a](#)].

Bayesian approach supplies a flexible framework by utilizing prior information as well as the inference tools to any unknown quantities [[Idi08](#)]. In the sense of the application, different priors are closely linked to features of interest, while the powerful inference tools for parameters or hyperparameters of the model bring a more accurate solution, thus the resolution of SAR images can be improved, useful features can be well enhanced and finally a recognition-oriented SAR imaging can be realized.

According to the inversion approach proposed in Chapter 3, this chapter will be organized as follows:

CHAPTER 4. BAYESIAN APPROACH FOR MONO- AND BI-STATIC SAR IMAGING

In Section 4.2, experiments for MAP estimation with simple priors are conducted.

In Section 4.3, experiments for marginalization with hyperparameters estimation are conducted.

In Section 4.4, experiments for Total Variation (TV) prior and hierarchical Bayesian estimation are implemented.

Experimental results demonstrate the feasibility of the proposed approach.

4.2 Simple Priors with MAP Estimation

Figure 4.1 summarizes the proposed Bayesian approach for SAR imaging:

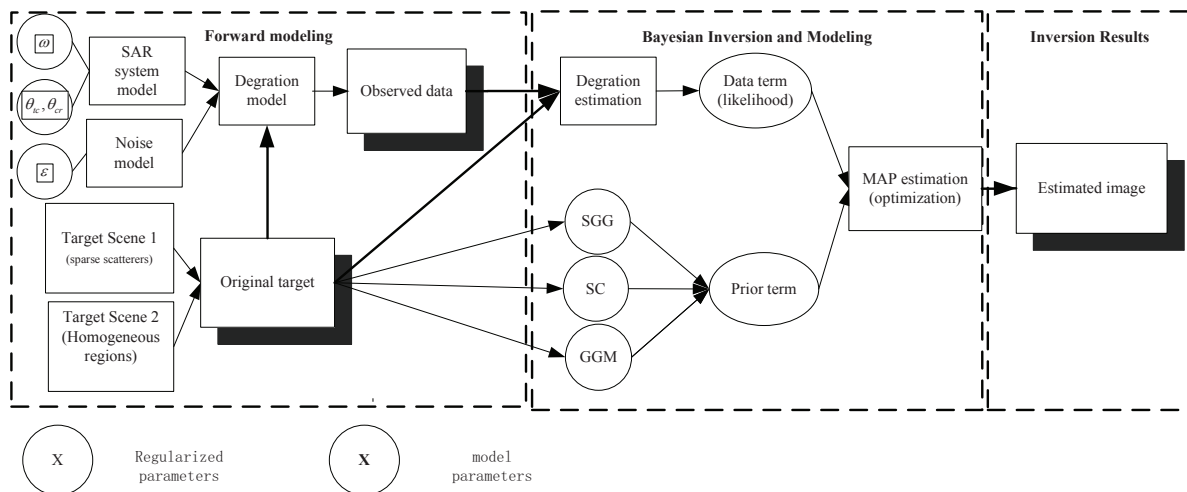


Figure 4.1: Graphic model of forward modeling and Bayesian inversion.

1. In the left bloc the forward model and prior information on the target are described.
2. In the middle bloc, the two main steps of the Bayesian approach which are obtention of likelihood and prior terms are summarized. In this section, we limited ourselves to simple priors with MAP estimation when the hyperparameters were given.
3. In order to demonstrate the performances of our proposed method, we define the relative distance errors to evaluate the reconstructed results.

For synthetic data, where it is possible for us to know the original \mathbf{f} , we use the following criterion

$$\text{Relative distance}(\mathbf{f}, \hat{\mathbf{f}}) = \frac{\|\mathbf{f} - \hat{\mathbf{f}}\|_2^2}{\|\mathbf{f}\|_2^2} \quad (4.1)$$

where $\hat{\mathbf{f}}$ is the estimated term. This criterion represents the reconstruction error to measure the performance of the reconstructions in simulation.

For real data, we do not know the original \mathbf{f} . One solution in this case is to use the following scheme in Figure 1.4, and compare $\hat{\mathbf{g}} = \mathbf{H}\hat{\mathbf{f}}$ with \mathbf{g} using

$$\text{Relative distance}(\mathbf{g}, \hat{\mathbf{g}}) = \frac{\|\mathbf{g} - \hat{\mathbf{g}}\|_2^2}{\|\mathbf{g}\|_2^2} \quad (4.2)$$

which is a normalized residual error.

In the next section, we will demonstrate the capabilities of the proposed Bayesian approach with several experiments. As usual we are interested in point scatterers along with homogeneous regions in a SAR image. The synthetic scenes are generated to simulate metallic point scatterers or manmade homogeneous targets. Real scenes composed by more complicated targets will also be used to verify the performance of the proposed method.

4.2.1 Results with synthetic data

We give simulated results on two synthetic target scenes $f(x, y)$: point targets and extended targets. We simulate different target scenes with the combination of these two kinds of targets. The relation between the Fourier transform of the measured data and the unknown target scene is modeled by a 2D spatial FT. The inverse problem becomes then a FS problem which depends on the geometry of the data acquisition. Only the set of locations in the Fourier space are different. Based on this, we propose the steps of generating synthetic data as following:

1. We first generate the synthetic target with scattering coefficients $f(x, y)$ with magnitude 1. For complex coefficients $f(x, y)$, the phase is generated randomly with uniform distribution in $[-\pi, \pi]$
2. We do Fourier Transform on $f(x, y)$ to obtain its spectral data $F(k_x, k_y)$;
3. We define a binary function $M(k_x, k_y)$ representing the sampling in the wavenumber domain under different observations and geometries. $M_1(k_x, k_y), M_2(k_x, k_y)$ are used for simulating data support with two bands of radar transmitter and different observation angles;
4. Then we get observed wavenumber data through $G(k_x, k_y) = M(k_x, k_y)F(k_x, k_y)$.
5. The additive complex gaussian noised $\epsilon(k_x, k_y)$ is generated based on the SNR and is added to $G(k_x, k_y)$. Our aim turns to reconstruct the original target $f(x, y)$ from its partial observed data $G(k_x, k_y)$.

Here we apply the proposed method in experiments with various synthetic and real target scenes and compare them with those of the conventional IFFT-based imaging methods and the classical regularization methods to demonstrate achieved improvements in performance.

Experiment 1: Target 1/Target 2

We start with two simple targets. Figure 4.2 shows the two targets. Target 1, illustrated in the first row, represents a target composed of regions; while Target 2 in

4.2.1 - Results with synthetic data

the second row, represents a target composed of strong scatterers. The first column shows the two synthetic targets which are the magnitude of $f(x, y)$, i.e., $|f(x, y)|$. The second column shows the magnitude of Fourier Transform, the third column shows the masks which are corresponding to the different observation geometry and the generated data are shown in the fourth column.

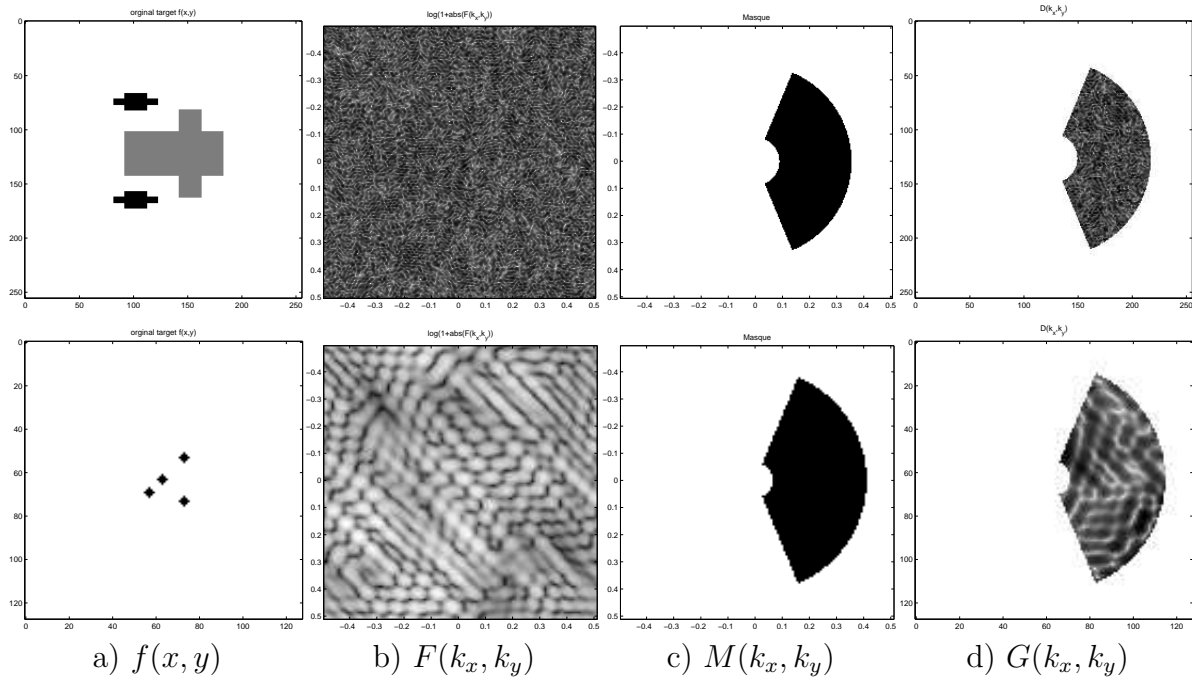


Figure 4.2: Two simulated targets and generated complex data sets, magnitude displayed in reverse video: a) Original Targets: Target 1 and Target 2; b) Fourier Transform; c) Masks; d) Observed data.

We can see that, Target 1, is more realistic to a scene composed by homogeneous regions. And the reason we choose such a special geometry for Target 2 is actually for simulating the experimental scene which will be given in the next chapter. The masks represents datasets with different geometry and bandwidth.

Results Analysis

Figure 4.3 shows the reconstructed results for the two targets (the first row for Target 1 and the second row for Target 2) with complex scattering coefficients. Comparing with different inversion methods, those from regularization methods as well as the proposed Bayesian methods with different priors are better than those from classical deterministic imaging methods. The improvement comes from the introduction of the prior information.

If we examine the results in the first row in Figure 4.3, we could find for Target 1, the inversion results based on the proposed Bayesian method using the GGM prior is better than those obtained using other priors. while comparing results in the second row, we could find that for Target 2 which has the typical scattering characteristics of isolated

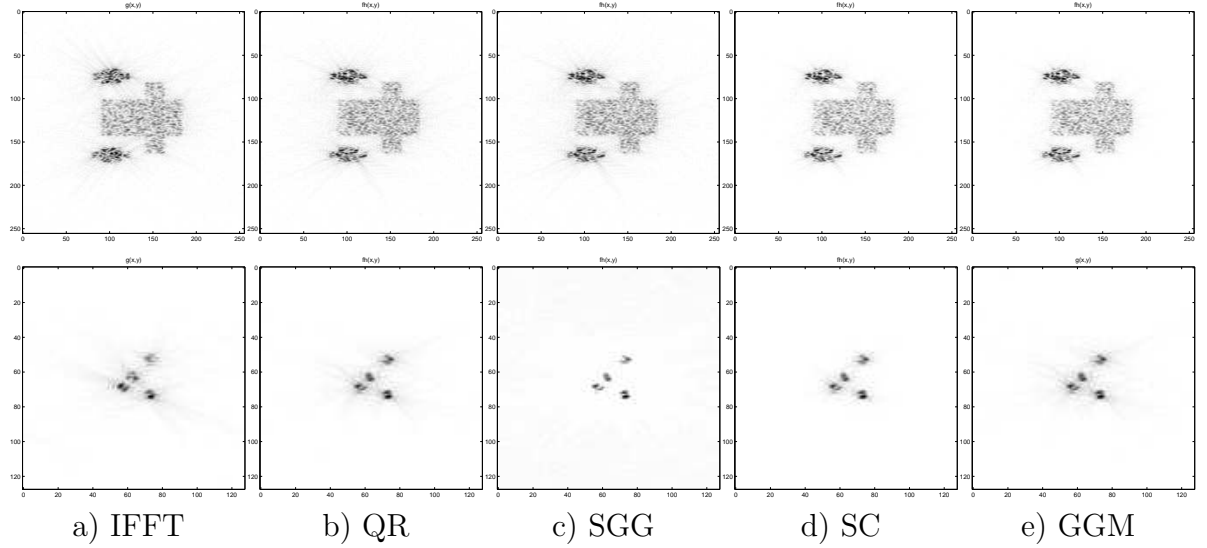


Figure 4.3: Reconstructed results on simulated complex data, magnitude displayed with the first row on data set 1 and the second row on data set 2 displaying in reverse video: a) Inverse Fast Fourier Transform (IFFT); b) Quadratic Regularization (QR); c) Separable Generalized Gaussian (SGG); d) Separable Cauchy (SC); e) Generalized Gaussian Markov (GGM).

points, results based on the proposed Bayesian method using the SGG prior ($\beta = 1$) perform better than those using other priors.

The Table 4.1 presents the results for the targets with complex values. For Target 1 under SNR of 30dB and 20dB, the proposed Bayesian method with GGM prior present the best performance. For Target 2, the proposed Bayesian method with SGG prior is always the best under different SNR of 30dB, 20dB, 10dB and 5dB.

The proposed Bayesian method shows a comparatively strong robustness. From the analysis, we can see that in order to obtain a good reconstruction results, for targets of dominant scattering structures, sparse distributions can be chosen for prior modeling; In contrast, for targets containing several regions, smoothen priors could be used for enhancing the region features of the targets.

Table 4.1: Statistical results of reconstructed relative distance errors on two targets (Target 1/Target 2) with complex scattering coefficients

SNR	30dB	20dB	10dB	5dB
IFFT	0.86/0.87	0.89/0.90	0.94/0.92	0.94/0.94
QR	0.84/0.86	0.86/0.90	0.89/0.92	0.89/0.94
SGG	0.83/0.82	0.85/0.84	0.88/0.85	0.93/0.90
SC	0.86/0.84	0.86/0.86	0.87/0.85	0.91/0.92
GGM	0.82/0.83	0.84/0.85	0.88/0.85	0.88/0.92

4.2.2 - Results with real data

4.2.2 Results with real data

To be more realistic, we now perform the experiments on data collected in MSTAR (Moving and Stationary Target Acquisition and Recognition program) public target data set.

Real data description

The data set was collected in September of 1995 at the Redstone Arsenal, Huntsville, AL by the Sandia National Laboratory (SNL) SAR sensor platform. The collection was jointly sponsored by DARPA and Air Force Research Laboratory as part of the MSTAR program. SNL used an X-band SAR sensor in one foot resolution spotlight mode¹.

The MSTAR dataset consists of SAR images of various ground military vehicles including T72 tanks, BMP2 tanks and BTR70 armed personnel carriers as well as the standard SLICY targets. These images were taken at X band, at 17° and 15° depression angles respectively and evenly spaced (in about 5°) in Azimuth(aspect angle) to cover 360° [CKC02, WW09]. The parameters of MSTAR target is illustrated in Table 4.2.

Phase history data generation

We take the SLICY data (HB14957.015) and T72 data (HB03333.015) for the experiment. The original targets of slicy and T72 tank are shown in Figure 4.4². The data sets we get are complex-valued SAR images, with 54×54 and 128×128 for SLICY and T72, respectively. We perform operations of FFT, remove zeroes and windows on the images data and get the phase history data as in [CKC02]. We then apply our method with the phase history data.

The magnitudes of the phase history data on the two targets are shown in Figure 4.5.

Table 4.2: MSTAR public targets

	Targets	Target Description
SLICY	Multiple simple geometric shaped static target	CAD Model November '96 Imagery: TBD in Jan '97
T72	T-72 Tank	3 replicate targets: each collected at 15° & 17° degree dep. angles and full aspect coverage

Results on MSTAR

Figure 4.6 illustrates the experimental results on MSTAR, with the first and the second row showing reconstructed results on the standard Slicy data and T72 Tank,

1. Data from <https://www.sdms.afrl.af.mil/index.php?collection=mstar&page=targets>
2. Pictures from http://www.wagenman.org/thesis/MSTAR/MT_15_45/15_deg/col2/scene1/slicy/target.htm, <http://www.army-technology.com/projects/t72/>



Figure 4.4: The original target: a) Target chip for Slicy at 15° ; b) T72 tank at 15° .

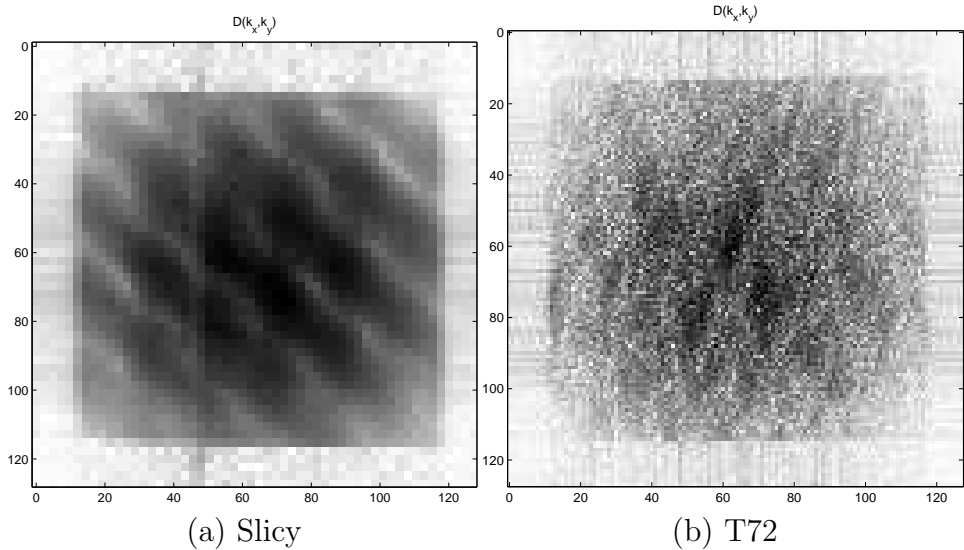


Figure 4.5: The magnitude of phase history data displaying in reverse video
: (a) Slicy; (b) T72.

respectively.

We again use the relative distance error defined in Equation (4.2) to evaluate the reconstructed results. Table 4.3 illustrates the comparative reconstruction errors of IFFT, QR and the proposed MAP method with priors of SGG, SC and GGM, respectively.

4.2.3 Analysis and discussions

Figure 4.6 shows the inversion results based on the real data of MSTAR. Because of non-zero background clutters as well as the specific distributed regions, the reconstruction of these targets are not sharp and clear as the previous scene. It is shown that bright artifacts that are noticeable around strong reflectors in the focused images. However, the resultant reconstructed images remain in good agreement with the true

4.2.3 - Analysis and discussions

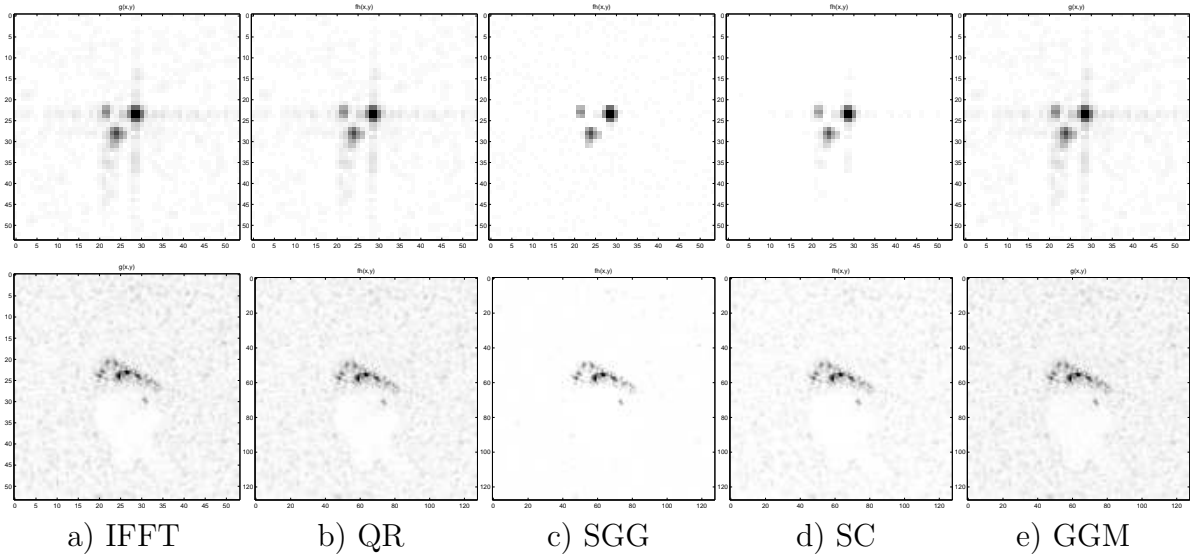


Figure 4.6: Reconstructed results, with first row on Slicy data and the second row on MSTAR data (complex values), magnitude displayed in reverse video: a) Inverse Fast Fourier Transform (IFFT); b) Quadratic Regularization (QR); c) Separable Generalized Gaussian (SGG); d) Separable Cauchy (SC); e) Generalized Gaussian Markov (GGM).

Table 4.3: Statistical results of reconstructed relative distance error on two real targets (SLICY and T72 Tank)

	IFFT	QR	SGG	SC	GGM
SLICY	0.32	0.31	0.29	0.30	0.32
T72 Tank	0.35	0.34	0.32	0.31	0.30

image.

Table 4.3 presents the relative distance error of inversion results. From it, we can see that by making use of the prior information of targets to do inversion, not only certain characteristics of targets can be well enhanced (or preserved), but also the robustness of inversion results on targets under low SNR can be firmly strengthened.

Figure 4.7 illustrates that for the distribution of SGG, reconstruction errors on Target 2 change with different values of regularized parameters λ and β , from which we could see the effectiveness of the sparse priors for this kind of targets. Figure 4.8 illustrates for Cauchy distribution, reconstruction errors on Target 2 changing with different values of parameter λ .

Based on the above analysis, we can see that with an appropriate prior, a better estimation result can be get. For the target scene mainly composed of point sources (representing small size metallic targets, for example), it is moderate to utilize the SGG or SC prior, which could enhance features specially as strong scattering points; instead, for the scene mainly incorporating regions (representing comparatively large targets or scene), it is nearly perfect to employ the GGM prior which could smoothen regions as well as preserving edges.

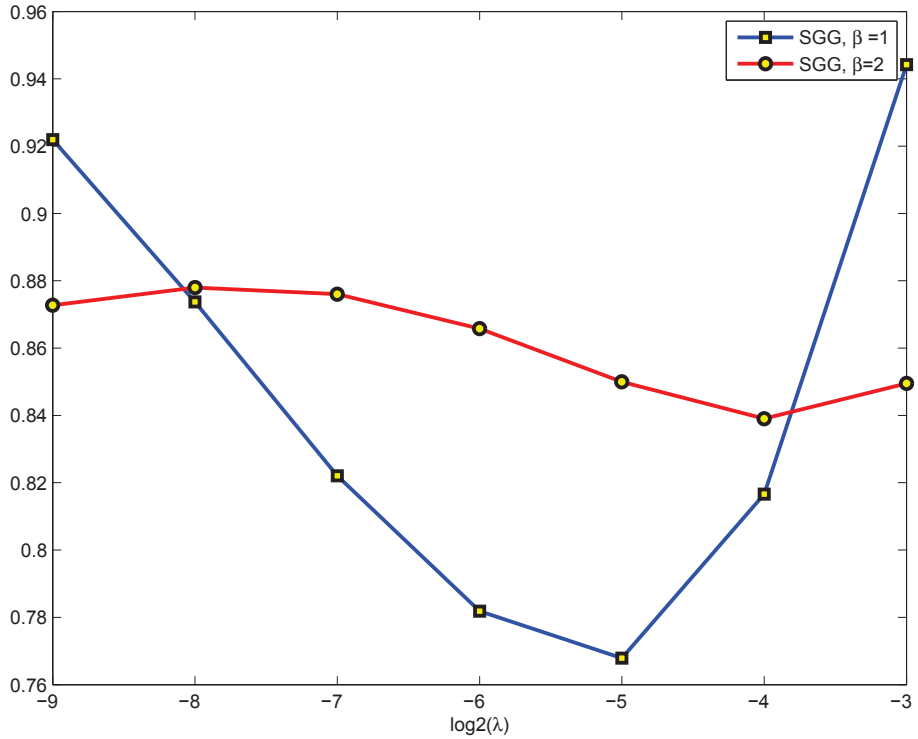


Figure 4.7: Different reconstruction errors with parameters λ and β in prior SGG.

4.3 JMAP for Hyperparameters Estimation

In the section above, we have investigated Bayesian method by assuming that the parameters of the distributions are known. But this is unreal in practical. The parameters are generally unknown so it is necessary to do estimation as well. Bayesian method provides an efficient way to jointly estimate the target and the hyperparameters. Figure 4.9 illustrates the JMAP process of this estimation method based on alternate optimization of $p(\mathbf{f}, \boldsymbol{\theta} | \mathbf{g})$.

Figure 4.10 shows the marginalization steps:

We apply the marginalization algorithm as illustrated in Figure 4.10 for two Gaussian priors proposed in the section 3.4.2. In the following section, we will show some experiments based on:

1. Gaussian prior when we estimate σ_ϵ^2 and σ_f^2 ,
2. Sparse Gaussian prior when we estimate σ_ϵ^2 and σ_i^2 ,

and compare the marginalization estimation results.

4.3.2 - Results with real data

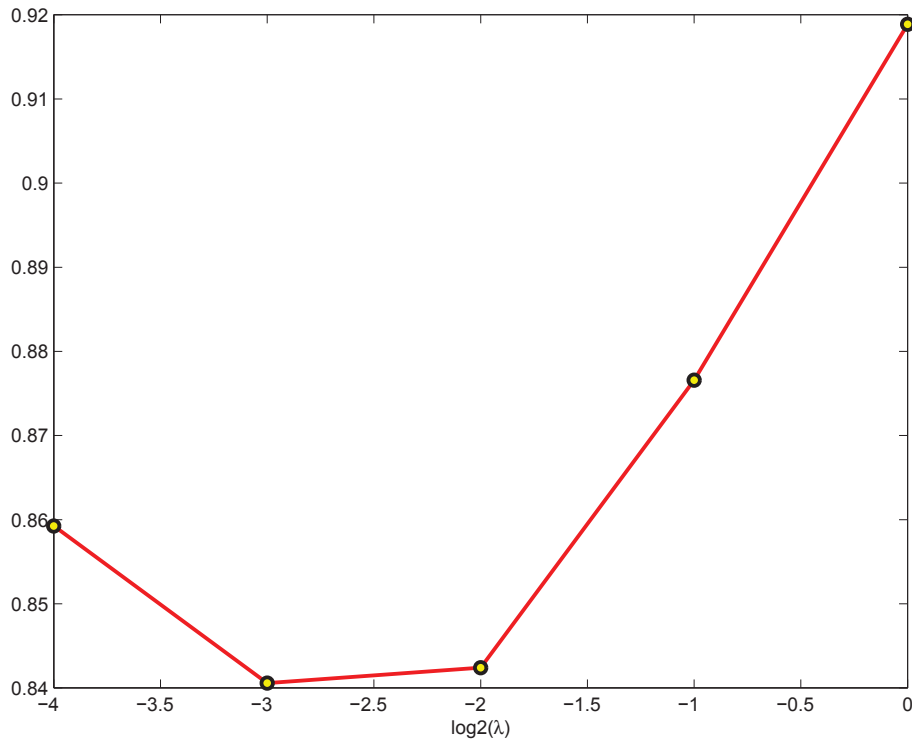


Figure 4.8: Different reconstruction errors with the parameter λ in prior SC.

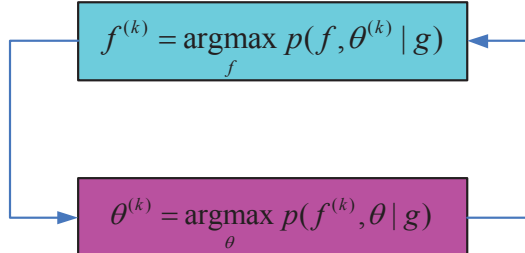


Figure 4.9: Jointly estimate the target and the hyperparameters.

4.3.1 Results with synthetic data

In this section, we conduct experiments on synthetic data to validate our proposed method. Data generation steps are defined as the same in Section 4.2.1, as illustrated in Figure 4.2.

Figure 4.11 shows the Bayesian reconstructed results $\hat{f}(x, y)$ obtained with the proposed two priors for the target of complex-valued data. Table 4.4 lists the relative distance error of the inversion results for the targets of complex data.

4.3.2 Results with real data

We now also perform the experiments on real data on MASTAR data set. As before, two targets (Slicy and T72) are used. The reconstruction results are shown in

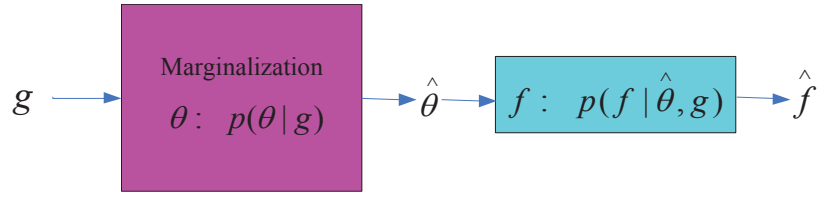


Figure 4.10: Marginalization with hyperparameters.

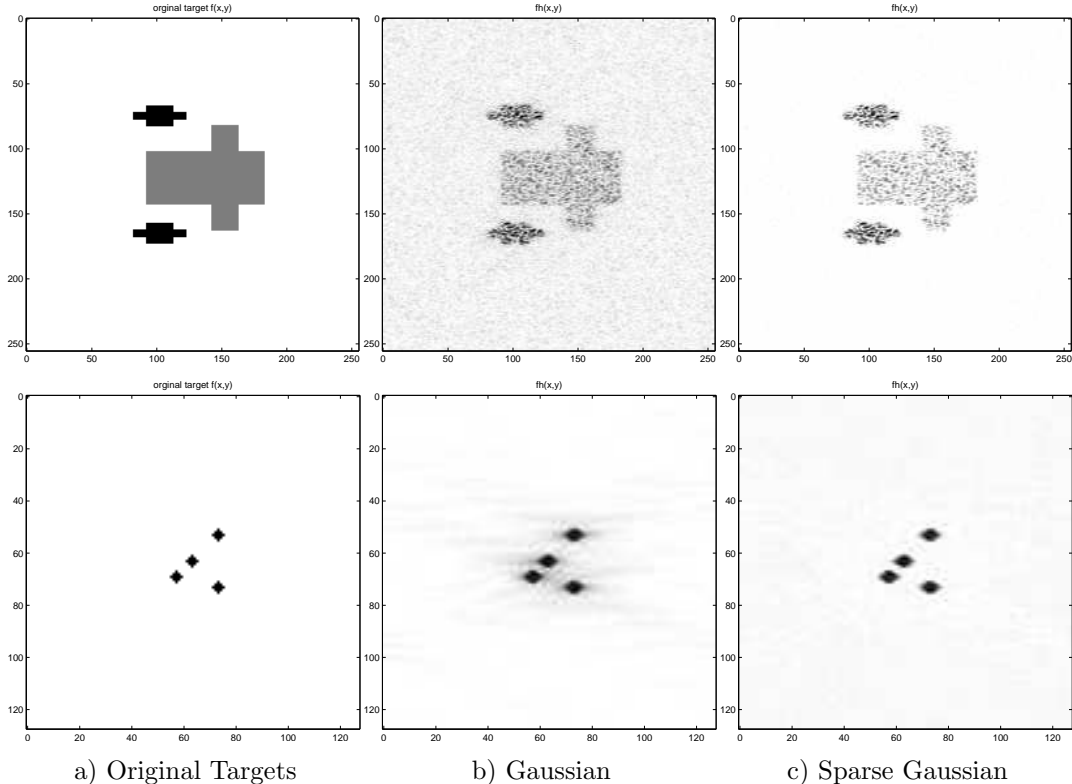


Figure 4.11: Synthetic data (complex values), magnitude displayed in reverse video: a) Original targets and Bayesian reconstructed results with different priors with hyperparameter estimation; b) Gaussian Prior; c) Sparse Gaussian Prior.

Table 4.4: Statistical results of reconstructed relative distance error on the two synthetic targets of complex values with Bayesian methods

	Gaussian	Sparse Gaussian
Target 1	0.88	0.73
Target 2	0.70	0.68

Figure 4.12, with the first row and the second row of Slicy and T72, respectively.

We again use the relative distance defined in Equation (4.2) to evaluate the recon-

4.3.3 - Analysis and discussions

structed results. Table 4.5 illustrates the relative distance error of reconstruction with the proposed marginalization method. Again, the results demonstrate the effectiveness of the proposed method with Gaussian and especially with Sparse Gaussian prior.

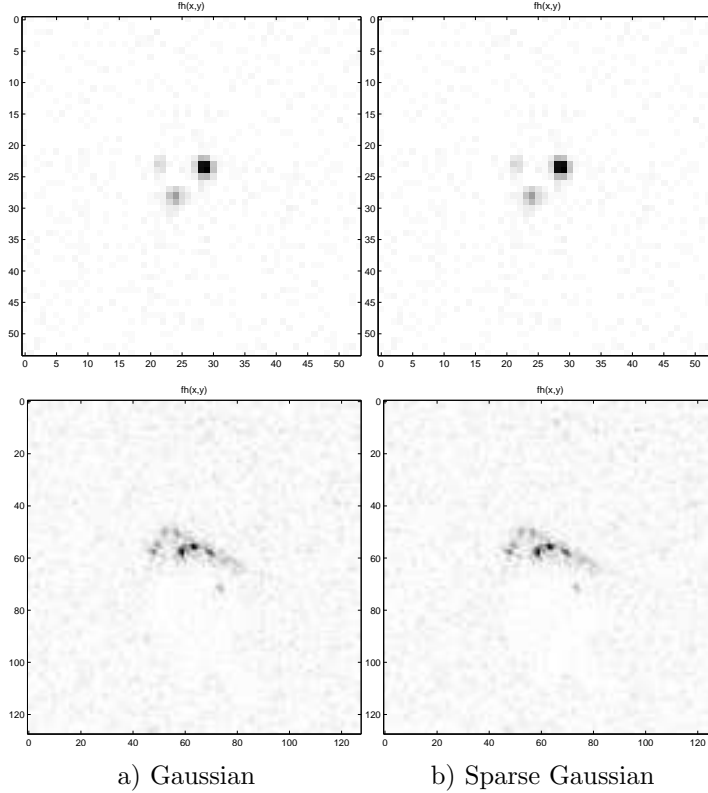


Figure 4.12: Bayesian reconstructed results with different priors with hyperparameters estimation, magnitude displayed in reverse video: a) Gaussian prior; b) Sparse Gaussian prior.

Table 4.5: Statistical results of reconstructed relative distance error on two realistic targets (SLICY and T72 Tank)

	Gaussian	Sparse Gaussian
SLICY	0.21	0.20
T72 Tank	0.40	0.34

4.3.3 Analysis and discussions

Results based on simulated data is shown in Figure 4.11, with the first row and the second row showing the results on Target 1 and Target 2, respectively. From them, we can see with the proposed method, real target scene can be reconstructed accurately.

Results based on real data is shown in Figure 4.12 also demonstrate the success of the proposed method. Thanking the introduction of the prior information, as well as the marginalization inference, hyperparameter estimation can be implemented at the same time.

4.4 TV Prior and Hierarchical Bayesian Estimation

Fig. 4.13 show the graphic model with TV prior and the corresponding estimation process.

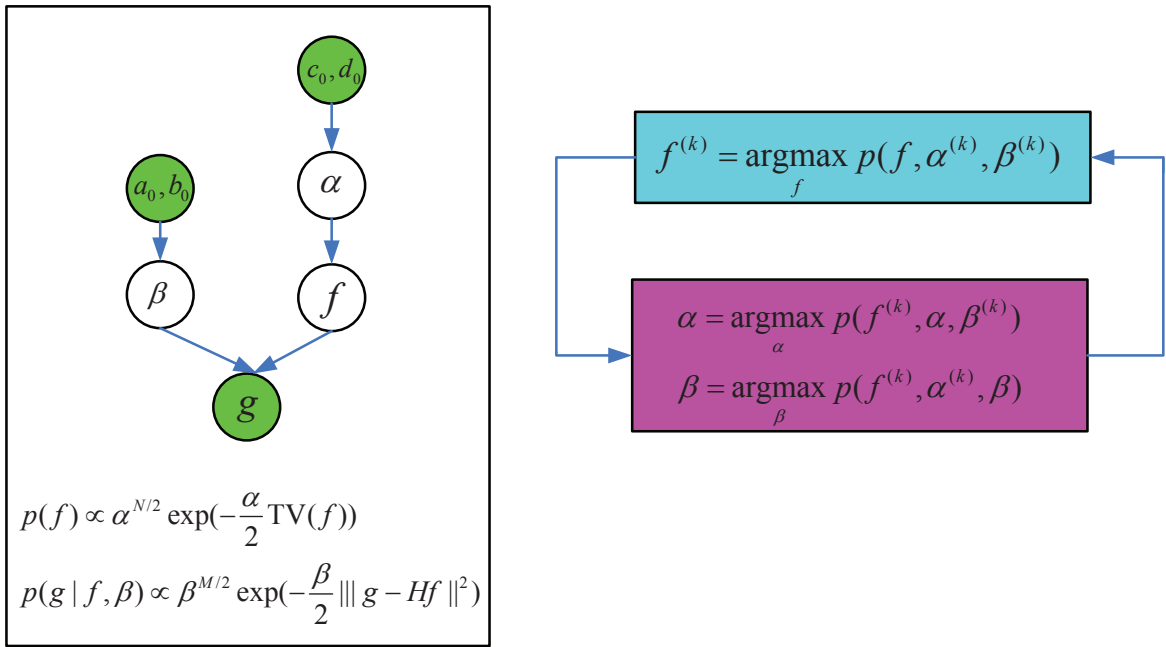


Figure 4.13: Jointly estimate the target and the hyperparameters with TV prior.

4.4.1 Results with synthetic data

Again we first demonstrate the proposed method on synthetic data. As shown in Figure 4.14, the steps of the data generation are done as before, where we first create the original targets $f(x, y)$ and its Fourier Transform $F(k_x, k_y)$ in wavenumber domain, and then define the mask $M(k_x, k_y)$ which gives the partial observation in the frequency domain. Finally the observation $G(k_x, k_y)$ is generated by $G(k_x, k_y) = F(k_x, k_y)M(k_x, k_y) + \epsilon(k_x, k_y)$. Our goal is to reconstruct $\hat{f}(x, y)$ from the noisy and partial observation $G(k_x, k_y)$. The first row is the targets of real values and the second is the targets of complex values.

The simulated targets are specially chosen as the scene composed of homogeneous regions, in order to accurately verify the proposed method.

4.4.2 - Results with real data

Figure 4.15 shows the reconstructed images of targets of complex values with Inverse Fast Fourier Transform (IFFT) and the proposed Bayesian TV method (BTV) with two different operators \mathbf{D} formed by two filters respectively.

$$d_1 = \begin{bmatrix} 0 & -1 & 0 \\ -1 & 4 & -1 \\ 0 & -1 & 0 \end{bmatrix} \quad (4.3)$$

$$d_2 = \begin{bmatrix} -1 & 1 \\ 1 & -1 \end{bmatrix} \quad (4.4)$$

Table 4.6 lists the relative distance error of reconstructions. In each column, comparing the three results from IFFT, BTV- $d1$ and BTV- $d2$, we can clearly see that under the same SNR, the reconstruction results from TV priors are better than that from the conditional method of IFFT; while in each row, comparing results from each method, we can find the results from TV priors are robust even under low SNR.

Table 4.6: Relative distance error of reconstruction on synthetic complex data

SNR	30dB	20dB	10dB	5dB
IFFT	0.84	0.85	0.88	0.90
BTV- $d1$	0.82	0.83	0.87	0.89
BTV- $d2$	0.83	0.83	0.87	0.89

4.4.2 Results with real data

Figure 4.17 shows the reconstructed results based on public real SAR data, of which the first, the second rows are from Sandia, Isleta Lake, Isleta Pueblo, New Mexico and the third row are from MSTAR of T72 respectively. Since the data is already an image, we turn it into the complex phase domain as real received echoes. The steps are done as before. Figure 4.16 illustrates the frequency magnitude of two parts of the lake, named as lake 1 and lake 2.

It shows that with the TV prior, the region features of the objects are smoothed, e.g., the dark areas, while the edges are preserved and enhanced, e.g., the white lines in the images in the second row. The noise is suppressed greatly. Table 4.7 lists the relative distance error of reconstructions, which shows the BTV- $d1$ brings a better performance for reconstruction. The reason is that the filter d_1 considers more neighbor pixels than the filter d_2 .

Table 4.7: Relative distance error of reconstruction on real data

	IFFT	BTV- $d1$	BTV- $d2$
Lake 1	0.89	0.82	0.82
Lake 2	0.79	0.76	0.77
T72	0.84	0.80	0.81

4.4.3 Analysis and discussions

From the results on both synthetic and real data, it is shown that the region can be smoothed while the edges can be preserved and enhanced with TV prior. The main reason is that TV prior is a sparse prior with l_1 on spatial difference to model the edges in images. So for the region targets, we can use the proposed TV prior to enhance the edge features in a SAR image. The proposed method with feature enhanced images can well benefit the following tasks, such as SAR image interpretation and target recognition.

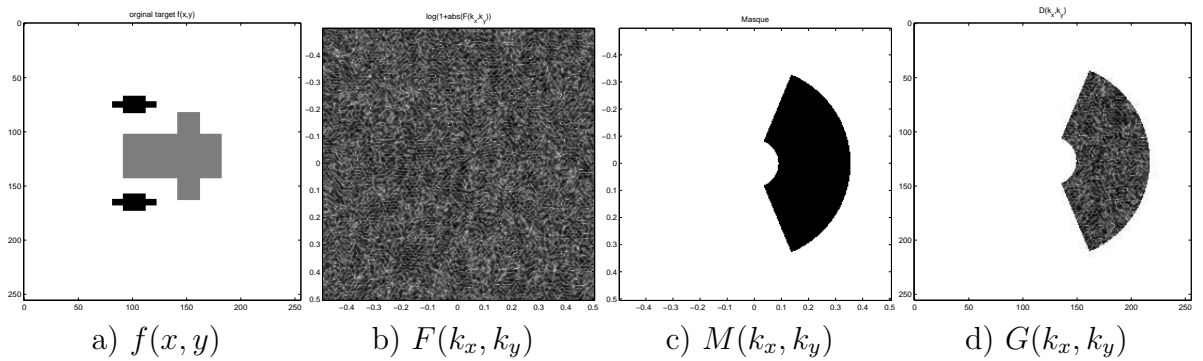


Figure 4.14: Synthetic data (complex values), magnitude displayed in reverse video.

4.5 Conclusions

In this chapter, we applied the proposed Bayesian approach to Mono- and Bi-static SAR imaging. A detailed modeling of the data acquisition process was simulated. Then several experiments were conducted on both synthetic and real data. The results demonstrated the feasibility of the proposed method, with the advantages as following: i) bringing high resolution to the images; ii) enhancing interested target features while imaging; iii) adaptively estimating the hyperparameters while imaging; iv) improving the robustness of the optimal estimation as the solution to the inverse problem.

From the sense of target recognition, Bayesian SAR imaging method is distinct from conventional methods which consider radar imaging and feature extraction as independent processes. With assigning appropriate priors, it offers a promising solution in improving target recognition capability for real SAR systems.

It is to be noted that the content and results of this chapter are mainly from the papers [ZMDLM11, ZMLW12].

4.4.3 - Analysis and discussions

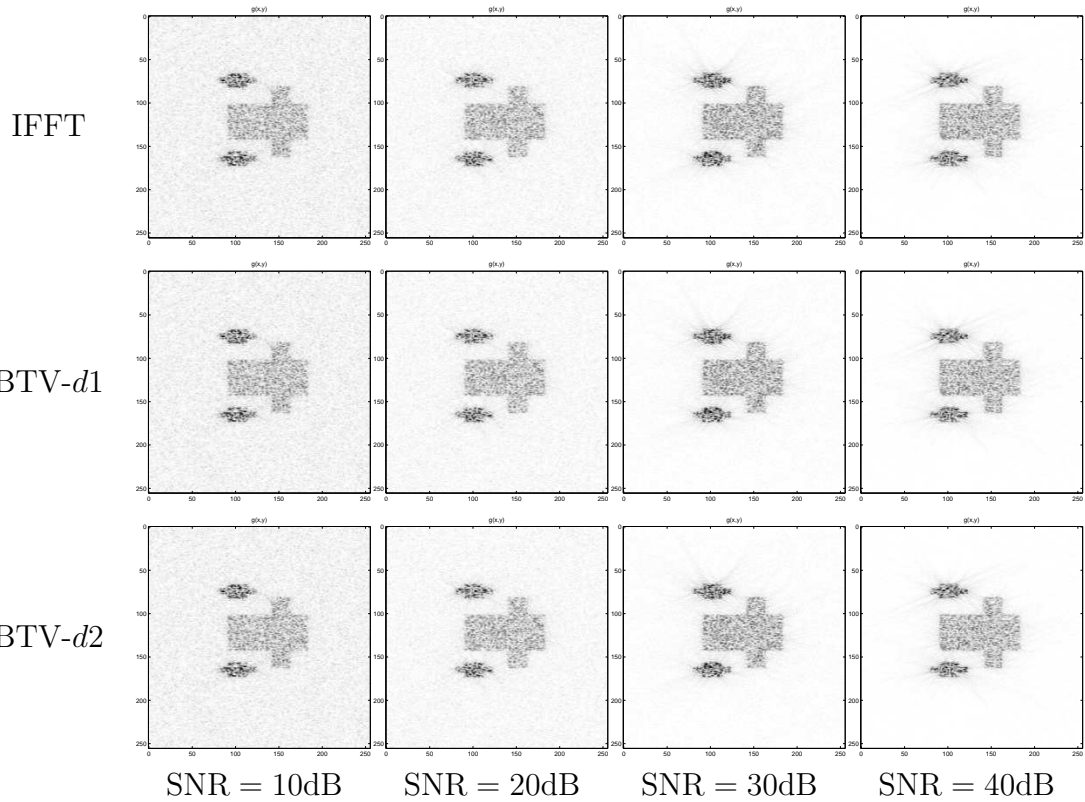


Figure 4.15: Reconstruction results of the targets of complex values with IFFT and the proposed method versus different SNR, magnitude displayed in reverse video
: a) 5 dB; b) 10dB; c) 20 dB; d) 30dB.

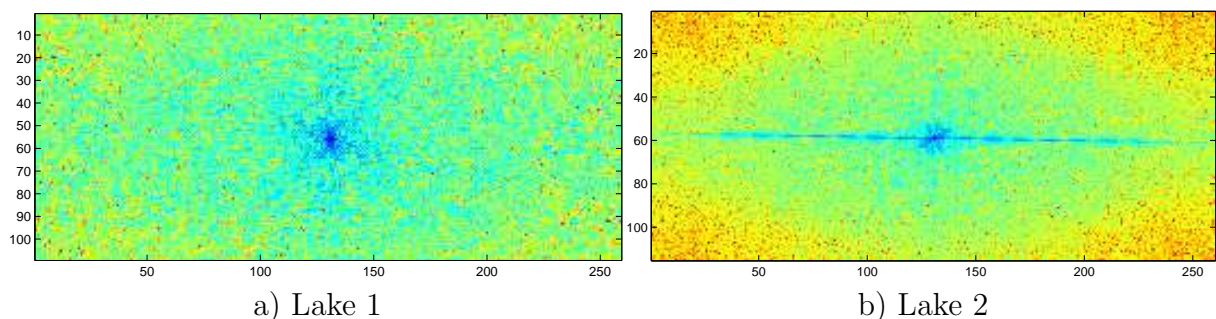


Figure 4.16: Frequency magnitude of Isleta lake: a) Lake 1; b) Lake 2.

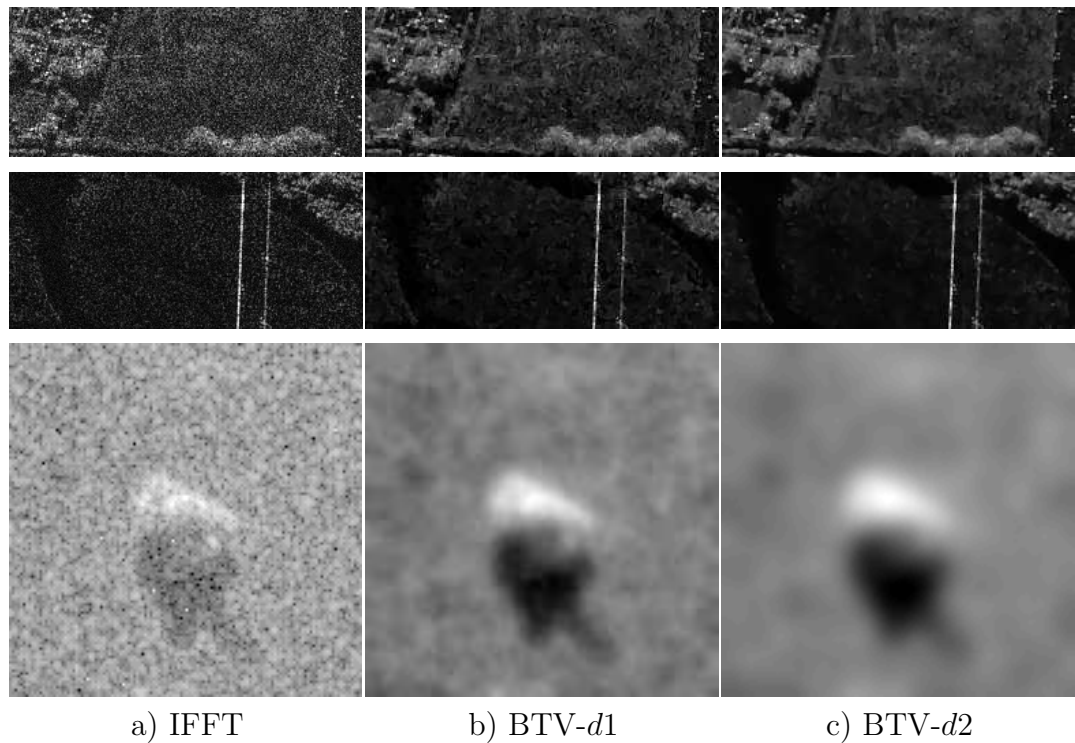


Figure 4.17: Real data reconstruction (complex values), magnitude displayed: a) IFFT; b) BTV- d_1 ; c) BTV- d_2 .

5

Bayesian Approach for Multi-static SAR Imaging

5.1 Introduction

The objective of this chapter is to apply the proposed Bayesian approach to Multi-static SAR imaging.

Theoretically speaking, the proposed method in the previous chapter can also be applied to Multi-static case, which needs to make use of more than one data set to do data fusion and inversion.

Multi-static SAR has been paid more and more attention for its importance in cooperative surveillance. One important application is the satellite-borne space distribution SAR [WG07, FG02, CB09]. In essence, it is an ill-posed problem of image reconstruction from multi observations over the same target to obtain a high resolution image. However, real measurements are corrupted by noise. Meanwhile, the reconstructed images by conventional methods suffer from artifacts. There is then a need for developing appropriate inversion and data fusion methods.

Many methods have been developed for multi-static or multi-frequency SAR data fusion. Statistically based fusion methods present distinct potentials for uncertainties arising from information incompleteness [YMTP12, Zha04, Li07]. [Bro03] demonstrated the benefits for classification by employing a Bayesian approach on multiple-view data at different incoherent views. [OTM⁺03, OTM⁺01, CTC⁺04] discussed the benefits of fused SAR images for feature extraction and target detection. [LHYS07] proposed an innovative multi-to-multi image fusion method against noise. [SLP01] proposed a Bayesian approach on sensor image fusion and [CTC⁺04, HP11] specially studied the fusion strategies on SAR images. In this chapter, we propose a Bayesian fusion method to explore the abundant information contained in echo data [MD03]..

This chapter is organized as follows: in Section 5.2 we introduce the application background of the distributed satellite multi-static SAR, analyzing the drawbacks of traditional fusion methods; in Section 5.3, we propose three different fusion schemes; in Section 5.4, we conduct the experiments on both simulated and real data to demonstrate the performance of the proposed method; in Section 5.5, we draw conclusions of this chapter.

5.2 Distributed Satellite Multi-Static SAR

Recently, SAR techniques show its potential in the configurations of multi-static passive SAR system. Current typical spaceborne distributed satellite SAR systems such as Techsat21 system [BMLM00] in USA, Cartwheel system in France [Mas01] and TanDEM-X system in Germany [GA07] have played important roles in remote sensing, detection and military surveillance. Different from Mono-static SAR, at the lowest points of passive receivers, Multi-static SAR could obtain a promising resolution at each direction of forward looking, down looking and back looking with the movement of receivers. These characteristics strengthen imaging regions, which could bring applications in new fields [GA07, WHB06, GD02]. [KFHM03] presents a typical distributed satellites SAR system, with main parameters given in Table 5.1.

Table 5.1: System main measurement parameters

Main satellite position /km	35850
Small satellites position /km	400
Radar transmitter wavelength /cm	3.1
Range resolution /m	3
Cross range resolution /m	3

By utilizing its distributed characteristics, the range resolution and cross range resolution of the main satellite could be improved. For a given ground target area, based on the simultaneous observations from satellites at different slant angles and pitch angles, making coherent integration of received echoes spectra to synthesize a wide spectra and then doing reconstruction. This coherent processing method yields an assumption that the received echo signals from each position could be completely coherent for the distances between satellites are very small and the whole antennas compose an effective large antenna. However, in practice, the received signals at each receiving antenna may be interfered by the scattering signals. This is mainly due to received signals from different channels can never be completely coherent integrating; and partly due to adding bandwidth resulting in additive thermal noise at the receiver, which decreases the SNR of SAR images [ZBXH07].

Besides, instead of using phase information, barely making use of amplitude information, a class of incoherent processing for distributed satellites is formed, which is implemented by incoherently combination of multiple channels, or by multi-look technique within one channel. The former doesn't decrease resolution of the single channel, however, the latter does. And image registration is required for both before amplitudes adding.

We conclude the challenges of conventional methods are:

1. When the received echoes of multiple satellites receivers are considered as echoes from one satellite at different time, the resolution of the fusion is then affected by the phase compensation error. Supposing that the phase compensation has been done, conventional imaging methods based on IFFT [CGM95b] will also lead to the loss of information and the low resolution.
2. By making use of multi spectral images to do data level fusion, the fused images suffer from color distortion and data (bands) dependency of different satellites [PVG98, SFM⁺02, Zha10]. Moreover, this method neglects consideration on distributed geometries and can not be considered as an effective estimation method for uncertainties.

At the same time, in reality, significantly affected by the noise and clutters from background, the resolution of a distributed satellites SAR image decreases severely, which also suppresses the information in the image of fusion.

5.3 Multi-Static SAR Imaging as a Data Fusion Problem

5.3.1 Different data fusion schemes

Distributed satellites SAR is made of multiple channels and each channel could be viewed as a separate Bi-static SAR system. Thus for each channel, we consider the forward model of Bi-static SAR.

To handle the multichannel data processing characteristics in distributed satellites SAR systems, we propose three fusion schemes [MDZDF10].

Method 1: separate inversion followed by image fusion

Implementing inversion in the frequency domain for each set of data separately and then doing fusion in the spatial domain:

We first do inversion in the frequency domain for each set of data separately to get multi images, and then do incoherent processing to do spatial fusion.

This method is summarized as follows:

$$\begin{aligned}
 & G_1(k_x, k_y) - \boxed{\text{Inversion}} - \hat{f}_1(x, y) \\
 & M_1(k_x, k_y) \longrightarrow \boxed{\text{Fusion}} \longrightarrow \hat{f}(x, y) \longrightarrow \hat{G}(k_x, k_y) \\
 & G_2(k_x, k_y) - \boxed{\text{Inversion}} - \hat{f}_2(x, y) \\
 & M_2(u, v)
 \end{aligned}$$

which means that: we use each data set to do image reconstruction independently and then combine the results to obtain final results. We have to notice that the images in the fusion step need registration. Then, the inversion can be safely operated as image reconstruction with one data set.

5.3.2 - Bayesian data fusion

Method 2: data fusion followed by inversion

Implementing fusion in the frequency domain and then doing inversion in the spatial domain:

By coherent processing method, we first do fusion in the frequency domain and then based on the fused data to get the final image. This algorithm needs compensation for time delay and makes use of the overlap spectra to realize multi channel coherent adding.

The core problem is how to realize coherent adding in the frequency domain [MDDF09].

This method can be summarized as follows:

$$\begin{array}{c} G_1(k_x, k_y) \\ M_1(k_x, k_y) \\ \hline | \longrightarrow \quad G(k_x, k_y) \\ G_2(k_x, k_y) \\ M_2(k_x, k_y) \end{array} \longrightarrow \boxed{\text{Inversion}} \longrightarrow \hat{f}(x, y) \longrightarrow \widehat{G}(k_x, k_y)$$

To get data fusion of $G_1(k_x, k_y)$ and $G_2(k_x, k_y)$, we use mean value of common regions and use them individually in other independent regions:

$$G(k_x, k_y) = \begin{cases} (G_1(k_x, k_y) + G_2(k_x, k_y))/2 & (k_x, k_y) \in M_1(k_x, k_y) \cap M_2(k_x, k_y) \\ G_1(k_x, k_y) & (k_x, k_y \in M_1(k_x, k_y)) \\ G_2(k_x, k_y) & (k_x, k_y \in M_2(k_x, k_y)) \end{cases}$$

Method 3: joint data fusion and inversion

Implementing joint fusion and inversion:

$$\begin{array}{c} G_1(k_x, k_y) \\ M_1(k_x, k_y) \\ \hline | \longrightarrow \boxed{\text{Fusion} \\ \text{and} \\ \text{Inversion}} \longrightarrow \hat{f}(x, y) \longrightarrow \begin{array}{c} -\widehat{G}_1(k_x, k_y) \\ -\widehat{G}_2(k_x, k_y) \end{array} \\ G_2(k_x, k_y) \\ M_2(k_x, k_y) \end{array}$$

5.3.2 Bayesian data fusion

By utilizing two data sets simultaneously, we do joint fusion and inversion. Assuming that we have two data set $G_1(k_x, k_y)$ and $G_2(k_x, k_y)$, the objective is to get the original target $f(x, y)$. Accordingly, the forward model can be written as

$$\begin{cases} \mathbf{g}_1 = \mathbf{H}_1 \mathbf{f} + \boldsymbol{\epsilon}_1 \\ \mathbf{g}_2 = \mathbf{H}_2 \mathbf{f} + \boldsymbol{\epsilon}_2 \end{cases} \quad (5.1)$$

which can be directly solved by

$$p(\mathbf{f} | \mathbf{g}_1, \mathbf{g}_2) \propto p(\mathbf{g}_1 | \mathbf{f}) p(\mathbf{g}_2 | \mathbf{f}) p(\mathbf{f}) \quad (5.2)$$

Suppose ϵ_1 and ϵ_2 are i. i. d. Gaussian white noise, with given variances $\sigma_{\epsilon_1}^2$ and $\sigma_{\epsilon_2}^2$, we have

$$p(\mathbf{f} | \mathbf{g}_1, \mathbf{g}_2) \propto \exp[-J(\mathbf{f})] \quad (5.3)$$

where

$$J(\mathbf{f}) = \frac{1}{\sigma_{\epsilon_1}^2} \|\mathbf{g}_1 - \mathbf{H}_1 \mathbf{f}\|_2^2 + \frac{1}{\sigma_{\epsilon_2}^2} \|\mathbf{g}_2 - \mathbf{H}_2 \mathbf{f}\|_2^2 - \ln p(\mathbf{f}) \quad (5.4)$$

by which to find the optimal estimation of \mathbf{f} . The expression of the solution depends on the choice of $p(\mathbf{f})$. For the Gaussian prior $p(\mathbf{f}) \propto \exp(-\frac{1}{\sigma_f^2} \|\mathbf{f}\|_2^2)$, we obtain:

$$-\ln p(\mathbf{f}) = \frac{1}{\sigma_f^2} \|\mathbf{f}\|_2^2 \quad (5.5)$$

and in this case there is an analytic solution which can be obtained by equating to zero the gradient of the $J(\mathbf{f})$:

$$\nabla J(\mathbf{f}) = -\frac{2}{\sigma_{\epsilon_1}^2} \mathbf{H}_1^t (\mathbf{g}_1 - \mathbf{H}_1 \mathbf{f}) - \frac{2}{\sigma_{\epsilon_2}^2} \mathbf{H}_2^t (\mathbf{g}_2 - \mathbf{H}_2 \mathbf{f}) + \frac{2}{\sigma_f^2} \mathbf{f} \quad (5.6)$$

which results in

$$\mathbf{f} = \left(\frac{1}{\sigma_{\epsilon_1}^2} \mathbf{H}_1^t \mathbf{H}_1 + \frac{1}{\sigma_{\epsilon_2}^2} \mathbf{H}_2^t \mathbf{H}_2 + \frac{1}{\sigma_f^2} \mathbf{I} \right)^{-1} \left(\frac{1}{\sigma_{\epsilon_1}^2} \mathbf{H}_1^t \mathbf{g}_1 + \frac{1}{\sigma_{\epsilon_2}^2} \mathbf{H}_2^t \mathbf{g}_2 \right) \quad (5.7)$$

One great difficulty in this fusion inversion method is the estimation of the hyperparameters $\sigma_{\epsilon_1}^2$, $\sigma_{\epsilon_2}^2$ and σ_f^2 .

This can be done if we assign them Inverse Gamma (IG) priors

$$\begin{cases} p(\sigma_{\epsilon_1}^2) = \text{IG}(\sigma_{\epsilon_1}^2 | \alpha_1, \beta_1) \\ p(\sigma_{\epsilon_2}^2) = \text{IG}(\sigma_{\epsilon_2}^2 | \alpha_2, \beta_2) \\ p(\sigma_f^2) = \text{IG}(\sigma_f^2 | \alpha_f, \beta_f) \end{cases} \quad (5.8)$$

and then considering the posterior $p(\mathbf{f}, \boldsymbol{\theta} | \mathbf{g})$ and then using either a JMAP or a VBA method.

The expression of the criterion of JMAP is obtained by

$$(\hat{\mathbf{f}}, \hat{\boldsymbol{\theta}}) = \arg \max_{\mathbf{f}, \boldsymbol{\theta}} p(\mathbf{f}, \boldsymbol{\theta} | \mathbf{g}) \quad (5.9)$$

by alternate optimization with respect to \mathbf{f} , then to each of the three variables of $\boldsymbol{\theta} = (\sigma_{\epsilon_1}^2, \sigma_{\epsilon_2}^2, \sigma_f^2)$.

Data fusion with Separable Generalized Gaussian Distribution

To exploit the sparsity of scene, we adopt the Separable Gaussian Distribution to model the prior distribution of the target complex reflectivity.

$$p(\mathbf{f}) \propto \exp \left\{ -\gamma \sum_j |f_j|^\beta \right\} \propto \exp \left\{ -\gamma \|\mathbf{f}\|_\beta^\beta \right\} \quad (5.10)$$

5.4.1 - Results with synthetic data

In this case, the gradient of the $J(\mathbf{f})$ becomes

$$\nabla J(\mathbf{f}) = -\frac{2}{\sigma_{\epsilon_1}^2} \mathbf{H}_1^t (\mathbf{g}_1 - \mathbf{H}_1 \mathbf{f}) - \frac{2}{\sigma_{\epsilon_2}^2} \mathbf{H}_2^t (\mathbf{g}_2 - \mathbf{H}_2 \mathbf{f}) + \frac{2}{\sigma_f^2} \beta \Lambda(\mathbf{f}) \mathbf{f} \quad (5.11)$$

where

$$\Lambda(\mathbf{f}) = \text{diag} [(|f_j|^2 + \zeta)^{\beta/2-1}] \quad (5.12)$$

5.4 Experiments and Analysis

5.4.1 Results with synthetic data

Simulation 1: complex data of (Target 1/Target 2)

In this section, we consider Target 1 and Target 2 with complex reflectivity. Figure 5.1 show the reconstruction results of Target 1 from the two partial frequency observation separately. The fusion results are shown in Figure 5.2. Figure 5.3 show the reconstruction results of Target 2 from the two partial frequency observation separately. The fusion results are shown in Figure 5.4.

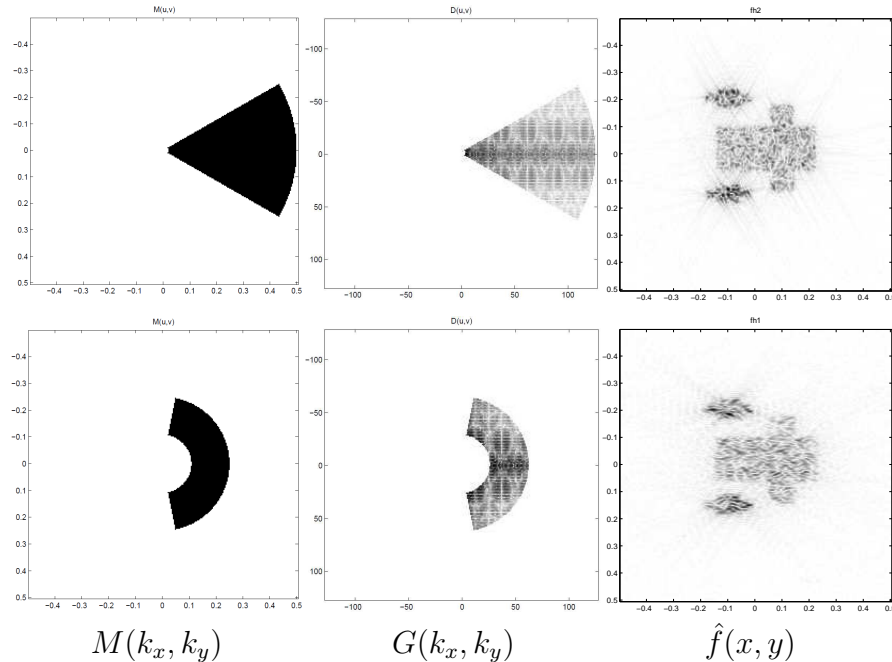


Figure 5.1: Reconstruction results for two different geometries and bandwidths observed data on Target 1 (complex values), magnitude displayed in reverse video.

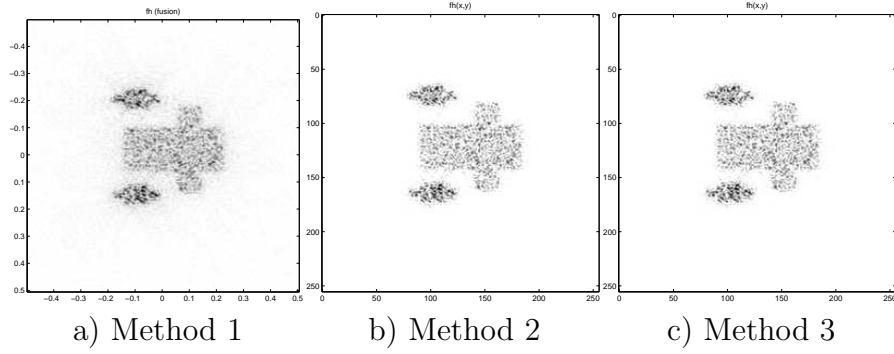


Figure 5.2: Fusion results on Target 1 (complex values), magnitude displayed in reverse video: a) Method 1: separate inversion and fusion; b) Method 2: data fusion and inversion; c) Method 3: joint data fusion and inversion.

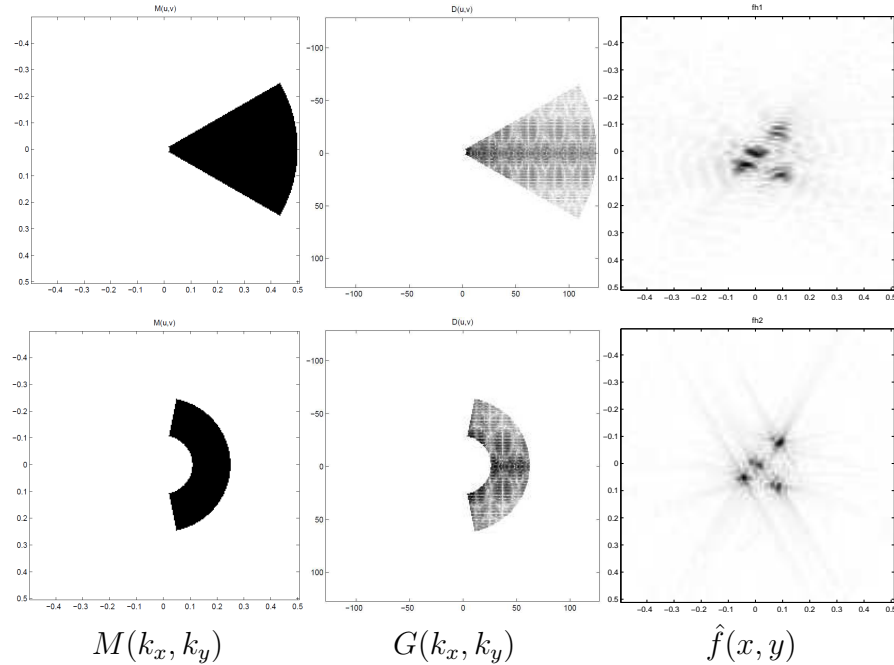


Figure 5.3: Reconstruction results for two different geometries and bandwidths observed data on Target 2 (complex values), magnitude displayed in reverse video.

Simulation results analysis

Based on the fusion results, we can see that all three fusion methods have improved the resolution. Reconstructed target images looking clearer and easier to interpret. Among them, with method 3, the Bayesian joint fusion and reconstruction method, the result shows certain distinct features. The resolution is also improved.

Table 5.2 illustrates the relative distance for reconstruction results with different fusion methods. The proposed Bayesian method with the least relative reconstruction errors, has the best performance compared with the other two methods.

5.4.2 - Results with experimental data

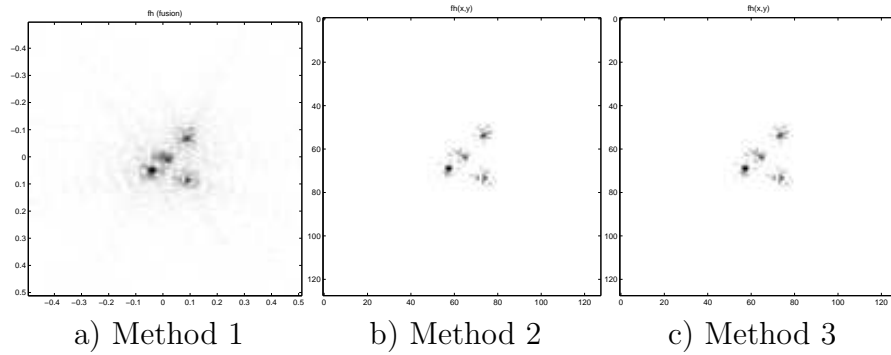


Figure 5.4: Fusion results on Target 2 (complex values), magnitude displayed in reverse video: a) Method 1: separate inversion and fusion; b) Method 2: data fusion and inversion; c) Method 3: joint data fusion and inversion.

Table 5.2: Comparison of reconstruction performances of three methods on two complex-valued targets.

Fusion methods	Target 1	Target 2
Method 1 ($I \rightarrow F$)	0.89	0.69
Method 2 ($F \rightarrow I$)	0.54	0.59
Method 3 ($F \& I$)	0.51	0.54

5.4.2 Results with experimental data

The proposed method has been applied on the experimental data of the French Aerospace Lab. The measurement is done with the stepped frequency signal. There are three target compositions, for each composition, using two full polarization radar bandwidth observed data to do inversion [Far08].

Measurement system description

The measurement system mainly consists of:

- A vector network analyzer;
- A positioning system for moving the receiving antenna on a circular arc;
- Antenna polarization horizontal and vertical of the transmitter and receiver;
- A set of four spheres constituting the measured scene.

Figure 5.5 [Far08] illustrates the imaging geometry. Table 5.3 presents the measurement parameters.

Results analysis

Figure 5.6 illustrates the inversion results on real data measurements. In the first row, three different original targets made of 1 sphere, 2 and 4 spheres are presented. In the second, the third and the fourth rows, the inversion results of three original targets are presented, using Band 1, Band 2 and Band 1& Band 2 with the proposed Bayesian method (Method 3), respectively.

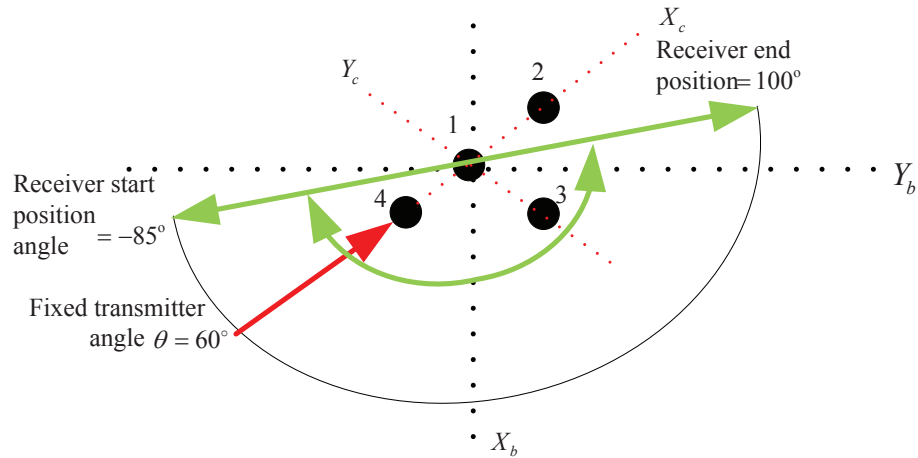


Figure 5.5: Real data imaging geometry.

Table 5.3: Experimental measurement parameters

Observed target	three target compositions (1,2,4 spheres)
Transmitter position	The fixed position of transmitter
Receiver position	The emission axis passes through the center stage 0 with an elevation angle of 35° to the plan (Xb, Yb) and 60° to the Plan (Zb, Xb).
Transmitter bandwidth	The receiver moves in the (Xb, Yb) on a circular path of 5m.
	BF1=(1.16-1.98)GHz, VV polarization BF2=(1.47-1.68)GHz, VV polarization

Comparing the results of both simulated and real data, we can see that:

1. Method 1, using multi images inverted in the frequency domain to do data-level fusion, has the problem of data dependency, the fused result is not satisfying;
2. Method 2, using a simple combination of the spectrum data, whose performance is affected by the average result; meanwhile, for neglecting the unknown information in the frequency domain, the resolution of reconstruction is limited.
3. Method 3, using a joint fusion and reconstruction, has the best reconstruction performance. The advantages of the proposed methods include: based on Bayesian inference, by combining all observations to supply a unique and optimal estimation, the more accurate results can be obtained. Thanks to the prior information introduced by the proposed inversion method taking into account of features of the target as well as the system imaging geometry into the forward modeling.

5.5 Conclusions

Based on the Bayesian MAP estimation, three data fusion and inversion methods for distributed satellite SAR were proposed. Through comparing results on simulated and real data, the Bayesian joint fusion and reconstruction method performed better than the other two methods. An optimal estimation based on different frequency bands was realized. Problems of target information loss as well as the data bands dependency caused by conventional methods were avoided. The proposed method showed the application potential in distributed SAR systems.

The content and experimental results of this chapter are also in papers [[MDZDF10](#), [MDDF09](#)].

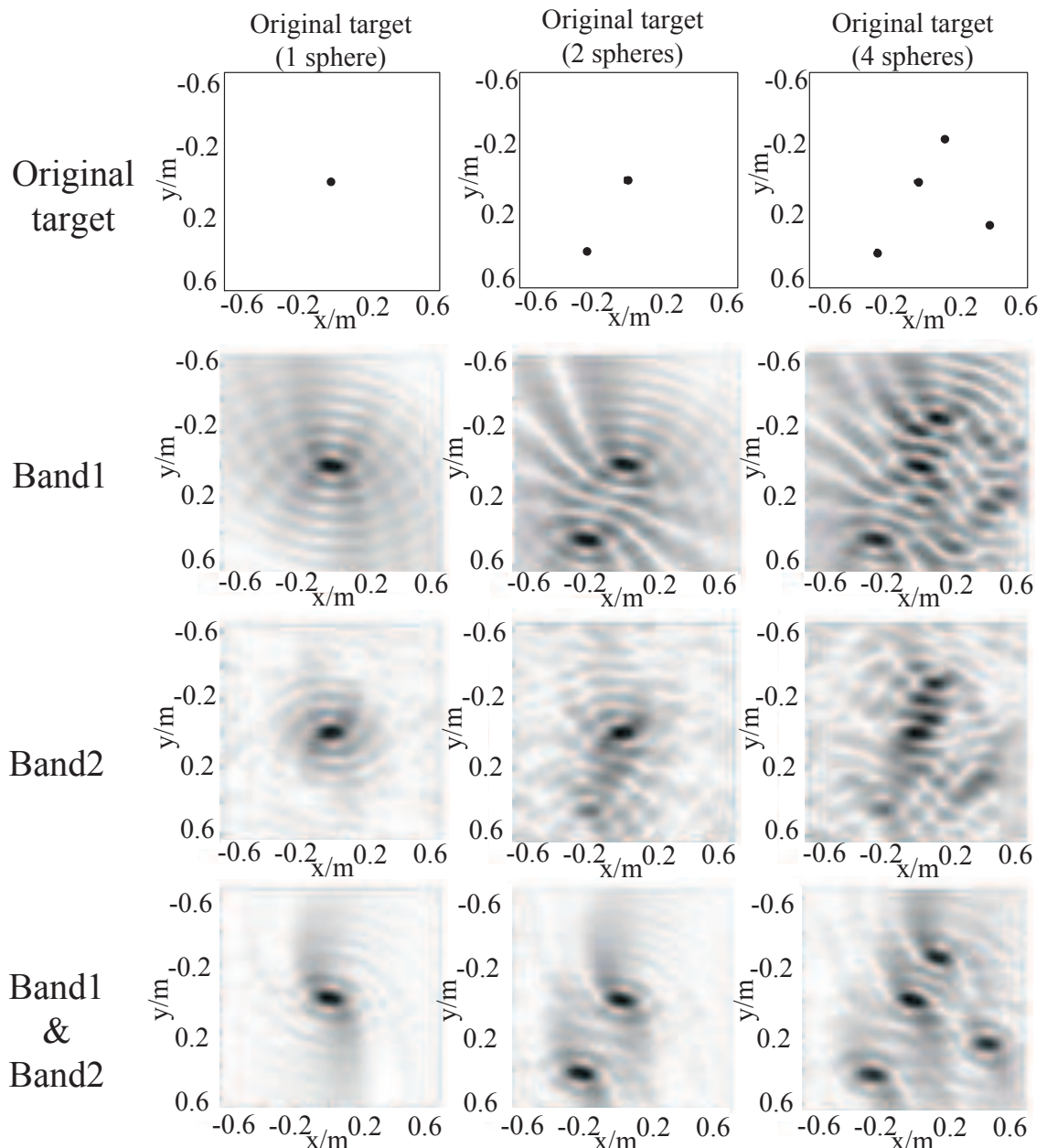


Figure 5.6: Results on real data (complex values), magnitude displayed in reverse video.

Part III

Application to SAR Micromotion Target Imaging

6

Bayesian Approach for SAR Micro-Motion Target Imaging

6.1 Introduction

In the previous chapters, we have studied the problem of SAR imaging for different geometries. The problem is considered as a linear inverse problem of Fourier Synthesis (FS). Then, we combine our knowledge of the unknown target scene with observed data and solve the imaging problem in a Bayesian framework.

All the targets above are considered as stationary. For a moving target, unfortunately, the problem becomes to be more complicated. Although there exists a well known technique of SAR Ground Moving Target Indication (SAR-GMTI) for the air- and spaceborne radar, which takes advantage of the movement of the target and sensor by defocusing and/or displacement induced by target motions. However, it no longer works for the situation that the target experiences non-uniform accelerating translation, especially for more complex motions such as rotation, vibration, sinusoidal motion and rocking (named as micromotion) [DWQ⁺09].

Micromotion results in complicated nonlinear phase histories on SAR echo. Unfortunately the classical imaging methods can not handle it any more. The effects induced by micromotion on SAR images include gray strip, disordered lines, ghost points, fences, blurred lines, displaced points, *etc.*, making it more difficult to be interpreted.

In this chapter, we consider the problem of micromotion target imaging as a signal sparse representation problem. We adopt a parametric model and propose a Bayesian approach for the solution.

This chapter is organized as follows. In Section 6.2 we analyze the micromotion effect on SAR imaging, and give an overview of current research on SAR micromotion target imaging. Based on the analysis, we propose a BCS (Bayesian Compressive Sensing)

6.2.2 - Effects on SAR imaging

method to solve this problem. To do this, firstly, in 6.4 we establish the SAR echo model on micromotion target. In Section 6.5.1 we review the different sparse modeling and optimization criteria. In particular, l_1 regularization approach conducts us to the Bayesian approach which is developed in Section 6.5.2. We propose two priors as Separable Generalized Gaussian prior and *Student-t* prior. In Section 6.6 we carry out simulations and analyze the performance of the proposed approach. Finally in Section 6.7, we draw our conclusions.

6.2 Micromotion Effect on SAR Imaging

6.2.1 Definition of micromotion

In nature, micromotion widely spreads in variety forms, such as the movement of human's body, the swing of legs, the vibration of a bridge, *etc.*; in the military context, such as the rotating antenna in air defense positions, a large fan for the air-conditioned vehicle engine, rotating windmills, wheels, vibrated bumps of a moving vehicle, swing ships, rotation antenna of ship-borne radar, the rotor with the rotation high-speed of helicopter, *etc.* [TSQ⁺10]. All these non-uniformly accelerated motion of targets or target components (such as vibration and rotation) are commonly referred as micromotion.

Definition 2. *Micromotion is a collective definition referred to slightly back and forth movement or the movement of the target or target component along the cross direction relatively to radar*

For a single scattering target, micromotion presents in its back and forth movement; For multiple scattering target, micromotion presents in its non-rigid movement. Non-rigid body motion refers to the relative motion between the constituent parts of a target, such as vibration and rotation of parts. Back and forth is a broader concept than cyclical, may contain more than one periodic component. In addition, although this definition excludes the simple accelerated motion, yet accelerated motion can be viewed as the combination components of translation and micromotion [Den11].

6.2.2 Effects on SAR imaging

Target micromotion and micro-Doppler are attracting an increasingly wide interest from the SAR community for providing additional and favorable information of targets. Micromotion parameters, such as the rotating frequency and radius, record the attributed information. Thus their estimation is very important for micromotion compensation and focusing in SAR imagery. The estimated results can also be directly used as features for target recognition.

However, it is a huge challenge for micromotion parameter estimation in SAR, because i) micromotion-target signals are hard to be separated from stationary-clutter ones, ii) they are also distributed over multiple range cells (especially for large rotating radii), i.e. Range Cell Migration (RCM), which is disadvantageous for target energy integration and iii) they will cause Doppler aliasing in the slow time domain when the

maximum micro-Doppler exceed the Pulse Repetitive Frequency (PRF). It is not practical to estimate them in the SAR gray image domain because of defocusing, ghost image and other energy-spread image characteristics induced by target micromotion.

Figure 6.1 [LDQL11] illustrates the different micromotion effect on SAR imaging, with the presence on the frequency-time plane.

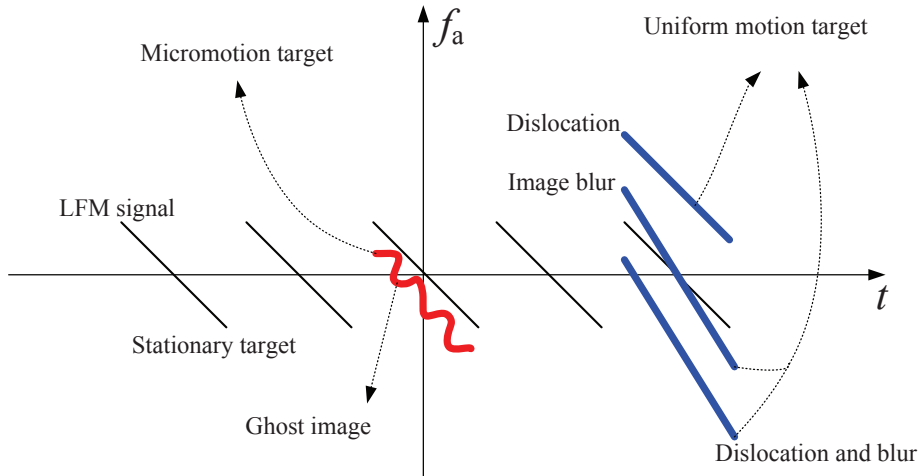


Figure 6.1: Micromotion effect on SAR imaging (time-frequency plane).

Conventional SAR/GMTI [GLB11, EGM08, GS07, SGC06] technology takes the target motion as to be uniform or only with radial acceleration and perform the focusing process with the second order distance model. It can achieve target detection with uniform motion in a SAR stationary scene, parameter estimation and re-focusing imaging of the position and movement.

However, for micromotion targets, due to the more complicated movements than uniform motion, conventional MTI technology can no longer be used.

6.3 Conventional Methods for SAR Micromotion Target Imaging

6.3.1 Conventional imaging methods

A few algorithms have been proposed for the estimation of SAR micromotion targets [TSQ⁺10, STC98, SK03, Spa05]. All of them manipulate a single range cell and take micromotion-target azimuthal echoes as Sinusoidal Frequency-Modulated (SFIM) signals. The cyclic spectral density [STC98], a time-frequency method [Spa05] and the adaptive optimal kernel one [SK03] have been used to estimate the vibrating frequency of simulated or real SAR targets. Then in [TSQ⁺10], the wavelet or chirplet decomposition is used to separate the signal of a rotating radar dish from that of stationary clutter and then auto correlation is utilized to get its rotating frequency.

6.3.2 - Compressive Sensing (CS) methods

All these methods, however, haven't addressed the aforementioned three key problems ever-present in SAR, i.e., clutter, RCM and Doppler aliasing, which hinder their application in reality. In effect, unlike uniformly moving targets, RCM correction is very difficult for micromotion ones due to their sinusoidal range history [DWQ⁺09].

Matched Filter (MF) [TG60] plays an important role in moving target imaging [WHB06, CB08], which performs a multidimensional reconstruction at every pixel for every possible velocity of the motion, resulting in a huge space-velocity cube [WHB06]. Worse still, for the fact that each slice of the velocity is estimated independently, it brings in ambiguous results. To improve this, an adaptive matched filtering method, called filtered back projection was proposed [CB08]. However, all these methods yield high computational cost and ambiguity unavoidably caused by the independent estimation. Figure 6.2 illustrates the parameter quantitative (super)cube of MF method for SAR micromotion target imaging [Den11].

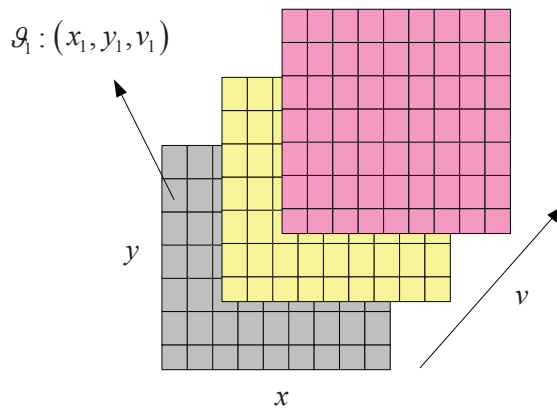


Figure 6.2: Parameter quantitative (super)cube.

For micromotion target imaging, conventional imaging method deals with it simply by increasing micro-parameters which leads to a huge parameter cube. In addition, the resolution is limited by high side lobes.

6.3.2 Compressive Sensing (CS) methods

According to Nyquist sampling theorem, the minimum requirement of sampling rate to accurately reconstruct a signal is twice of its bandwidth. For SAR high resolution imaging, depending on the classical sampling theory, high sampling rate is obligatorily needed. However, in large scale problems it may lead to serious computational problems.

Fortunately, by CS [Don92, Don06b, Don06a, CRT06b, CRT06a, CRT08] and sparse signal representation [SK10b, SK10c, PSZ08, ZWL08], it is possible to reconstruct the sparse signals accurately from a highly incomplete number of samples [CICB10, DT10, FL09, ZR11]. [SK10b] proposed a joint spatial reflectivity signal inversion method based on an over-complete dictionary of target velocities for SAR moving targets imaging.

In this chapter, we focus on the parametric method to solve SAR micromotion target imaging problem, which circumvents the tough issues mentioned above. The scattering

center model thus must also include target micromotion parameters. However, higher dimensions of parameters will bring difficulties to fast and global optimization. Fortunately, we observe a fine sparsity of target due to the increase of the parameter space dimension.

Thus, based on the fact that typical underlying scenes exhibit sparsity, if we consider the imaging observation system as a transform matrix which turns to be an over-complete dictionary, the imaging process can be viewed as the sparse signal representation of observed data by use of this dictionary.

It is noteworthy that CS-based method is sensitive to noise and clutters. In addition, in the problem of parameter estimation, the valuation of model parameters is difficult to be determined and normally affects the accuracy. Fortunately, Bayesian accounts for additive noise encountered in the compressed measurement process [XPC12]. Moreover, with Bayesian approach, optimal model parameters can also be automatically estimated [BMK10a, JYC08, LXC08]. So we can combine CS theory with the Bayesian method for this parameter estimation problem.

6.3.3 Comprehensive analysis

In summary, the preliminary study of SAR micromotion target imaging has been carried out, with the research mainly focused on the micro-target separation, time-frequency analysis and parameter estimation. However, there are still various challenges for current methods:

1. Target motion model is still relatively simple;
2. Not accounting for noise and clutter;
3. Not considering the micro additional range cell migration;
4. Not considering the situation that multi targets with different motion parameters.

We recast the problem with a parametric model and propose a Bayesian CS (BCS) method approach to exploit target priors, to account for noise and to estimate the model parameters based on the sparse signal representation. Figure 6.3 illustrates the frame of our proposed approach [Den11, ZMDW⁺12].

The proposed approach for SAR micromotion imaging presents the following advantages:

1. Realizing the joint estimation of motion and scattering parameters estimation;
2. Dealing with missing data;
3. Achieving high resolution imaging with narrow main lobe (super resolution) and low side lobe;
4. Especially solving the problem of multiple targets within the same range cell.

6.4 Forward Modeling

The forward model in this section directly works on echo domain, with the goal to establish the measurement model for target with any motion. The proposed observation

6.3.3 - Comprehensive analysis

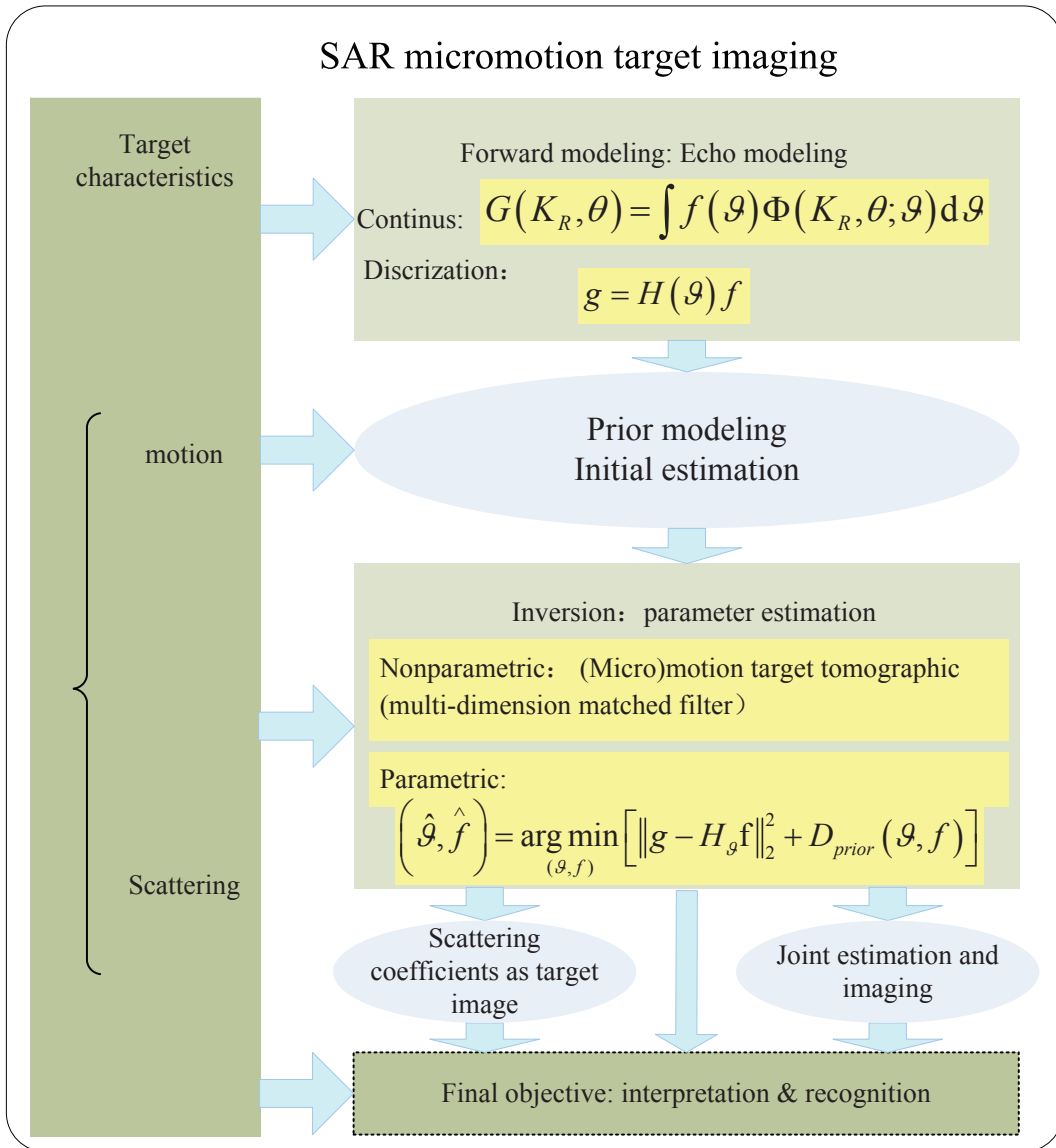


Figure 6.3: Joint estimation and imaging frame.

model can be viewed as the first class of Fredholm equation. Parameters of micromotion are combined with scattering centers to form a motion-scattering mixed model. The objective is to obtain the parametric information of the existence, the movement and the scattering information.

As illustrated in Figure 6.4, the radar moves at velocity V_a . Then for slowtime t it moves to

$$y' = V_a t = R_c \tan \theta \approx R_c \theta. \quad (6.1)$$

R_c is the vertical distance of the sensor path to the origin of the target scene. We may see that θ has the similar meaning as slow time t . In real case, R_c is comparatively very large, while θ is very small.

Considering an arbitrarily moving target, let vector ϑ represent the target micro-motion parameters, such as the initial position (x, y) , velocity, rotation frequency, etc.

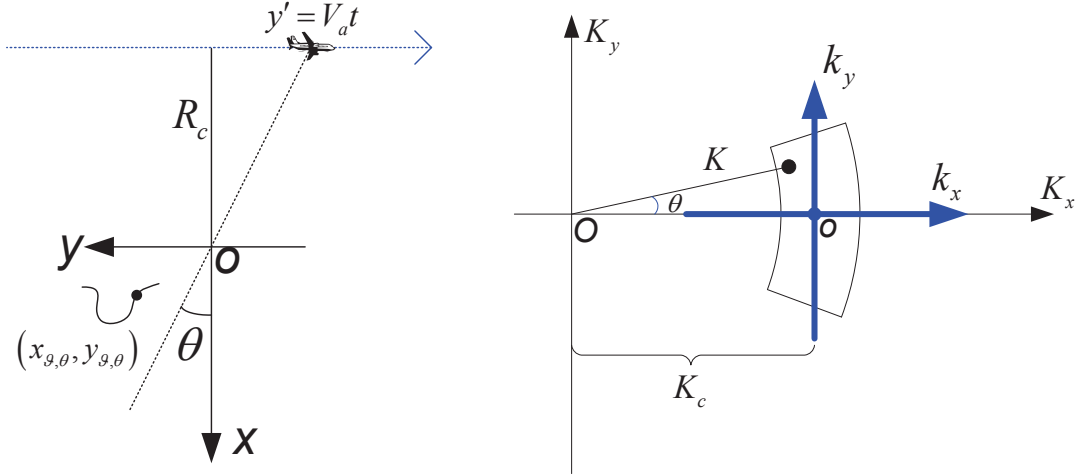


Figure 6.4: Micromotion target imaging geometry: a) The SAR imaging geometry in slant plane; b) The corresponding configuration in wavenumber space.

Suppose the target moves to $(x_{\vartheta,\theta}, y_{\vartheta,\theta})$ when radar is located at y' . $f(\vartheta)$ is the scattering coefficient. Thus the distance model of the target is

$$\begin{aligned} R_\vartheta(\theta) &= \sqrt{(R_c + x_{\vartheta,\theta})^2 + (y' + y_{\vartheta,\theta})^2} \\ &\approx \sqrt{R_c^2 + y'^2} + x_{\vartheta,\theta} \cos \theta + y_{\vartheta,\theta} \sin \theta \end{aligned} \quad . \quad (6.2)$$

Spotlight SAR echo of the target could be represented in the wavenumber domain as

$$\begin{aligned} s(K, \theta; \vartheta) &= P(K) \exp \left[-jK \sqrt{R_c^2 + y'^2} \right] \\ &\cdot \exp [-jK(x_{\vartheta,\theta} \cos \theta + y_{\vartheta,\theta} \sin \theta)], \end{aligned} \quad (6.3)$$

where $P(K)$ is the Fourier transform (FT) of the transmitted signal. Then the total echoes of all targets are

$$S_{\text{total}}(K, \theta) = \int f(\vartheta) s(K, \theta; \vartheta) d\vartheta. \quad (6.4)$$

After range compression and motion compensation, the first two terms of $s(\cdot)$ in Equation (6.3) disappear, and then the target signal model becomes

$$G(K, \theta) = \int f(\vartheta) \exp [-jK(x_{\vartheta,\theta} \cos \theta + y_{\vartheta,\theta} \sin \theta)] d\vartheta. \quad (6.5)$$

When the target experiences micromotion, e.g., rotation or vibration, we have

$$x_{\vartheta,\theta} = x + r_m \cos (2\pi f_m t + \varphi^0), \quad (6.6)$$

$$y_{\vartheta,\theta} = y + r_m \sin (2\pi f_m t + \varphi^0), \quad (6.7)$$

6.3.3 - Comprehensive analysis

where micromotion parameters compose a parameter vector

$$\vartheta \triangleq (x, y, r_m, f_m, \varphi^0) \quad (6.8)$$

and (x, y) is the position of the micromotion center, r_m is the micromotion amplitude, i.e., rotating radius or vibrating amplitude, f_m is the micromotion frequency and φ^0 is the initial micromotion phase. Substituting Equations (6.6) and (6.7) into (6.5) leads to

$$G(K, \theta) \approx \int f(\vartheta) \cdot h(K, \theta; \vartheta) d\vartheta, \quad (6.9)$$

where

$$\begin{aligned} h(K, \theta; \vartheta) &\triangleq \exp(-jKx \cos \theta - jKy \sin \theta) \\ &\cdot \exp\left(-jK r_m \cos\left(\frac{2\pi f_m R_c}{V_a} \tan \theta + \varphi^0\right)\right) \end{aligned} \quad (6.10)$$

We can clearly see that, Equation (6.10) has an additional exponential component representing target micromotion, compared with the stationary scattering center model [SK03].

We now try to discretize Equation (6.10). Without loss of generality, suppose there are I rotated targets. Then for the i th one, let f_i denote the scattering coefficient, ϑ_i denote the micromotion parameter, both of which are unknown. The model of Equation (6.9) can be discretized as

$$G(K, \theta) = \sum_{i=1}^I f_i \cdot h(K, \theta; \vartheta_i) + \epsilon_i(K, \theta), \quad (6.11)$$

where noise has been added via $\epsilon_i(K, \theta)$. Note K and θ can also be discretized into M and N values respectively. Therefore Equation (6.11) can be expressed in a matrix form as

$$\mathbf{g} = \mathbf{H}\mathbf{f} + \boldsymbol{\epsilon}, \quad (6.12)$$

where

$$\mathbf{g} = [G(K_1, \theta_1), \dots, G(K_1, \theta_N), G(K_2, \theta_1), \dots, G(K_2, \theta_N), \dots, G(K_M, \theta_1), \dots, G(K_M, \theta_N)]^T \quad (6.13)$$

is a vector of size MN representing the data,

$$\boldsymbol{\epsilon} = [\epsilon(K_1, \theta_1), \dots, \epsilon(K_1, \theta_N), \epsilon(K_2, \theta_1), \dots, \epsilon(K_2, \theta_N), \dots, \epsilon(K_M, \theta_1), \dots, \epsilon(K_M, \theta_N)]^T \quad (6.14)$$

is a vector of size MN representing the errors (modeling and measurement),

$$\mathbf{H} = \begin{bmatrix} h(K_1, \theta_1; x_1, y_1, r_{m_1}, f_{m_1}, \varphi_1^0) & h(K_1, \theta_1; x_1, y_1, r_{m_1}, f_{m_1}, \varphi_2^0) & \dots & h(K_1, \theta_1; x_{N_x}, y_{N_y}, r_{m_P}, f_Q, \varphi_J^0) \\ h(K_1, \theta_2; x_1, y_1, r_{m_1}, f_{m_1}, \varphi_1^0) & h(K_1, \theta_2; x_1, y_1, r_{m_1}, f_{m_1}, \varphi_2^0) & \dots & h(K_1, \theta_2; x_{N_x}, y_{N_y}, r_{m_P}, f_Q, \varphi_J^0) \\ \vdots & \vdots & \ddots & \vdots \\ h(K_M, \theta_N; x_1, y_1, r_{m_1}, f_{m_1}, \varphi_1^0) & h(K_M, \theta_N; x_1, y_1, r_{m_1}, f_{m_1}, \varphi_2^0) & \dots & h(K_M, \theta_N; x_{N_x}, y_{N_y}, r_{m_P}, f_Q, \varphi_J^0) \end{bmatrix} \quad (6.15)$$

is a matrix of dimensions $MN \times N_x N_y P Q J$ representing the forward modeling matrix system and

$$\mathbf{f} = \{[A(x_{n_x}, y_{n_y}, r_{m_p}, f_{m_q}, \varphi_j^0)], n_x = 1, \dots, N_x, n_y = 1, \dots, N_y, m_p = 1, \dots, P, m_q = 1, \dots, Q, j = 1, \dots, J\} \quad (6.16)$$

is a vector of size $N_x N_y P Q J$ of parameters representing targets in the scene. In this expression $A(x_{n_x}, y_{n_y}, r_{m_p}, f_{m_q}, \varphi_j^0)$ is the coefficient at position (x_{n_x}, y_{n_y}) with micromotion frequency f_q , micromotion range r_p and initial micromotion phase φ_j^0 .

Then, the problem of scattering and micromotion parameter estimation can be formulated as a linear inversion problem subject to sparsity constraints.

6.5 Bayesian Inversion

6.5.1 Sparse signal representation and deterministic optimization

The main idea behind sparse signal representation is, to find the most compact representation of a signal as a linear combination of a few elements (or atoms), in an over-complete dictionary [Don06a, BCDH10, DET06, DH01]. Compared with the conventional orthogonal transform representation, this most parsimonious representation of a signal over a redundant collection of generated basis offers efficient capability of signal modeling. Finding such a sparse representation of a signal involves solving an optimization problem. Mathematically, it can be formulated as follows. For Equation (6.12), assume $\mathbf{g} = \mathbf{H}\mathbf{f}$ in absence of noise where $\mathbf{g} \in \mathbb{C}^{M \times 1}$ is a vector of data, $\mathbf{H} \in \mathbb{C}^{M \times N}$ a matrix whose elements can be considered as an over-complete dictionary as its columns and $\mathbf{f} \in \mathbb{C}^{N \times 1}$ the corresponding linear coefficients. In particular, $M \ll N$ leads the null space of Φ to be non-empty such that there are many different possibilities to represent \mathbf{g} with the elements in \mathbf{H} . The problem of sparse representation is then to find the coefficients \mathbf{f} with the most few non-zero elements, i.e., $\|\mathbf{f}\|_0$ is minimized while $\mathbf{g} = \mathbf{H}\mathbf{f}$. Formally,

$$\min_{\mathbf{f}} \|\mathbf{f}\|_0 \quad s.t. \quad \mathbf{g} = \mathbf{H}\mathbf{f} \quad (6.17)$$

where $\|\mathbf{f}\|_0$ is the l_0 norm which is the cardinality of \mathbf{f} . However, the combinatorial optimization problem Equation (6.17) is NP-hard and intractable. A large body of approximation methods are proposed to address this optimization problem, such as greedy pursuit [TGS06] based methods like matching pursuit [NV10], or convex-relaxation [Tro06] based methods that replace the l_0 with the l_1 norm,

$$\min_{\mathbf{f}} \|\mathbf{f}\|_1 \quad s.t. \quad \mathbf{g} = \mathbf{H}\mathbf{f} \quad (6.18)$$

Candes et al. [CRT06a] show that for K -sparsity signal that only has K non-zero element in \mathbf{f} , the reconstruction of \mathbf{f} with $M \geq O(K \log(N/K))$ [Don06a] measures can be achieved with high probability by l_1 norm minimization. Moreover, to efficiently reconstruct \mathbf{f} , the mapping matrix \mathbf{H} should satisfy the *Restricted Isometry Property* (RIP) [CRT08, YBZS10] which requires that

$$(1 - \delta_s) \|\mathbf{f}\|_2^2 \leq \|\mathbf{H}\mathbf{f}\|_2^2 \leq (1 + \delta_s) \|\mathbf{f}\|_2^2 \quad (6.19)$$

This RIP of \mathbf{H} is connected to the mutual coherence between the atoms of the dictionary which is defined as

$$\mu(\mathbf{H}) = \max_{i \neq j} \frac{|\langle h_i, h_j \rangle|}{\|h_i\|_2^2 \|h_j\|_2^2} \quad (6.20)$$

where the h_i is the i th column of \mathbf{H} . Large mutual coherence indicates that two atoms that are closely related will degrade the reconstruction algorithm. Hence, the dictionary

6.5.2 - Bayesian sparse reconstruction

is required to have low coherence so that the submatrix \mathbf{H} with K atoms is nearly orthogonal [DH01].

If the observation \mathbf{g} is noisy, the problem of the sparse representation for a noisy signal can be formulated as

$$\min_{\mathbf{f}} \|\mathbf{f}\|_1 \quad s.t. \quad \|\mathbf{g} - \mathbf{H}\mathbf{f}\|_2^2 \leq \delta, \quad (6.21)$$

where δ is a noise allowance. Equivalently, the Equation (6.21) can be reformulated to minimize the following objective function

$$L(\mathbf{f}; \lambda) = \|\mathbf{g} - \mathbf{H}\mathbf{f}\|_2^2 + \lambda \|\mathbf{f}\|_1, \quad (6.22)$$

where $\lambda > 0$ is the regularization parameter that balances a trade-off between the reconstruction error and the sparsity of \mathbf{f} . The formulation Equation (6.22) can also be interpreted as the MAP estimation in the Bayesian philosophy as we will see in the next section.

To this end, the micromotion parameter estimation is now cast as the sparse reconstruction of \mathbf{f} associated with the parameter hypothesis at the position of non-zero elements of \mathbf{f} . There are a large number of methods to solve the Equations (6.21) or (6.22), such as the method of compressive sampling matching pursuit (CoSaMP) presented in [NT08] which has been widely used for its simplification and effectiveness. Here, we will compare our proposed method with this method.

6.5.2 Bayesian sparse reconstruction

Even if the sparse representation has originally been introduced as an optimization problem such as Equations (6.17), (6.18), (6.21), or (6.22), it can also be presented as a Bayesian MAP estimation problem [MD06a, Tip01]:

$$\hat{\mathbf{f}} = \arg \max_{\mathbf{f}} \{p(\mathbf{f}|\mathbf{g})\}, \quad (6.23)$$

where

$$p(\mathbf{f}|\mathbf{g}) = \frac{p(\mathbf{g}|\mathbf{f}) p(\mathbf{f})}{p(\mathbf{g})} \propto p(\mathbf{g}|\mathbf{f}) p(\mathbf{f}), \quad (6.24)$$

To understand this, firstly let us assume the error ϵ in Equation (6.12) is centered, Gaussian and white: $\epsilon \sim \mathcal{N}(\epsilon|0, \sigma_\epsilon \mathbf{I})$. It brings us to the expression of the likelihood:

$$p(\mathbf{g}|\mathbf{f}) = \mathcal{N}(\mathbf{H}\mathbf{f}, \sigma_\epsilon \mathbf{I}) \propto \exp \left\{ -\frac{1}{2v_\epsilon} \|\mathbf{g} - \mathbf{H}\mathbf{f}\|_2^2 \right\} \quad (6.25)$$

Secondly, choose the separable double exponential probability density [Wil95] as the prior of \mathbf{f} :

$$p(\mathbf{f}) \propto \exp \left\{ -\gamma \sum_j |f_j| \right\}, \quad (6.26)$$

it is then easy to see that the MAP estimation with this prior becomes

$$\hat{\mathbf{f}} = \arg \max_{\mathbf{f}} \{p(\mathbf{f}|\mathbf{g})\} = \arg \min_{\mathbf{f}} \{-\ln p(\mathbf{f}|\mathbf{g})\} = \arg \min_{\mathbf{f}} \{J(\mathbf{f})\} \quad (6.27)$$

with

$$J(\mathbf{f}) = \|\mathbf{g} - \mathbf{H}\mathbf{f}\|_2^2 + \lambda\|\mathbf{f}\|_1, \quad \text{with } \lambda = 2v_\epsilon \quad (6.28)$$

which can be compared to Equation (6.22).

The prior information that the targets are sparsely distributed in the observation scene can be modeled by the two following probability density functions (PDF) [MD12, MD11]:

- Generalized Gaussian priors:

$$p(\mathbf{f}) \propto \exp \left\{ -\gamma \sum_j |f_j|^\beta \right\}, \quad (6.29)$$

which give the double exponential for $\beta = 1$ and Gaussian for $\beta = 2$ and are also more useful for sparse representation with $0 < \beta < 1$. With these priors, the MAP estimate can be computed by optimizing the following criterion:

$$J(\mathbf{f}) = \frac{1}{2\sigma_\epsilon^2} \|\mathbf{g} - \mathbf{H}\mathbf{f}\|_2^2 + \gamma \sum_j |f_j|^\beta, \quad (6.30)$$

which can be done with any gradient based algorithm when $1 < \beta \leq 2$. There also exist appropriate algorithms for $\beta = 1$ and $0 < \beta < 1$. In this thesis, we used a gradient based algorithm.

- *Student-t* priors:

$$p(\mathbf{f}|\nu) = \prod_j \mathcal{St}(f_j|\nu) \propto \exp \left\{ -\frac{\nu+1}{2} \sum_j \log(1 + f_j^2/\nu) \right\} \quad (6.31)$$

where

$$\mathcal{St}(f_j|\nu) = \frac{1}{\sqrt{\pi\nu}} \frac{\Gamma((\nu+1)/2)}{\Gamma(\nu/2)} (1 + f_j^2/\nu)^{-(\nu+1)/2}. \quad (6.32)$$

These priors are interesting due to its link to l_1 regularization and secondly due to the mixture of Gaussian representation of the *Student-t* probability density:

$$\mathcal{St}(f_j|\nu) = \int_0^\infty \mathcal{N}(f_j|0, 1/\tau_j) \mathcal{G}(\tau_j|\nu/2, \nu/2) d\tau_j \quad (6.33)$$

which gives the possibility of proposing a hierarchical model via the positive hidden variables τ_j :

$$\begin{cases} p(\mathbf{f}|\boldsymbol{\tau}) = \prod_j p(f_j|\tau_j) = \prod_j \mathcal{N}(f_j|0, 1/\tau_j) \\ \propto \exp \left\{ -\frac{1}{2} \sum_j \tau_j f_j^2 \right\} \\ p(\tau_j|\alpha, \beta) = \mathcal{G}(\tau_j|\alpha, \beta) \propto \tau_j^{(\alpha-1)} \exp\{-\beta\tau_j\} \\ \text{with } \alpha = \beta = \nu/2 \end{cases}. \quad (6.34)$$

6.5.2 - Bayesian sparse reconstruction

Choice of Estimator and Approximations

Using this hierarchical model, we can write the joint prior of \mathbf{f} and $\boldsymbol{\tau}$

$$\begin{aligned} p(\mathbf{f}, \boldsymbol{\tau}) &= \prod_j p(f_j | \tau_j) p(\tau_j) = \prod_j \mathcal{N}(f_j | 0, 1/\tau_j) p(\tau_j) \\ &\propto \exp \left\{ -\frac{1}{2} \sum_j \tau_j f_j^2 + (\gamma - 1) \ln \tau_j - \beta \tau_j \right\} \end{aligned} \quad (6.35)$$

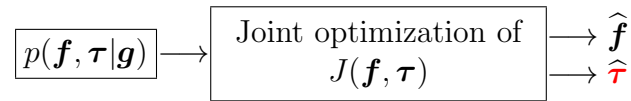
Then, using the Bayes rule, we obtain:

$$p(\mathbf{f}, \boldsymbol{\tau} | \mathbf{g}) \propto p(\mathbf{g} | \mathbf{f}) p(\mathbf{f}, \boldsymbol{\tau}) \propto \exp \{-J(\mathbf{f}, \boldsymbol{\tau})\} \quad (6.36)$$

where

$$J(\mathbf{f}, \boldsymbol{\tau}) = \frac{1}{2v_\epsilon} \|\mathbf{g} - \mathbf{H}\mathbf{f}\|_2^2 + \sum_j \frac{1}{2} \tau_j f_j^2 - (\alpha - 1) \ln \tau_j + \beta \tau_j \quad (6.37)$$

which is summarized as follows:



$$\hat{\mathbf{f}} = \arg \max_{\mathbf{f}} \{p(\mathbf{f} | \mathbf{g})\} = \arg \min_{\mathbf{f}} \{-\ln p(\mathbf{f} | \mathbf{g})\} = \arg \min_{\mathbf{f}} \{J(\mathbf{f})\} \quad (6.38)$$

Joint optimization of this criterion, alternatively with respect to \mathbf{f} (with fixed $\boldsymbol{\tau}$)

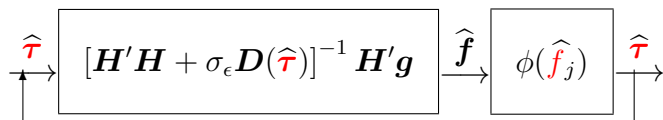
$$\begin{aligned} \hat{\mathbf{f}} &= \arg \min_{\mathbf{f}} \{J(\mathbf{f}, \boldsymbol{\tau})\} \\ &= \arg \min_{\mathbf{f}} \left\{ \frac{1}{2v_\epsilon} \|\mathbf{g} - \mathbf{H}\mathbf{f}\|_2^2 + \sum_j \frac{1}{2} \tau_j f_j^2 \right\} \end{aligned} \quad (6.39)$$

and with respect to $\boldsymbol{\tau}$ (with fixed \mathbf{f})

$$\begin{aligned} \hat{\boldsymbol{\tau}} &= \arg \min_{\boldsymbol{\tau}} \{J(\mathbf{f}, \boldsymbol{\tau})\} \\ &= \arg \min_{\boldsymbol{\tau}} \left\{ \sum_j \frac{1}{2} \tau_j f_j^2 - (\alpha - 1) \ln \tau_j + \beta \tau_j \right\} \end{aligned} \quad (6.40)$$

results in the following iterative algorithm:

$$\left\{ \begin{array}{l} \hat{\mathbf{f}} = [\mathbf{H}'\mathbf{H} + v_\epsilon \mathbf{D}(\hat{\boldsymbol{\tau}})]^{-1} \mathbf{H}'\mathbf{g} = \mathbf{D}(\hat{\boldsymbol{\tau}})\mathbf{H}'(\mathbf{H}\mathbf{D}(\hat{\boldsymbol{\tau}})\mathbf{H}' + v_\epsilon \mathbf{I})^{-1} \mathbf{g} \\ \hat{\tau}_j = \phi(\hat{f}_j) = \frac{\alpha}{\hat{f}_j^2 + \beta} \\ \mathbf{D}(\hat{\boldsymbol{\tau}}) = \text{diag}[1/\hat{\tau}_j, \quad j = 1, \dots, n] \end{array} \right. \quad (6.41)$$



Note that τ_j is inverse of a variance and we have $1/\tau_j = (f_j^2 + \beta)/\alpha$. We can interpret this as an iterative quadratic regularization inversion followed by the estimates of variances τ_j which are used in the next iteration to define the variance matrix $\mathbf{D}(\boldsymbol{\tau})$. This algorithm is simple to implement. However, we are not sure about its convergency. To obtain a better solution and at the same time to be able to estimate the variance of the noise, we propose to use the VBA [SQ05, Bis06, CCPV07] which consists in approximating the joint posterior by a separable one and then using it to do the inference.

Here we summarize this approach:

- Model for the noise:

$$\begin{cases} p(\mathbf{g}|\mathbf{f}, v_\epsilon) = \mathcal{N}(\mathbf{g}|\mathbf{H}\mathbf{f}, v_\epsilon \mathbf{I}), & \tau_\epsilon = 1/v_\epsilon \\ p(\tau_\epsilon) = \mathcal{G}(\tau_\epsilon|\alpha_{\epsilon 0}, \beta_{\epsilon 0}) \end{cases} \quad (6.42)$$

- Model for the sparse signal:

$$\begin{cases} p(\mathbf{f}|\mathbf{v}) = \prod_j p(f_j|\mathbf{v}_j) = \prod_j \mathcal{N}(f_j|0, \mathbf{v}_j) = \mathcal{N}(\mathbf{f}|0, \mathbf{V}) \\ \mathbf{V} = \text{diag}[\mathbf{v}], \quad \tau_j = 1/\mathbf{v}_j, \quad \text{diag}[\boldsymbol{\tau}] = \mathbf{V}^{-1} \\ p(\boldsymbol{\tau}) = \prod_j \mathcal{G}(\tau_j|\alpha_0, \beta_0) \end{cases} \quad (6.43)$$

- Joint posterior:

$$p(\mathbf{f}, \boldsymbol{\tau}, \tau_\epsilon | \mathbf{g}) \propto p(\mathbf{g}|\mathbf{f}, \tau_\epsilon) p(\mathbf{f}|\boldsymbol{\tau}) p(\boldsymbol{\tau}) p(\tau_\epsilon) \quad (6.44)$$

- VBA: $p(\mathbf{f}, \boldsymbol{\tau}, \tau_\epsilon | \mathbf{g})$ is approximated by

$$q(\mathbf{f}, \boldsymbol{\tau}, \tau_\epsilon) = q(\mathbf{f}) \prod_j q(\tau_j) q(\tau_\epsilon) \quad (6.45)$$

where

$$\begin{cases} q(\mathbf{f}) = \mathcal{N}(\mathbf{f}|\tilde{\boldsymbol{\mu}}, \tilde{\Sigma}) \\ \tilde{\boldsymbol{\mu}} = \tilde{\Sigma} \mathbf{H}' \mathbf{g} = \tilde{\mathbf{V}} \mathbf{H}' \left(\mathbf{H} \tilde{\mathbf{V}} \mathbf{H}' + \tilde{\tau}_\epsilon \mathbf{I} \right)^{-1} \mathbf{g} \\ \tilde{\Sigma} = (\tilde{\tau}_\epsilon \mathbf{H}' \mathbf{H} + \tilde{\mathbf{V}})^{-1} = \tilde{\mathbf{V}} - \tilde{\mathbf{V}} \mathbf{H}' \left(\mathbf{H} \tilde{\mathbf{V}} \mathbf{H}' + \tilde{\tau}_\epsilon \mathbf{I} \right)^{-1} \mathbf{H} \tilde{\mathbf{V}}, \text{ with } \tilde{\mathbf{V}} = \text{diag}[\tilde{\mathbf{v}}], \end{cases} \quad (6.46)$$

$$\begin{cases} q(\tau_\epsilon) = \mathcal{G}(\tau_\epsilon|\tilde{\alpha}_\epsilon, \tilde{\beta}_\epsilon) \\ \tilde{\alpha}_\epsilon = \tilde{\alpha}_{\epsilon 0} + (n+1)/2 \\ \tilde{\beta}_\epsilon = \beta_{\epsilon 0} + 1/2 \\ \tilde{\tau}_\epsilon = \tilde{\alpha}_\epsilon / \tilde{\beta}_\epsilon, \end{cases} \quad (6.47)$$

6.5.2 - Bayesian sparse reconstruction

$$\left\{ \begin{array}{l} q(\tau_j) = \mathcal{G}(\tau_j | \tilde{\alpha}_j, \tilde{\beta}_j) \\ \tilde{\alpha}_j = \alpha_{00} + 1/2 \\ \tilde{\beta}_j = \beta_{00} + \langle f_j^2 \rangle / 2 \\ \tilde{v}_j = \tilde{\beta}_j / \tilde{\alpha}_j \end{array} \right. \quad (6.48)$$

and the expressions of the needed expectations are:

$$\left\{ \begin{array}{l} \langle \mathbf{f} \rangle = \tilde{\mu} \\ \langle \mathbf{f} \mathbf{f}' \rangle = \Sigma + \mu \mu' \\ \langle f_j^2 \rangle = [\Sigma]_{jj} + \mu_j^2 \\ \langle \tau \rangle = \tilde{\tau} = \tilde{\alpha}_\tau / \tilde{\beta}_\tau \\ \langle a_j \rangle = \tilde{a}_j = \tilde{\alpha}_j / \tilde{\beta}_j \end{array} \right. \quad (6.49)$$

This algorithm can be summarized as follows:

– Initialization: $\tilde{\tau}_\epsilon = 0.1$, $\tilde{\mathbf{V}} = \text{diag}[\tilde{\tau}_j / \tilde{\tau}_\epsilon]$ with $\tilde{\tau}_j = 1$

– Iterations:

compute $\tilde{\Sigma} = [\tau_\epsilon \mathbf{H}' \mathbf{H} + \tilde{\mathbf{V}}]^{-1}$ and $\tilde{\mu} = \Sigma \mathbf{H}' \mathbf{g}$

compute $\langle f_j^2 \rangle = \tilde{\Sigma}_{jj} + \tilde{\mu}_j^2$

compute $\tilde{\alpha}_\epsilon, \tilde{\beta}_\epsilon$ and so $\tilde{\tau}_\epsilon = \tilde{\alpha}_\epsilon / \tilde{\beta}_\epsilon$

compute $\tilde{\alpha}_j, \tilde{\beta}_j$ and so $\tilde{\tau}_j = \tilde{\alpha}_j / \tilde{\beta}_j$

The only difficult and costly part is the estimation of $\tilde{\Sigma}$ and $\tilde{\mu}$. Due to the fact that we only need $\tilde{\mu}$ and $\tilde{\Sigma}_{jj}$, we propose the following approximation:

- $\tilde{\mu}$ is computed through the optimization of $J(\mathbf{f}) = \tau_\epsilon \|\mathbf{g} - \mathbf{H}\mathbf{f}\|_2^2 + \frac{1}{2} \sum_j \tau_j f_j^2$ with respect to \mathbf{f} ;
- $\tilde{\Sigma}_{jj}$ which is the variance of f_j is approximated by the empirical variance of f_j during the iterations of the optimization algorithm.

This is the method we implemented, tested and compared to other classical methods.

6.6 Simulation Results

In this section, we conduct several numerical experiments to demonstrate our method based on the sparse signal representation. The imaging geometry is shown in Figure 6.4. The range R_0 from the original to the center of the target is 10 km and the velocity of the platform V_a is 200 m/s. The central frequency f_c is 10 GHz with bandwidth $B = 400$ MHz associated with the Rayleigh resolution along the range direction 0.375 m. The angular extent of azimuth is 10° with cross-range resolution 0.0861 m. We generate the received signal with the parameters and then applied proposed the method to estimate such parameters. The performance is evaluated by carrying out Monte Carlo experiments.

6.6.1 Sampling pattern

Based on CS principle, compared to conventional imaging methods, targets can be recovered with a smaller randomly sampled measures. Figure 6.5 shows that sampling pattern in the wavenumber domain, the uniform sampling in Figure 6.5a and the randomly sampling in Figure 6.5b.

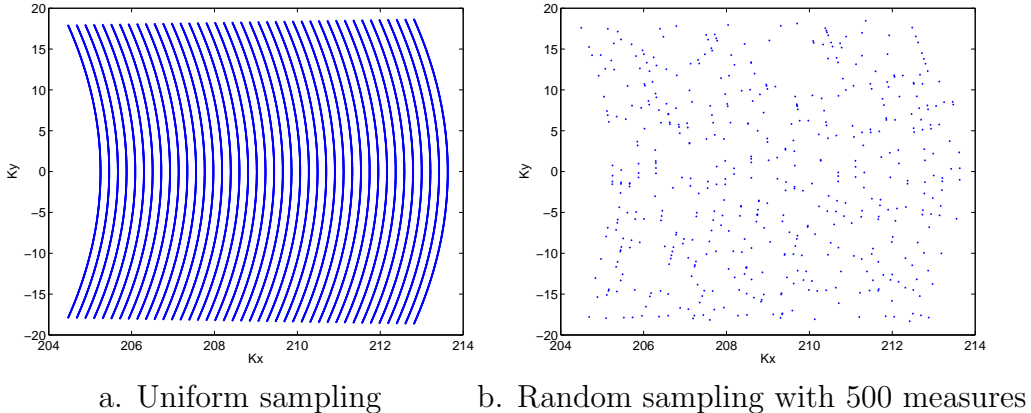


Figure 6.5: Sampling pattern in wavenumber space: a) The uniform sampling pattern; b) The random sampling pattern.

6.6.2 Reconstruction when no micromotion

In the first experiment, a scene consisting of three point targets without micromotion is considered. The three targets parameters are only about positions, with $(\hat{x}, \hat{y}) = (0, 0), (2, 2)$, and $(4, 4)$, respectively.

With the randomly sampled measures, Figure 6.6 compares the reconstruction results between the conventional imaging method of IFFT, the CoSaMP and the proposed Bayesian method when no micromotion.

The noisy measurement leads to the presence of the artificial scattering centers and energy loss of true scattering centers. With conventional FFT-based method, results

6.6.5 - Reconstruction with MF method

can be easily seen with side lobes.

Both the CoSaMP and the proposed Bayesian method come out with clearer images and are capable of recovering the true position of targets, even with smaller randomly measures.

6.6.3 Reconstruction when micromotion is present

In the second experiment, a scene consisting of the same geometry of three point targets undergoing micromotion is considered. The micromotion frequency and micromotion range are different, with values being 0.5, 1, 1 (Hz) and 1, 0.5, 0.5 (m), respectively. For simplicity, the initial phases are assumed to be zeros. We list the target parameter vectors here: $(\hat{x}, \hat{y}, \hat{r}, \hat{f}_m, \hat{\phi}_0) = (0, 0, 1, 0.5, 0)$, $(2, 2, 0.5, 1, 0)$ and $(4, 4, 0.5, 1, 0)$.

In Figure 6.7b, the range profile appears distinctly in a micromotion pattern compared with Figure 6.6b. The presentation of micromotion blurs the reconstruction images without motion compensation as shown in Figure 6.7a, which is a poor result. The proposed joint parameter estimation method gains a well-focused image as illustrated in Figure 6.7d. As can be seen, three targets are reconstructed clearly with an excellent result. Figure 6.7c illustrates the reconstruction result via the CoSaMP method.

6.6.4 Reconstruction with micromotion and non-micromotion targets

In the third experiment, a scene consisting of both stationary and micromotion targets is considered. The objective of this experiment is to show the capability of reconstruction a mixed scene with both micromotion and non-micromotion targets by the proposed method. The associated parameters of the two targets are $(\hat{x}, \hat{y}, \hat{r}, \hat{f}_m, \hat{\phi}_0) = (0, 0, 0, 0, 0)$ and $(2, 2, 0.5, 1, 0)$, respectively.

Figure 6.8 shows the recovery results. The conventional IFFT based methods can not present the exact positions of targets. There are many other residual pixels which lead to the ambiguity of scatterers. Both CoSaMP and the proposed Bayesian method can handle this problem and estimate two targets accurately.

6.6.5 Reconstruction with MF method

In the fourth experiment, a scene consisting of two micromotion targets is considered. We carry out the experiment to show the micromotion parameters volume and their estimation with MF method. For simplicity, we again consider two micromotion targets with the same micromotion range 0.5 m and initial phase 0° for two targets but the micromotion frequencies are 0.5 and 1 Hz, respectively. The associated parameters of the two targets are $(\hat{x}, \hat{y}, \hat{r}, \hat{f}_m, \hat{\phi}_0) = (0, 0, 0.5, 0.5, 0)$, $(5, 1, 0.5, 1, 0)$. We adopt the matched filtering in the 3D range-Azimuth-micromotion frequency space by scanning a large number of possible scatterer positions and micromotion frequencies, resulting in a large space-micromotion frequency cube.

Figure 6.9a shows the 3D data cube. Figure 6.9b,c illustrate the two slices after matched filtering at micromotion frequencies $f_m = 1 \text{ Hz}$ and $f_m = 0.5 \text{ Hz}$, respectively. It is computationally expensive and not well focused being of low resolution. In addition, it is rather difficult to perform RCM such that the position cannot be estimated accurately. In contrast, the proposed method can overcome these drawbacks of traditional methods and yield a more precise estimate.

6.6.6 Reconstruction with closely located micromotion targets

In the fifth experiment, a scene consisting of two very closely micromotion targets is considered. The objective is to present the performance of the proposed method for super-resolution imaging.

Two very closely spaced micromotion targets localized at positions of $(0, 0)$ and $(0.25, 0.25)$, respectively, with micromotion parameters given $(\hat{x}, \hat{y}, \hat{r}, \hat{f}_m, \hat{\phi}_0) = (0, 0, 1, 0.5, 0)$ and $(0.25, 0.25, 0.5, 1, 0)$.

Figure 6.10 shows the results. The reconstruction image by IFFT is illustrated in Figure 6.10a and the corresponding range profile in Figure 6.10b. It shows that the range profiles of the two targets are overlapped and the conventionally reconstructed image suffers from high side lobes. Consequently the two targets can not be discriminated. However, Figure 6.10c, d present an excellent result of CoSaMP and the proposed Bayesian method. In contrast to the fail of conventional method as IFFT, the results in Figure 6.10d prove the capability of super-resolution of the proposed method.

6.6.7 Analysis and discussions

To further examine the performance, we implement the simulation of Root Mean Square (RMS) errors to evaluate the robustness of the proposed method. Figures 6.11 and Figure 6.12 depict the estimation error of RMS versus SNR. The results is obtained on a scene of two micromotion targets with the following parameters $(\hat{x}, \hat{y}, \hat{r}, \hat{f}_m, \hat{\phi}_0) = (0, 0, 1, 0.5, 0)$ and $(5, 1, 0, 5, 1, 0)$.

It is demonstrated that the proposed method can recover the parameters of target signatures accurately. It can be observed that the RMS decreases sharply as the SNR increases and arrives at high precision estimations after 0 dB, indicating the robustness of the method to uncertain, limited and noisy data.

Based on above simulated results, we can see that compared to conventional methods, the advantages of the proposed method mainly include:

1. Putting the micromotion target imaging and parameter estimation into a unifying Bayesian parameter estimation framework, which can also handle the hyperparameter estimation;
2. Breaking through the classic the Rayleigh resolution limit, providing the capability of super-resolution;
3. Being capable of estimating micromotion parameters from limited observations;
4. Being robust to noise.

6.7 Conclusions

Based on radar scattering characteristics and CS theory, the problem of SAR imaging can be considered as a high precision estimation problem of target parameters from finite observations. Then this estimation problem can be solved by sparse signal representation on a parametric model. Bayesian approach can be well combined to obtain the sparsest representation of the target and the optimal estimation. Based on this idea, in this chapter, we proposed a sparsity-inducing method to estimate the scattering and micromotion parameters of SAR targets jointly and further formatted it in the Bayesian framework. It was done by formulating the original nonlinear problem as a sparse representation problem over an over-complete dictionary. In addition, an efficient VBA method was proposed to account for the hierarchical Bayesian computation. The proposed method can exactly recover the scattering and micromotion parameters of targets and even achieve good performance for near spacing targets, as demonstrated by the simulation results.

Here too, we may remark that the contents and results of this chapter is also reflected in the paper [[ZMDW⁺12](#)].

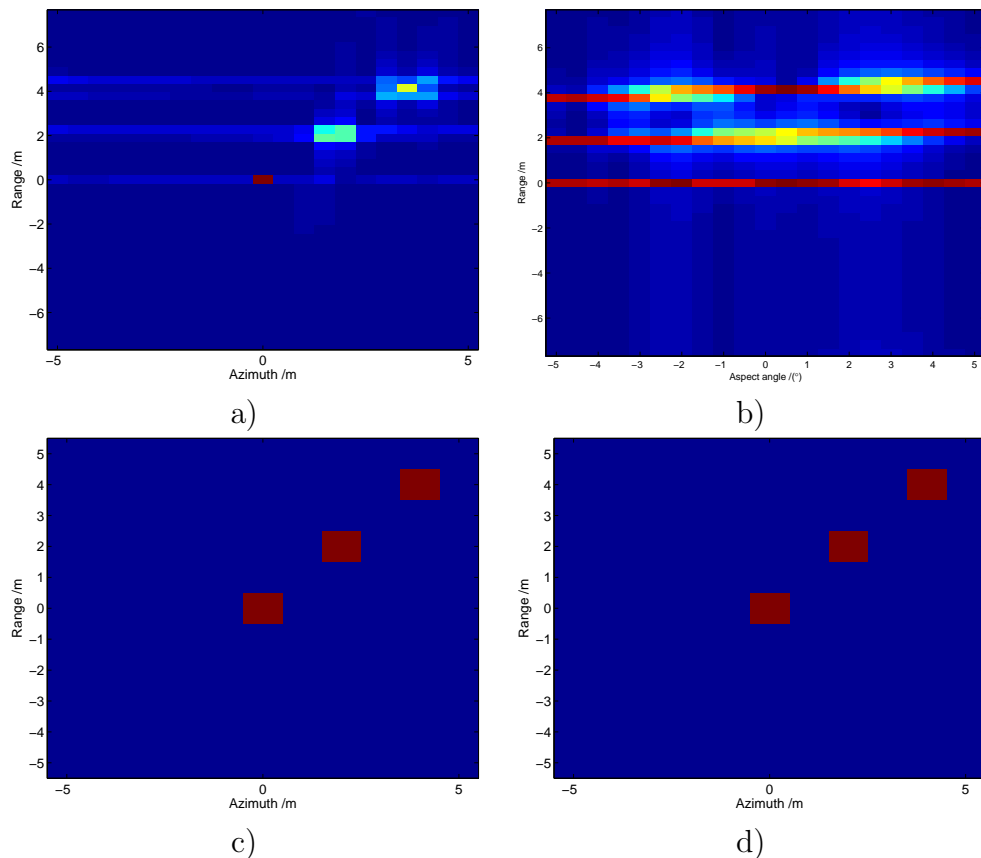


Figure 6.6: Reconstruction results when no micromotion: a) The reconstruction image by IFFT; b) The corresponding range profile; c) and d) The reconstruction images by CoSaMP method and the proposed Bayesian method respectively.

6.6.7 - Analysis and discussions

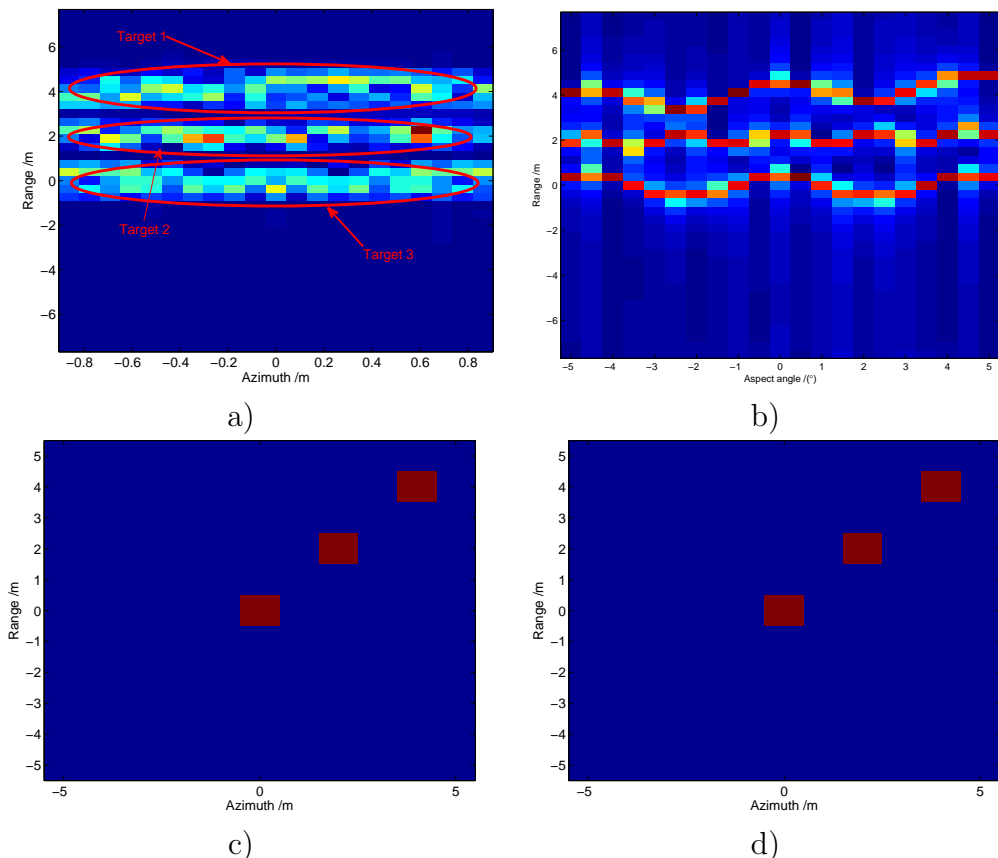


Figure 6.7: Reconstruction results when micromotion is present: a) The reconstruction image by IFFT; b) The corresponding range profile; c) and d) The reconstruction images by CoSaMP method and the proposed Bayesian method respectively.

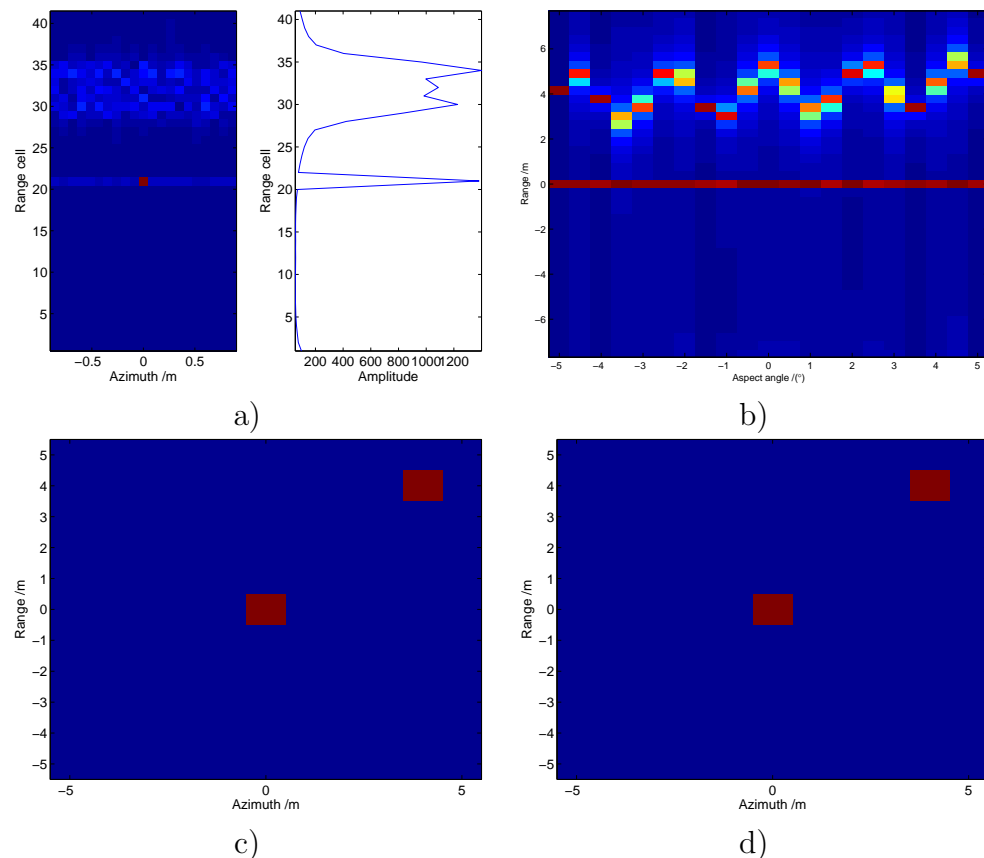


Figure 6.8: Reconstruction of a scene combined with both micromotion and stationary targets: a) The reconstruction image by IFFT; b) The corresponding range profile; c) and d) The reconstruction images by CoSaMP method and the proposed Bayesian method respectively.

6.6.7 - Analysis and discussions

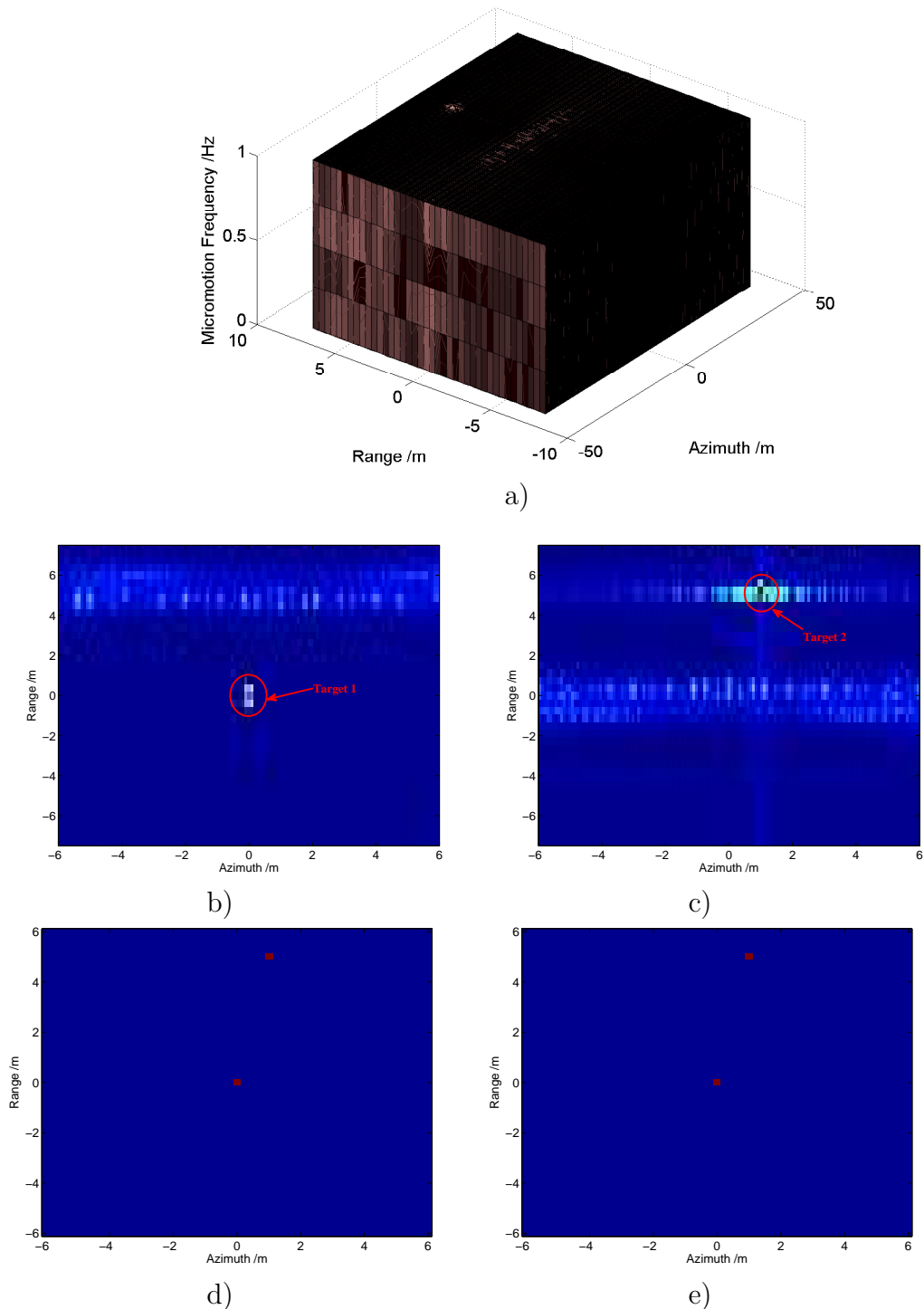


Figure 6.9: Reconstruction results with MF, CoSaMP, and the proposed Bayesian method when micromotion is present: a) The 3D space-micromotion frequency data volume; b) and c) The slices at $f_m = 1 \text{ Hz}$ and $f_m = 0.5 \text{ Hz}$, respectively after matched filtering; d) and e) The reconstruction images by CoSaMP method and the proposed Bayesian method respectively.

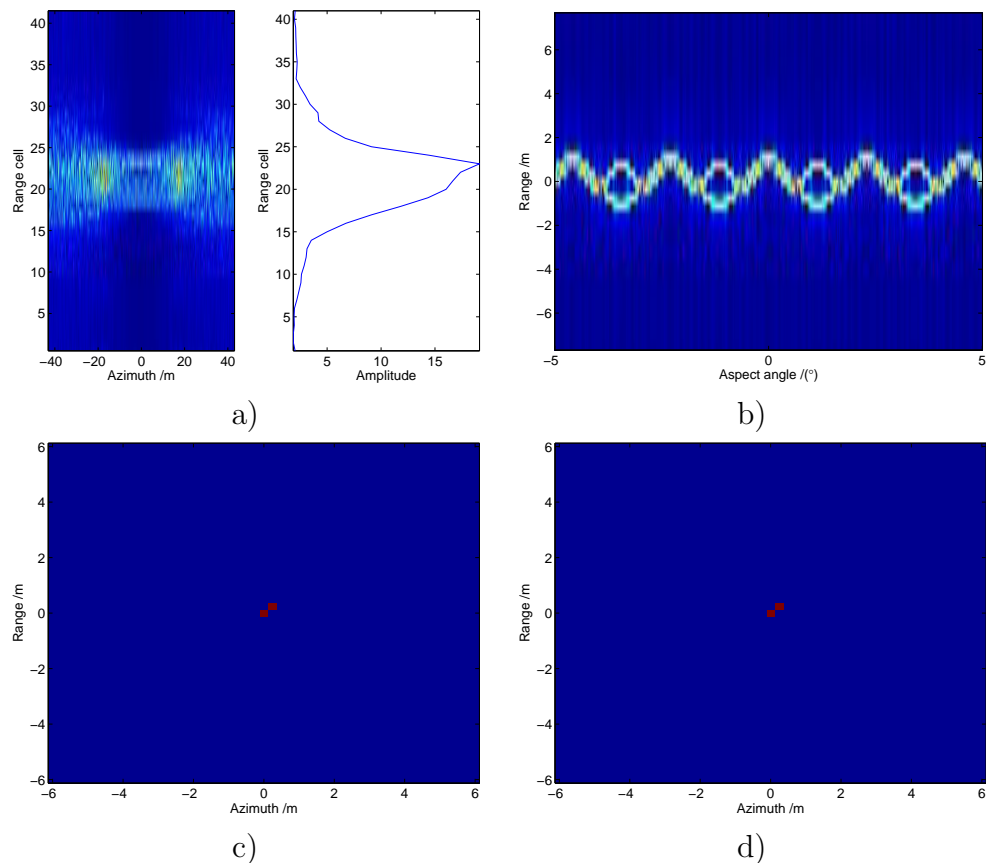


Figure 6.10: Reconstruction of two close targets when micromotion is present: a) For two closely localized micromotion targets, reconstruction image by IFFT; b) The corresponding range profile; c) and d) The reconstruction images by CoSaMP method and the proposed Bayesian method respectively.

6.6.7 - Analysis and discussions

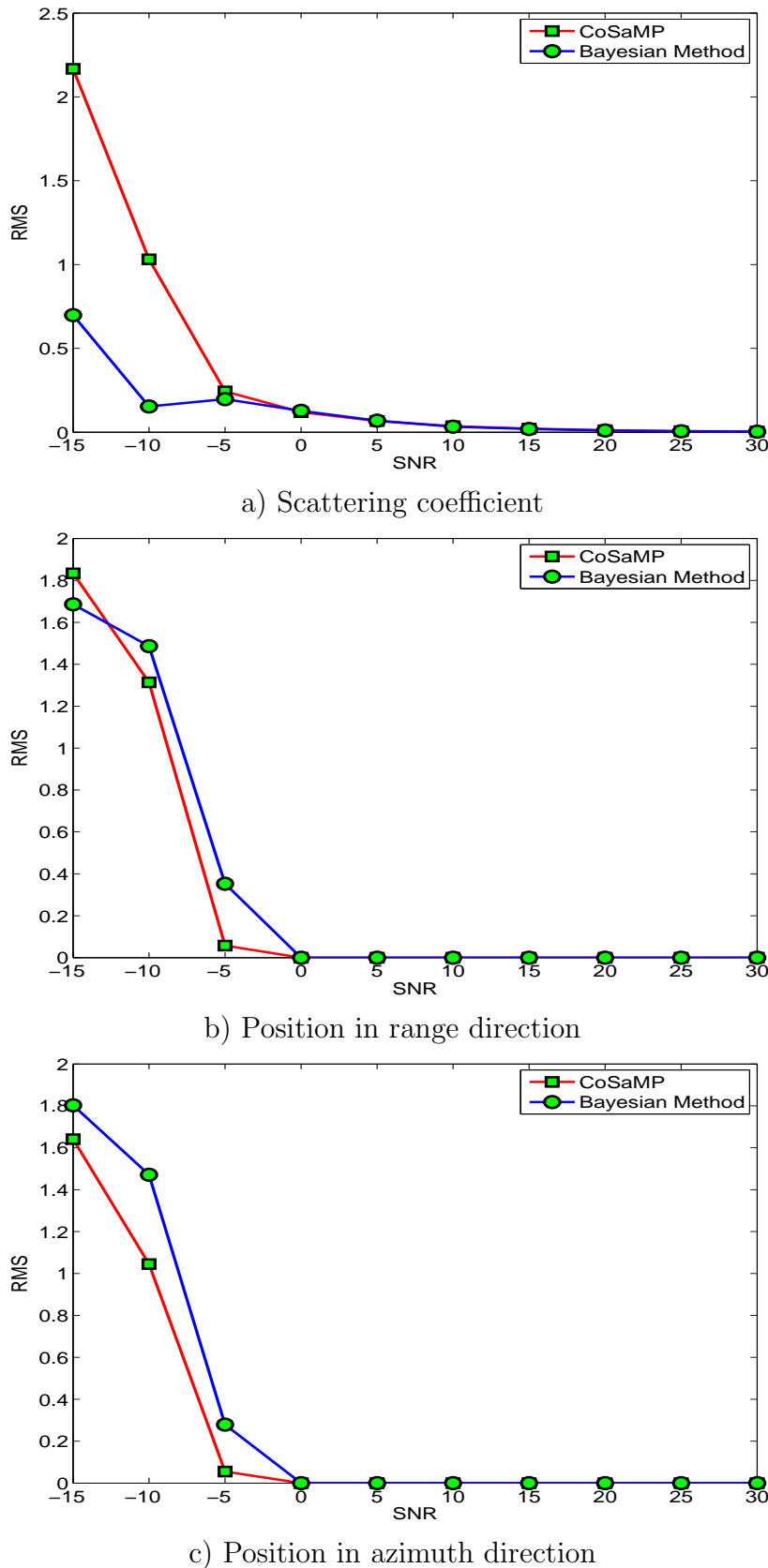
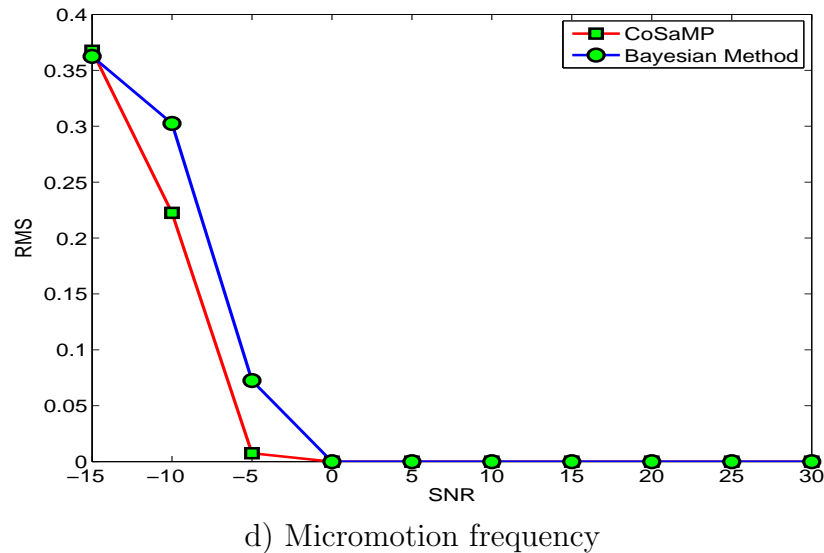
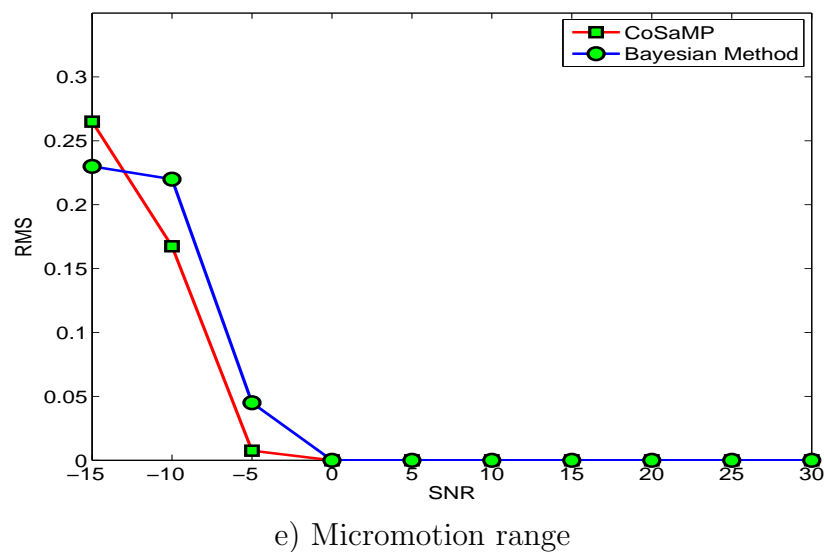


Figure 6.11: Reconstruction RMS: a–c) The root mean square error versus SNR by the CoSaMP method and the proposed Bayesian method for scattering coefficient, position in range direction and position in azimuth direction, respectively.



d) Micromotion frequency



e) Micromotion range

Figure 6.12: Reconstruction RMS: d–e) The root mean square error versus SNR by CoSaMP method and the proposed Bayesian method for micromotion frequency and micromotion range, respectively.

7

Conclusions and perspectives

7.1 Conclusions

In this thesis, we made contributions to Bayesian approach for the ill-posed inverse problems arising in SAR imaging for different situations. We systematically formulated the mathematical model for Mono-, Bi-, Multi-static SAR and the micromotion target imaging. We established a unifying Bayesian framework for various target scenes. We studied the physical mechanism of SAR imaging, proposed different priors and analyzed the effects on reconstruction. We solved the problem of SAR micromotion target parameter estimation. We combined our proposed Bayesian approach with CS theory, developed the Variational Bayesian Approximation method, realized jointly reflectivity scene reconstruction and micromotion parameters estimation. We presented efficiently computing optimization algorithms and the hyperparameters estimation. Experiments implemented on both synthetic and real data demonstrated the effectiveness of the proposed approach.

In chapter 2, we established a tomographic model for SAR imaging. Traditional methods dealing with this imaging problem based on the assumption that the Fourier domain information is complete, which is however an unrealistic assumption. Thus they have serious drawbacks of low resolution, high side lobe artifacts and not being robust. We consider two kinds of target modeling : extended targets and point targets. We analyzed the problem of SAR imaging in a linear case as a Fourier Synthesis (FS) problem, which constitutes the basis of our inversion approach.

However, we are aware that the FS problem as we modeled is not realistic, because the original data are not on a rectangular cartesian grid. But we wanted to focus on an idealized forward model particularly to study different inversion methods and their relative performance.

In chapter 3, we cast the ill-posed inverse problem of Fourier synthesis (FS) which

CHAPTER 7. CONCLUSIONS AND PERSPECTIVES

consisted in reconstructing a target from partial knowledge of its Fourier Transform (FT) in applications of Mono-, Bi- and Multi- static SAR imaging systems in a general Bayesian framework. The proposed Bayesian approach can conveniently translate our knowledge about the target to regularize the estimation. We proposed different priors for simple and complicated target scenes.

1. We proposed three simple priors: separable generalized Gaussian(SGG), separable Cauchy (SC) and Generalized Gauss-Markov (GGM). SGG or SC performs better for a scene consisting of point sources, while GGM is better for a scene consisting of homogeneous regions.
2. We proposed Generalized Gaussian prior and sparse Gaussian prior with hyperparameters;
3. We developed a generalized Total Variation (TV) prior which extends the classic TV with l_1 norm of first-order derivative to MRF model.

In particular, we have investigated the sparsity of SAR targets. The appropriate prior model leads to a stable and coherent reconstruction of the original targets from the partial observations.

In chapter 4, we applied the proposed approach to Mono- and Bi-static SAR imaging. Different from existing deterministic imaging methods and regularization methods, the Bayesian framework provides a flexible tool for estimation and inference. By incorporating appropriate priors of unknown targets, one can get promising reconstruction results with enhanced target features of interest. We conducted three groups of experiments:

1. MAP estimation on two typical radar targets on three simple priors;
2. Marginalization with hyperparameter estimation on two Gaussian priors;
3. Hierarchical Bayesian estimation based on a TV prior.

We also implemented the experiments on both synthetic and real data. The results demonstrated the performance of the proposed methods.

In chapter 5, we applied the proposed approach to Multi-static SAR imaging. We solved it as a data fusion problem. We proposed three different data fusion schemes and implemented each on synthetic and experimental data from a reduced-size laboratory experiment. By comparing the three proposed data fusion schemes, it is shown that the proposed Bayesian joint data fusion and inversion method had the best performance, with advantages of being robust to noise and the superresolution.

In chapter 6, we changed the strategy of forward modeling to account for moving target especially micromotion targets where the relation between the transmitted signals, the target and the received echo is no longer linear. Then again we proposed a Bayesian approach based on Compressive Sensing (CS) and Sparse signal representation. We firstly linearized the forward model as a linear combination of elements with an over-complete dictionary. It is then essential to find the nonzero coefficients which are associated with the scattering and micromotion parameters. Since micromotion targets are sparsely distributed in the observation scene, there are only few nonzero coefficients. Herein this sparse distribution of coefficients are modeled by Generalized Gaussian prior and *Student-t* prior. The proposed Bayesian approach can estimate the target micromotion and scattering parameters jointly. Simulation results demonstrated the effectiveness of the proposed approach.

7.2 Perspectives

7.2.1 Forward modeling and inversion developing perspectives

Bayesian inference is based on appropriate forward modeling, associated errors as well as uncertainties modeling and target scene prior modeling. For each step, we always need to propose models to do target scene modeling as well as to describe the interaction with transmitted signals in general context. Thus, to make an accurate inference, the hypothesis needs to be reasonable.

Thinking in a Bayesian way, the two main problems of SAR imaging are [MD12]:

- *How to predict the data based on hypothesis and forward model?*
- *How do the observed data support these hypothesis and model?*

Around these two basic problems, further research on Bayesian SAR imaging can be undertaken in the following aspects:

1. Establishing a more realistic scattering model

In this thesis, we have addressed the SAR target imaging based on an ideal scattering model, which is still very simple for real cases. A more realistic model is the attributed scattering center model, where the amplitude and frequency vary with different radar light directions. Further work can continue on more complicated scattering models such as attributed scattering center model (See Appendix A).

2. Modeling background clutters

We have modeled target scenes of both point targets and homogeneous regions via appropriate priors. However, we didn't discriminate the clutter effect from background. Further work can be undertaken on background clutter modeling [YSBZ11]. Bayesian approach provides various priors to model clutters. For example, for the homogeneous background, it can be modeled by Markov models. For a complicated scene containing background as well as point targets, it can be modeled by a mixture model.

3. Modeling targets with more complex motion

We have addressed SAR imaging problem for targets experiencing micromotion of rotation with a constant speed. However, in practice target may experience irregular movement or dynamic micromotion which even contain a certain degree of randomness, resulting in disturbances on echo data. Further work can be extended to a more complex target motion model with any arbitrary motion.

4. Developing hierarchical priors with hidden variables and efficient approximation methods

Hierarchical priors with hyperparameters and hidden variables provide more realistic descriptions of target scenes and models. However, it is very difficult to estimate hyperparameters and make approximations. Further work will be continued on this part.

7.2.2 - Application perspectives

5. Studying the convergence of algorithms and implementing computations

The work on the convergence of proposed algorithms will be continued. To improve the computation speed, further work can be undertaken by the combination of GPU to accelerate computation for satisfying real application requirements.

7.2.2 Application perspectives

Practically, the proposed Bayesian approach can be employed in the following potential applications:

1. For recognition-oriented Bayesian SAR imaging (Bayesian SAR-ATR)

We aim to develop a recognition-oriented Bayesian SAR imaging framework. In this framework, the prior knowledge of target scenes will be treated as restriction to the expected image based on Bayesian inference. SAR images of high resolution with feature enhancement as well as background suppression will be generated, which will be beneficial for Auto Target Recognition (ATR).

The proposed Bayesian SAR technique distinctly differs from conventional inversion, imaging and recognition techniques on the following aspects:

- (a) The proposed Bayesian SAR imaging method allows us not only obtain an accurate solution but also have feasibilities of feature-enhancement by prior modeling. For example, conventional SAR imaging methods make uniform focus on target and background. With Bayesian imaging method, by appropriately assigning priors for the target and the background, target features can be well enhanced while background clutters can be significantly suppressed. And these steps will be done simultaneously.
- (b) Conventional recognition methods treat imaging and feature extraction as independent procedures [HXS06]. However, with specific prior modeling of target scene, useful features start to be incorporated during the imaging process.

The Bayesian SAR-ATR system is illustrated in Figure 7.1.

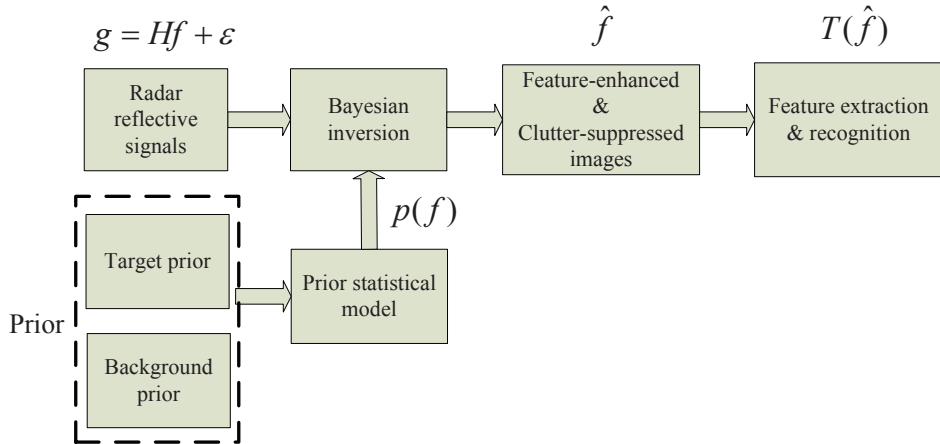


Figure 7.1: Bayesian SAR-ATR.

2. For Bayesian joint SAR MicroMotion Target Indication (Bayesian SAR-MMTI), parameter estimation and imaging

Conventional methods dealing with the problem of SAR/MMTI involve sequential steps of clutter suppression, detection, RCMC (Range Cell Migration Correction), signal separation, parameter estimation and imaging. The advantage is that for each step, the algorithm can be designed serially, which decreases the complexity of the algorithm. However, the disadvantages are also very obvious:

- Some process are still intractable such as clutter suppression and RCMC;
- The performance of the final detection and imaging is limited by many factors arising in each step.

In chapter 6, we operated directly on radar echo, formed the micromotion parameter as well as the scattering parameters into a mixed motion-scattering model and turned the problem of detection, parameter estimation and imaging into a unifying inverse problem framework. The proposed method can obtain the parametric, scattering and structure information of targets; meanwhile, it also has the capability for movement compensation. In such a way, it forms a joint technology for micromotion target detection, parameter estimation and imaging.

As illustrated in Figure 7.2, in the proposed Bayesian framework, first of all the full parametric modeling of the radar echo needs to be established, where the unknown parameters include the scattering reflectivity of the target, the target motion parameters and the unknown noise/clutter parameters. Then, by introducing the prior model of the interested target scene, the inverse problem will be solved with the realization of a joint estimation of the target image and motion parameters.

7.2.2 - Application perspectives

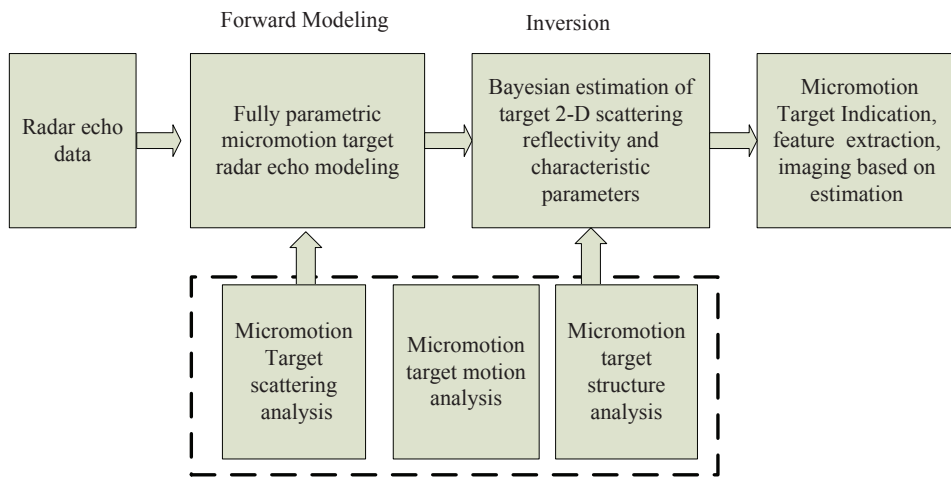
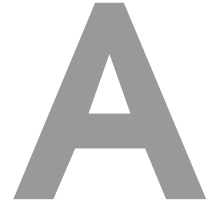


Figure 7.2: Jointly SAR MMTI.



ann

Attributed Scattering Model

Attributed scattering model is based on physical optics and Geometric Theory of Diffraction (GTD). When the wavelength of incident wave is smaller than the size of target, then the backscattering of target can be considered the composition of several individual scattering centers. For each scattering center, RCS can be represented as [KM99, PM97]:

$$E(\nu, \theta; \chi) = A(j \frac{\nu}{\nu_c})^\alpha \exp(-j \frac{4\pi\nu}{c} (x \cos \theta + y \sin \theta)) \cdot \sin c(\frac{2\pi\nu}{c} L_s \sin(\theta - \bar{\theta})) \exp(-2\pi\nu\gamma \sin \theta) \quad (\text{A.1})$$

where

- $\chi = [x, y, \alpha, \gamma, \bar{\theta}, L, A]$ represents the parameter set of scattering center;
- ν represents the frequency of the transmitter;
- θ represents the azimuth angle; When B represents the radar system bandwidth, ν_c represents the radar center frequency, $\mu = B/\nu_c$ represents the relative bandwidth, θ_m represents the total integration angle, $\nu \in [\nu_c(1 - \frac{\mu}{2}), \nu_c(1 + \frac{\mu}{2})]$ and $\theta \in [-\frac{\theta_m}{2}, \frac{\theta_m}{2}]$.
- $c = 3 \times 10^8 \text{ m/sec}$ represents the propagation velocity of light;
- x_i and y_i represent the positions on axis of the range and azimuth, respectively;
- A_i represents the complex amplitude of scattering center (complex reflectivity coefficient);
- $\alpha_i \in [-1, -0.5, 0, 0.5, 1]$ characterizes the frequency dependence of the response, called frequency influence coefficient;
- γ_i represents the dependency of local scattering centers on azimuth angle;
- L_{si} represents the length of an extended scattering center
- $\bar{\theta}_i$ represents the azimuth angle for an extended scattering center;

The frequency influence parameter α is related to the curvature information of the surface of scattering center. The parameters α and L contain information about the geometry of the scatters, the combination of which lead to a more accurate discrimination of the different kinds of scattering structures and a more abundant scattering characteristics for feature extraction and target recognition.

Model given in Equation (A.1) is called the scattering center model. Based on this model, we can do the following transform and approximation:

- let $\nu_x = \nu \cos \phi$ and $\nu_y = \nu \sin \phi$, which turn this model into the cartesian coordinate;
- let $(\frac{2\pi\nu}{c})^\alpha \approx \exp(-2\pi r_x \nu_x)$, where r_x is the damping factor;
- doing scale transform $\nu'_x = \nu_x / \nu_c$, $\nu'_y = \nu_y / \nu_c$;
- doing translation transform $\nu_x = \nu'_x - 1$, $\nu_y = \nu'_y$.

Then the scattering model becomes

$$E(\nu_x, \nu_y) = A \exp(-j \frac{4\pi}{\lambda_c} (x\nu_x + y\nu_y)) \exp(-2\pi(r_x \nu_x + r_y \nu_y)) \cdot \text{sinc}\left(-\frac{2\pi L_s \nu_c}{c} (\sin \bar{\theta} - \frac{2\pi L_s}{\lambda_c} (\nu_x \sin \bar{\theta} - \nu_y \cos \bar{\theta}))\right) \quad (\text{A.2})$$

where λ_c is the wavelength corresponding to radar center frequency.

Till now, we can see that the ideal scattering model adopted in this thesis, is a particularly simple case for the attributed scattering center model.

$$E(\nu, \theta) = \sum_{i=1}^n A_i \exp\left(\frac{-j4\pi\nu}{c} (x_i \cos \theta + y_i \sin \theta)\right) \quad (\text{A.3})$$

where n denotes the number of scattering centers, A_i denotes the amplitude of the i th scattering center, (x_i, y_i) denotes the scattering center position, c denotes the propagation velocity of wave, ν is the transmitted frequency of radar and θ is the azimuth angle.

As we can see, comparing to ideal scattering center model, attributed scattering center model contains a more explicit physical meaning, thus it can more accurately describe different types of scattering centers and more finely reflect the real scattering characteristics of targets.

Bibliography

- [AA10] M. AMIRMAZLAGHANI et H. AMINDAVAR : Two novel Bayesian multiscale approaches for speckle suppression in SAR images. *IEEE Trans. Geosci. Remote Sens.*, 48(7):2980–2993, Jul. 2010.
- [ASB03] A. ALESSIO, K. SAUER et C.A. BOUMAN : Map reconstruction from spatially correlated pet data. *IEEE Trans. Nuclear Science*, 50(5):1445–1451, Oct. 2003.
- [Bam92] R. BAMLER : A comparison of range-Doppler and wavenumber domain SAR focusing algorithms. *IEEE Trans. Geosci. Remote Sens.*, 30(4):706–713, Jul. 1992.
- [BB00] S. BASU et Y. BRESLER : $o(n^2 \log_2^n)$ filtered backprojection reconstruction algorithm for tomography. *IEEE Trans. Image Process.*, 9(10):1760–1773, Oct. 2000.
- [BC95] T. BOSE et M.Q. CHEN : Conjugate gradient method in adaptive bilinear filtering. *IEEE Trans. Signal Process.*, 43(6):1503–1508, Jun. 1995.
- [BCDH10] R.G. BARANIUK, V. CEVHER, M.F. DUARTE et C. HEGDE : Model-based compressive sensing. *IEEE Trans. Inf. Theory*, 56(4):1982–2001, Apr. 2010.
- [Bel08] D.P. BELCHER : Theoretical limits on SAR imposed by the ionosphere. *IET Radar Sonar Navig.*, 2(6):435–448, Dec. 2008.
- [Bis06] C.M. BISHOP : *Pattern Recognition and Machine Learning*. Springer-Verlag New York, Inc., Secaucus, NJ, USA, 2006.
- [BMK08] S.D. BABACAN, R. MOLINA et A.K. KATSAGGELOS : Parameter estimation in TV image restoration using variational distribution approximation. *IEEE Trans. Image Process.*, 17(3):326–339, Mar. 2008.
- [BMK10a] S.D. BABACAN, R. MOLINA et A.K. KATSAGGELOS : Bayesian compressive sensing using Laplace priors. *IEEE Trans. Image Process.*, 19(1):53–63, Jan. 2010.
- [BMK10b] S.D. BABACAN, R. MOLINA et A.K. KATSAGGELOS : Sparse Bayesian image restoration. In *Proc. IEEE Intl Conf. Image Process. (ICIP)*, pages 3577–3580, Sept. 2010.
- [BMLM00] R. BURNS, C.A. MC LAUGHLIN, J. LEITNER et M. MARTIN : TechSat 21: formation design, control and simulation. In *Proc. IEEE Aeros. Conf.*, volume 7(1), pages 19–25, 2000.
- [Bri88] E.O. BRIGHAM : *The fast Fourier transform and its applications*. Prentice-Hall, Inc., Upper Saddle River, NJ, USA, 1988.

BIBLIOGRAPHY

- [Bro03] M.Z. BROWN : Analysis of multiple-view Bayesian classification for SAR ATR. *In Proc. SPIE Algorithms for SAR Imagery X*, volume 5095(1), pages 265–274, 2003.
- [BSU87] J.J. BOWMAN, T.B.A. SENIOR et P.L.E. USLENGHI : *Electromagnetic and acoustic scattering by simple shapes (Revised edition)*. Hemisphere Publishing Corp., New-York, 1987.
- [BT09] A. BECK et M. TEBOULLE : Fast gradient-based algorithms for constrained total variation image denoising and deblurring problems. *IEEE Trans. Image Process.*, 18(11):2419–2434, Nov. 2009.
- [BXW05] Z. BAO, M.D. XING et T. WANG : *Radar imaging technology*. Electronic Industry Press, Beijing, 2005.
- [CB08] M. CHENEY et B. BODERN : Imaging moving targets from scattered waves. *Inverse Problems*, 24(3):035005, 2008.
- [CB09] M. CHENEY et B. BORDEN : Problems in Synthetic-Aperture Radar imaging. *Inverse Problems*, 25(12):123005, 2009.
- [CCPV07] C. CHAUX, P.L. COMBETTES, J.-C. PESQUET et R.W. VALÉRIE : A variational formulation for frame-based inverse problems. *Inverse Problems*, 23(4):1495, 2007.
- [CEPY05] T. CHAN, S. ESEDOGLU, F. PARK et A. YIP : Recent developments in total variation image restoration. *In Mathematical Models of Computer Vision*. Springer Verlag, 2005.
- [Çet01] M. ÇETIN : *Feature-enhanced Synthetic Aperture Radar imaging*. Ph.D. thesis, University of Boston, 2001.
- [CGM⁺95a] Walter G CARRARA, Ron S GOODMAN, Ronald M MAJEWSKI *et al.* : *Spotlight synthetic aperture radar: signal processing algorithms*. Artech House Boston, 1995.
- [CGM95b] W.G. CARRARA, R.S. GOODMAN et R.M. MAJEWSKI : *Spotlight Synthetic Aperture Radar: Signal Processing Algorithms*. Artech House, Norwood, MA, 1995.
- [Cha82] T.F. CHAN : An improved algorithm for computing the Singular Value Decomposition. *ACM Trans. Math. Software*, 8:72–83, 1982.
- [CHS06] H.J. CALLOW, R.E. HANSEN et T.O. SAEBO : Effect of approximations in fast factorized backprojection in Synthetic Aperture imaging of spot regions. *In Proc. Oceans*, volume 3721, pages 1–6, Boston, USA 2006.
- [CICB10] V. CEVHER, P. INDYK, L. CARIN et R.G. BARANIUK : Sparse signal recovery and acquisition with graphical models. *IEEE Signal Process. Mag.*, 27(6):92–103, Nov. 2010.
- [ÇK01] M. ÇETIN et W.C. KARL : Feature-enhanced Synthetic Aperture Radar image formation based on nonquadratic regularization. *IEEE Trans. Image Process.*, 10(4):623–631, Apr. 2001.
- [CKC02] M. CETIN, W.C. KARL et D.A. CASTANON : Analysis of the impact of feature-enhanced SAR imaging on ATR performance algorithms for SAR imagery. *In Proc. SPIE Algorithms for SAR Imagery IX*, volume 4727(1), pages 134–145, 2002.

- [ÇKCn03] M. ÇETIN, W.C. KARL et D.A. CASTANÓN : Feature enhancement and ATR performance using non-quadratic optimization-based sar imaging. *IEEE Trans. Aerosp. Electron. Syst.*, 39:1375–1395, Oct. 2003.
- [CM06] J.C. CURLANDER et R.N. McDONOUGH : *Synthetic Aperture Radar: systems and signal processing*. J. Wiley and Sons, New York, 2006.
- [CRT06a] E.J. Candes, J. ROMBERG et T. TAO : Robust uncertainty principles: exact signal reconstruction from highly incomplete frequency information. *IEEE Trans. Inf. Theory*, 52(2):489–509, Feb. 2006.
- [CRT06b] E.J. CANDÈS, J.K. ROMBERG et T. TAO : Stable signal recovery from incomplete and inaccurate measurements. *Comm. Pure Appl. Math.*, 59(8):1207–1223, Aug. 2006.
- [CRT08] E.J. CANDÈS, J.K. ROMBERG et T. TAO : The restricted isometry property and its implications for compressed sensing. *Comptes Rendus-Math*, 346(9-10):589–592, Mar. 2008.
- [CS00] W.C. CHEW et J.M. SONG : Fast Fourier transform of sparse spatial data to sparse Fourier data. In *IEEE Intl Antennas Propag. Symp.*, volume 4, pages 2324–2327, Salt Lake City, UT, 2000.
- [CTC⁺04] Y. CHAMBENOIT, E. TROUVE, N. CLASSEAU, J.-P. RUDANT et P. BOLON : Different fusion strategies to detect geographical objects by active contours in multitemporal sar images. In *Proc. IEEE Intl Geosci. Remote Sens. Symp. (IGARSS'04)*, volume 1, pages 1–7, Sept. 2004.
- [CW05] I.G. CUMMING et F.H. WONG : *Digital Processing of Synthetic Aperture Radar Data Algorithm and Implementation*. Artech House, Norwood, MA, 2005.
- [DeG98] S.R. DEGRAAF : SAR imaging via modern 2-D spectral estimation methods. *IEEE Trans. Image Process.*, 7(5):729–761, May 1998.
- [Den11] B. DENG : *Research on Synthetic Aperture Radar Micro-Motion Target Indication (SAR MMTI)*. Ph.D. thesis, National University of Defense Technology, 2011.
- [DET06] D.L. DONOHO, M. ELAD et V.N. TEMLYAKOV : Stable recovery of sparse overcomplete representations in the presence of noise. *IEEE Trans. Inf. Theory*, 52(1):6–18, Jan. 2006.
- [DFW⁺10] X.F. DING, M.M. FAN, X.Z. WEI, X. LI et H.T. XIAO : Narrowband imaging method for spatial precession cone-shaped targets. *Sci. China*, 55(4):1–8, 2010.
- [DH01] D.L. DONOHO et X. HUO : Uncertainty principles and ideal atomic decomposition. *IEEE Trans. Inf. Theory*, 47(7):2845 –2862, Nov. 2001.
- [DJ02] Y. DING et D.C. Munson JR. : A fast back-projection algorithm for bistatic SAR imaging. In *Proc. IEEE Intl Conf. on Image Processing*, pages 449–452, Rochester, NY, 2002.
- [Don92] D.L. DONOHO : Superresolution via sparsity constraints. *SIAM J. Math. Anal.*, 23(5):1309–1331, 1992.
- [Don06a] D.L. DONOHO : Compressed sensing. *IEEE Trans. Inf. Theory*, 52(4): 1289–1306, Apr. 2006.

BIBLIOGRAPHY

- [Don06b] D.L. DONOHO : For most large underdetermined systems of equations, the minimal l1-normnear-solution approximates the sparsest near-solution. *Comm. Pure Appl. Math.*, 59:907–934, 2006.
- [DS08] M. DEHMOLLAIAN et K. SARABANDI : Refocusing through building walls using Synthetic Aperture Radar. *IEEE Trans. Geosci. Remote Sens.*, 46(6):1589–1599, Jun. 2008.
- [DT10] N. DOBIGEON et J.Y. TOURNERET : Bayesian orthogonal component analysis for sparse representation. *IEEE Trans. Signal Process.*, 58(5):2675–2685, 2010.
- [DTR10] L. DENIS, F. TUPIN et X. RONDEAU : Exact discrete minimization for tv+lo image decomposition models,. In *International Conference on Image Processing*, September 2010.
- [DWQ⁺09] B. DENG, G.Z. WU, Y.L. QIN, H.Q. WANG et X. LI : SAR/MMTI: An extension to conventional SAR/GMTI and a combination of SAR and micro-motion techniques. In *Proc. IET Intl Radar Conf., Guilin, China*, pages 1–4, Apr. 2009.
- [EGM08] J.H.G. ENDER, C.H. GIERULL et D.C. MAORI : Improved space-based moving target indication via alternate transmission and receiverswitching. *IEEE Trans. Geosci. Remote Sens.*, 46(12):3960–3974, 2008.
- [Far08] Ph. FARGETTE : Compte-rendu d’experimentation. Technical Report, ONERA, Paris. DGA, Nov. 2008.
- [FBR⁺00] T. FRESE, C.A. BOUMAN, N.C. ROUZE, G.D. HUTCHINS et K. SAUER : Bayesian multiresolution algorithm for pet reconstruction. In *Proc. Intl Conf. Image Process.*, volume 2, pages 613–616, Sept. 2000.
- [FBS02] T. FRESE, C.A. BOUMAN et K. SAUER : Adaptive wavelet graph model for bayesian tomographic reconstruction. *IEEE Trans. Image Process.*, 11(7):756–770, Jul. 2002.
- [Fel09] W.B. FELEPE : Reconstruction d’images dans le contexte d’imagerie SAR bistatique. Technical Report, ONERA: Palaiseau. DEMR, Jun. 2009.
- [Fér06] O. FÉRON : *Champs de Markov Caches pour les problemes inverse application à la fusion de donnees et la reconstruction d’images en tomographie microonde*. Ph.D thesis, University paris-sud XI, Orsay, France, 2006.
- [FG02] A. FARINA et M. GRAZZINI : Radar fusion to detect targets - part II. *Signal Process.*, 82(8):1096–1108, 2002.
- [Fit88] J.P. FITCH : Synthetic aperture radar. *New York, Springer-Verlag*, 1988, 178 p., 1, 1988.
- [FL99] G. FRANCESCHETTI et R. LANARI : *Synthetic Aperture Radar Processing*. CRC Press, New York, 1999.
- [FL09] S. FOUCART et M.J. LAI : Sparsest solutions of underdetermined linear systems via lq-minimization for $0 < q \leq 1$. *Appl. Comput. Harmonic Anal.*, 26(3):395–407, 2009.
- [FM99] A. FROMMER et P. MAASS : Fast CG-based methods for Tikhonov Phillips regularization. *SIAM J. Sci. Comput.*, 20:1831–1850, 1999.

- [FN05] M. FIANI-NOUVEL : Feature-enhancement of SAR images by Bayesian regularization. *In Proc. IEEE Intl Radar Conf.*, pages 562 – 567, May 2005.
- [FRB⁺03] T. FRESE, N.C. ROUZE, C.A. BOUMAN, K. SAUER et G.D. HUTCHINS : Quantitative comparison of fbp, em, and bayesian reconstruction algorithms for the indypet scanner. *IEEE Trans. Medical Imaging*, 22(2):258–276, Feb. 2003.
- [GA07] K. GERHARD et O.M. ALBERT : A satellite formation for high resolution SAR interferometry. *IEEE Trans. Geosci. Remote Sens.*, 45(11):3317–3341, Nov. 2007.
- [GBM94] I.J. GUPTA, M.J. BEAK et A. MOGHADDAR : Data extrapolation for high resolution Radar imaging. *IEEE Trans. Antennas Propag.*, 42(11):1540–1545, Nov. 1994.
- [GD02] D. GLEICH et M. DATCU : Processing of multiple-receiver spaceborne arrays for wide-area SAR. *IEEE Trans. Geosci. Remote Sens.*, 40(4):841–852, Apr. 2002.
- [Ger74] R. W. GERCHBERG : Superresolution through error energy reduction. *Optica Acta*, 21(9):709–720, Sept. 1974.
- [GLB11] J. GUO, Z.F. LI et Z. BAO : Adaptive clutter suppression and resolving of velocity ambiguities for an experimental three-channelairborne Synthetic Aperture Radar-ground moving target indication system. *IET Radar Sonar Navig.*, 5(4):426–435, Apr. 2011.
- [GN92] J.C. GILBERT et J. NOCEDAL : Global convergence properties of conjugate gradient methods for optimization. *SIAM J. Optimization*, 2:21–42, 1992.
- [GPSG10] A.S. GOH, M. PREISS, N.J.S. STACY et D.A. GRAY : Bistatic SAR experiment with the Ingara imaging radar. *IET Radar Sonar Navig.*, 4(3):426–437, Jun. 2010.
- [GS07] M. GEBELE et I. SIKANETA : Motion parameter estimation of Doppler ambiguous moving targets in SAR-GMTI. *In IEEE Intl Radar Symp. (IRS)*, Sept. 2007.
- [Had23] J. HADAMARD : *Lectures on the Cauchy problems in linear partial differential equations*. Yale Univ Press, New Haven, 1923.
- [HBCW01] B. HIMED, H. BASCOM, J. CLANCY et M. C. WICKS : Tomography of moving targets (TMT). *In Proc. SPIC Sensors, Systems, and Next-Generation Satellites V*, volume 4540(1), pages 608–619, Dec. 2001.
- [HHM12] P. HEAS, C. HERZET et E. MEMIN : Bayesian inference of models and hyperparameters for robust optical-flow estimation. *IEEE Trans. Image Process.*, 21(4):1437 –1451, Apr. 2012.
- [HP11] R. HUAN et Y. PAN : Decision fusion strategies for SAR image target recognition. *IET Radar Sonar Navig.*, 5(7):747–755, Aug. 2011.
- [HXS06] C. HE, G.S. XIA et H. SUN : An adaptive and iterative method of urban area extraction from sar images. *IEEE Geosci. Remote Sens. Lett.*, 3(4):504–507, Oct. 2006.
- [HYX05] P.K. HUANG, H.C. YIN et X.J. XU : *Radar target scattering characteristics*. Electronic Industry Press, Beijing, 2005.

BIBLIOGRAPHY

- [HZF⁺11] J. HU, W. ZHOU, Y. FU, X. LI et N. JING : Uniform rotational motion compensation for ISAR based on phase cancellation. *IEEE Geosci. Remote Sens. Lett.*, 8(4):636–640, Jul. 2011.
- [IBG98] G. Jones III, B. BHANU et J. GUO : Geometrical and magnitude invariants for recognition of articulated and non-standard objects in mstar images. In *Proceedings DARPA Image Understanding Workshop*, pages 1163–1170, Monterey, California, November 1998.
- [Idi01] J. IDIER : *Approche bayésienne pour les problèmes inverses, Traité IC2, Série traitement du signal et de l'image*. Hermés, Paris, 2001.
- [Idi08] J. IDIER : *Bayesian approach to inverse problems*. Wiley, London, 2008.
- [IG93] J. IDIER et Y. GOUSSARD : Markov modeling for Bayesian restoration of two-dimensional layered structures. *IEEE Trans. Inf. Theory*, 39(4):1356–1373, Jul. 1993.
- [Jin12] B. JIN : A variational Bayesian method to inverse problems with impulsive noise. *J. Computational Physics*, 231:423–435, Jan. 2012.
- [JK08] H.R. JEONG et K.T. KIM : Application of subarray averaging and entropy minimization algorithm to stepped-frequency ISAR autofocus. *IEEE Trans. Antennas Propag.*, 56(4):1144–1154, Apr. 2008.
- [Jon86] M.C. JONES : The discrete Gerchberg algorithm. *IEEE Acoust., Speech, Signal Process.*, 34(3):624–626, Jun. 1986.
- [JwE⁺96] C.V. JAKOWATZ, D.E. WAHL, P.H. EICHEL, D.C. GHIGLIA et P.A. THOMPSON : *Spotlight-Mode Synthetic Aperture Radar: A Signal Processing Approach*. Springer, New York, 1996.
- [JYC08] S. JI, X. YA et L. CARIN : Bayesian compressive sensing. *IEEE Tran. Signal Process.*, 56(6):2346–2356, Jun. 2008.
- [JZ07] T. JIN et Z.M. ZHOU : Fraction and dispersion effects compensation for UWB SAR subsurface objects imaging. *IEEE Trans. Geosci. Remote Sens.*, 45(12):4059–4066, Dec. 2007.
- [KFHM03] G. KRIEGER, H. FIEDLER, D. HOUNAM et A. MOREIRA : Analysis of system concepts for bi- and multi-static SAR missions. In *IEEE Intl Geosci. Remote Sens. Symp. (IGARSS '03)*, volume 2, pages 770–772, Jul. 2003.
- [KM99] Michael A KOETS et Randolph L MOSES : Feature extraction using attributed scattering center models on sar imagery. In *AeroSense'99*, pages 104–115, 1999.
- [Kno85] E.F. KNOTT : *Radar cross section*. Artech House, Dedham, MA, 1985.
- [Kov76] J.J. KOVALY : *Synthetic Aperture Radar*. Artech House, Dedham, MA, 1976.
- [LC91] Y.D. LI et J. CHANG : *Signal reconstruction theories and applications*. Tsinghua Univ Press, Beijing, 1991. (In Chinese).
- [LCW04] R.O. LANE, K.D. CORPSEY et A.R. WEBB : A Bayesian approach to simultaneous autofocus and super-resolution. In *Proc. SPIE Alogorithms for SAR XI*, volume 5427(1), pages 133–142, Apr. 2004.

- [LDQL11] X. LI, B. DENG, Y.L. QIN et Y.P. LI : The influence of target micromotion on SAR and GMTI. *IEEE Trans. Geosci. Remote Sens.*, 49(8):2738–2751, Aug. 2011.
- [LHYS07] N. LI, C. HE, L. YU et H. SUN : Pixel-level image fusion based on multi-to-multi turbo iterative. In *Proc. Asian-Pacific Conf. SAR (APSAR'07)*, pages 793–796, Nov. 2007.
- [Li07] Z.X. LI : *Multi-location Inverse Synthetic Aperture Radar image fusion at the data level*. Ph.D. thesis, Pennsylvania State University, 2007.
- [LLZ10] Y.X. LIU, X. LI et Z.W. ZHUANG : Estimation of micro-motion parameters based on micro-Doppler. *IET Signal Process.*, 4(3):213–217, Jun. 2010.
- [Lut90] S.P. LUTTRELL : Bayesian autofocus/super-resolution theory. In *IEE Colloquium on Role of Image Processing in Defence and Military Electronics*, pages 1–6, Apr. 1990.
- [LXC08] S.H. LI, Y. XUE et L. CARIN : Bayesian compressive sensing. *IEEE Trans. Signal Process.*, 57(6):2346–2356, Jun. 2008.
- [Mas01] D. MASSONNET : Capabilities and limitations of the interferometric cartwheel. *IEEE Trans. Geosci. Remote Sens.*, 39:506–520, 2001.
- [MBM08] E. MARTINI, O. BREINBJERG et S. MACI : Reduction of truncation errors in planar near-field aperture antenna measurements using the Gerchberg-Papoulis algorithm. *IEEE Trans. Antennas Propag.*, 56(11):3485–3493, Nov. 2008.
- [MD03] A. MOHAMMAD-DJAFARI : Bayesian approach for inverse problems in optical coherent and noncoherent imaging. In *Proc. SPIE Optical Information Systems*, volume 5202(1), pages 209–218, 2003.
- [MD06a] A. MOHAMMAD-DJAFARI : Bayesian inference for inverse problems in signal and image processing and applications. *Intl J. Imaging Syst. Technol. Special Issue: Computer Vision*, 16(5):209–214, 2006.
- [MD06b] A. MOHAMMAD-DJAFARI : Inverse problems in imaging systems and the general Bayesian inversion frame work. *J. Iranian Association of Electrical and Electronics Engineering*, 3(2), 2006.
- [MD09a] A. MOHAMMAD-DJAFARI : *Inverse problems in vision and tomography*. Wileys, London, 2009.
- [MD09b] A. MOHAMMAD-DJAFARI : *Problèmes inverses en imagerie et en vision*. Hermès, Lavoisier, Paris, France, 2009.
- [MD11] A. MOHAMMAD-DJAFARI : Probabilistic models which enforce sparsity. In *Proc. 4th Workshop on Signal Processing with Adaptive Sparse Structured Representations, Edinburgh, Scotland, UK*, pages 1–107, 2011.
- [MD12] A. MOHAMMAD-DJAFARI : Bayesian approach with prior models which enforce sparsity in signal and image processing. *EURASIP J. Adv. Signal Process.*, 2012(1):52, 2012.
- [MDDF09] A. MOHAMMAD-DJAFAR, F. DAOUT et Ph. FARGETTE : Développement de méthodes de fusion et d'inversion de données SAR multistatique. In *Symp. Signal Image Process. (GRETSI'09)*, Dijon, France, 2009.

BIBLIOGRAPHY

- [MDZDF10] A. MOHAMMAD-DJAFARI, S. ZHU, F. DAOUT et Ph. FARGETTE : Fusion of multistatic Synthetic Aperture Radar data to obtain a super-resolution image. *In J. Phys.: Conf Ser. 8th Intl Workshop Inf. Opt. (WIO'09)*, volume 206(1), pages 258–265, Jul. 2010.
- [MJOJ83] D.C. MUNSON, J.D. JR. O'BRIEN et W.K. JENKINS : A tomographic formulation of spotlight-mode Synthetic Aperture Radar. *Proc. IEEE*, 71(9):917–925, Aug. 1983.
- [MM07] A.K. MISHRA et B. MULGREW : Bistatic SAR ATR. *IET Radar Sonar Navig.*, 1(6):459–469, Dec. 2007.
- [MMJ07] R.L. MORRISON, N. DO MINH et D.C. MUNSON JR. : SAR image autofocus by sharpness optimization: A theoretical study. *IEEE Trans. Image Process.*, 16(9):2309–2321, Sept. 2007.
- [MML99] J. MITTERMAYER, A. MOREIRA et O. LOFFELD : Spotlight SAR data processing using the frequency scaling algorithm. *IEEE Trans. Geosci. Remote Sens.*, 37(5):2198–2214, May 1999.
- [MR96] J. MCCORKLE et M. ROFHEART : An order $N^2 \log(N)$ backprojector algorithm for focusing wide-angle wide-bandwidth arbitrary-motion Synthetic Aperture Radar. *In Proc. SPIE Radar Sensor Tech.*, volume 2427(1), pages 25–36, 1996.
- [NT08] D. NEEDELL et J.A. TROPP : CoSaMP: iterative signal recovery from incomplete and inaccurate samples. *Appl. Comput. Harmonic Anal.*, 26(3):301–321, 2008.
- [NV10] D. NEEDELL et R. VERSHYNIN : Signal recovery from incomplete and inaccurate measurements via regularized orthogonal matching pursuit. *IEEE J. Sel. Topics Signal Process.*, 4(2):310–316, Apr. 2010.
- [NW99] J. NOCEDAL et S.J. WRIGHT : *Numerical optimization*. Springer verlag, 1999.
- [OC12] N.O. ONHON et M. CETIN : A sparsity-driven approach for joint SAR imaging and phase error correction. *IEEE Trans. Image Process.*, 21(4):2075–2088, Apr. 2012.
- [OTM⁺01] V.P. ONANA, E. TROUVE, G. MAURIS, J.P. RUDANT et E. TONYE : Thin linear features extraction in sar images by fusion of amplitude and coherence information. *In Proc. IEEE Intl Geosci. Remote Sens. Symp. (IGARSS'01)*, volume 7, pages 3012–3014, 2001.
- [OTM⁺03] V. de P. ONANA, E. TROUVE, G. MAURIS, J.-P. RUDANT et E. TONYE : Linear features extraction in rain forest context from interferometric sar images by fusion of coherence and amplitude information. *IEEE Trans. Geosci. Remote Sens.*, 41(11):2540–2556, Nov. 2003.
- [Pap75] A. PAPOULIS : A new algorithm in spectral analysis and band-limited extrapolation. *IEEE Trans. Circ. Sys.*, CAS22(9):735–742, 1975.
- [PEPC10] L.C. POTTER, E. ERTIN, J.T. PARKER et M. CETIN : Sparsity and compressed sensing in Radar imaging. *In Proc. IEEE*, volume 98(6), pages 1006–1020, Jun. 2010.
- [PK08] V. PICKALOV et D. KAZANTSEV : Iterative Gerchberg-Papoulis algorithm for fan-beam tomography. *In IEEE Intl Conf. Computational Technologies*

- in Electrical and Electronics Engineering (SIBIRCON'08)*, pages 218–222, Jul. 2008.
- [PM97] Lee C POTTER et Randolph L MOSES : Attributed scattering centers for sar atr. *IEEE Transactions on Image processing*, 6(1):79–91, 1997.
- [PSZ08] L. C. POTTER, P. SCHNITER et J. ZINIEL : Sparse reconstruction for radar. *In Proc. SPIE Algorithms for SAR Imagery XV*, volume 6970, pages 697003 1–15, May 2008.
- [PVG98] Cle POHL et JL VAN GENDEREN : Review article multisensor image fusion in remote sensing: concepts, methods and applications. *International journal of remote sensing*, 19(5):823–854, 1998.
- [QD01] M. QUARTULLI et M. DATCU : Bayesian model based city reconstruction from high resolution ISAR data. *In Proc. IEEE/ISPRS Remote Sens. Data Fusion Over Urban Areas*, pages 58–63, 2001.
- [Ric05] M. RICHARDS : *Fundamentals of Radar Signal Processing*. McGraw-Hill, New York, 2005.
- [ROF92] L.I. RUDIN, S. OSHER et E. FATEMI : Nonlinear total variation based noise removal algorithms. *Physica D: Nonlinear Phenomena*, 60(1-4):259–268, Nov. 1992.
- [RRB⁺94] R.K. RANEY, H. RUNGE, R. BAMLER, I.G. CUMMING et F.H. WONG : Precision SAR processing using chirp scaling. *IEEE Trans. Geosci. Remote Sens.*, 32(4):786–799, Jul. 1994.
- [RT07] A. RAJ et K. THAKUR : Fast and stable Bayesian image expansion using sparse edge priors. *IEEE Trans. Image Process.*, 16(4):1073–1084, Apr. 2007.
- [SCMS09] S. SAMADI, M. ÇETİN et M.A. MASNADI-SHIRAZI : Multiple feature-enhanced Synthetic Aperture Radar imaging. *In Proc. SPIE Algorithms for SAR Imagery XVI*, volume 7337, pages 1–10, Apr. 2009.
- [SCMS11] S. SAMADI, M. ÇETİN et M.A. MASNADI-SHIRAZI : Sparse representation-based Synthetic Aperture Radar imaging. *IET Radar Sonar Navig.*, 5(2):182–193, Feb. 2011.
- [SFM⁺02] Giovanni SIMONE, Alfonso FARINA, Francesco Carlo MORABITO, Sebastiano B SERPICO et Lorenzo BRUZZONE : Image fusion techniques for remote sensing applications. *Information fusion*, 3(1):3–15, 2002.
- [SGC06] J.J. SHARMA, C.H. GIERULL et M.J. COLLINS : The influence of target acceleraration on velocity estimation in dual-channel SAR GMTI. *IEEE Trans. Geosci. Remote Sens.*, 44(1):134–147, Jan. 2006.
- [Shk04a] Y.V. SHKVARKO : Unifying regularization and Bayesian estimation methods for enhanced imaging with remotely sensed data- part II: Implementation and performance issues. *IEEE Trans. Geosci. Remote Sens.*, 42(5):932–940, May 2004.
- [Shk04b] Y.V. SHKVARKO : Unifying regularization and Bayesian estimation methods for enhanced imaging with remotely sensed data part I: Theory. *IEEE Trans. Geosci. Remote Sens.*, 42(5):923–931, May 2004.
- [Shk10a] Y.V. SHKVARKO : Unifying experiment design and convex regularization techniques for enhanced imaging with uncertain remotesensing data-part I: Theory. *IEEE Trans. Geosci. Remote Sens.*, 48(1):69–72, Jan. 2010.

BIBLIOGRAPHY

- [Shk10b] Y.V. SHKVARKO : Unifying experiment design and convex regularization techniques for enhanced imaging with uncertain remotesensing data-part II: Adaptive implementation and performance issues. *IEEE Trans. Geosci. Remote Sens.*, 48(1):69–82, Jan. 2010.
- [SK03] T. SPARR et B. KRANE : Micro-Doppler analysis of vibrating targets in SAR. *IEE Proc. Radar, Sonar Navig.*, 150(4):277–283, Aug. 2003.
- [SK10a] P. SAMCZYNSKI et K.S. KULPA : Coherent MapDrift technique. *IEEE Trans. Geosci. Remote Sens.*, 48(3):1505–1517, Mar. 2010.
- [SK10b] I. STOJANOVIC et W.C. KARL : Imaging of moving targets with multi-static SAR using an overcomplete dictionary. *IEEE J. Sel. Topics Signal Process.*, 4:164–176, Feb. 2010.
- [SK10c] Ivana STOJANOVIC et William Clem KARL : Imaging of moving targets with multi-static sar using an overcomplete dictionary. volume 4, pages 164–176, 2010.
- [Sko70] M.I. SKOLNIK : Radar handbook. 1970.
- [Sko01] M.I. SKOLNIK : *Introduction to radar systems*. McGraw-Hill, New York, 2001.
- [Sko08] M.I. SKOLNIK : *RADAR Handbook*. McGraw-Hill, New York, 2008.
- [SLM02] Y. SHKVARKO et L. LEYVA-MONTIEL : Theoretical aspects of Bayesian approach to aperture synthesis for Radar imaging. In *Proc. IEEE Antennas Propag. Intl Symp.*, volume 4, pages 322–325, Jun. 2002.
- [SLP01] R.K. SHARMA, T.K. LEEN et M. PAVEL : Bayesian sensor image fusion using local linear generative models. *Opt. Eng.*, 40:1364–1376, 2001.
- [SMW05] A. SPRIET, M. MOONEN et J. WOUTERS : Stochastic gradient-based implementation of spatially preprocessed speech distortion weighted multichannel wiener filtering for noise reduction in hearing aids. *IEEE Trans. Image Process.*, 53(3):911–925, Mar. 2005.
- [Sou91] M. SOUMEKH : Bistatic Synthetic Aperture Radar inversion with application in dynamic target imaging. *IEEE Trans. Signal Process.*, 39(9):2044–2055, Sept. 1991.
- [Sou92] M. SOUMEKH : system model and inversion for Synthetic Aperture Radar imaging. *IEEE Trans. Image Process.*, 1(1):64–76, Jan. 1992.
- [Sou99] M. SOUMEKH : *Synthetic Aperture Radar Signal Processing With MATLAB Algorithms*. J. Wiley and Sons, New York, 1999.
- [Spa05] T. SPARR : Moving target motion estimation and focusing in SAR images. In *Proc. IEEE Intl Radar Conf.*, pages 290–294, May 2005.
- [SQ05] V. SMIDL et A. QUINN : *The variational Bayes method in signal processing*. Springer, Berlin, 2005.
- [SSD99] M. SCHRODER, K. SEIDEL et M. DATCU : Bayesian modeling of remote sensing image content. In *Proc. Geosci. Remote Sens. Symp. (IGARSS '99), Hamburg, Germany*, volume 3, pages 1810–1812, Jul. 1999.
- [STC98] N.S. SUBOTIC, B.J. THELEN et D.A. CARRARA : Cyclostationary signal models for the detection and characterization of vibrating objects in SAR data. In *Proc. IEEE Thirty-Second Asilomar Conference on Signals,*

- Systems & Computers, Pacific Grove, CA, USA*, pages 1304–1308, Nov. 1998.
- [Sul04] R.J. SULLIVAN : *Radar foundation for imaging and advanced concepts*. SciTech Publishing, Raleigh, NC, 2004.
- [SYCS10] G.F. SHENG, W. YANG, L.J. CHEN et H. SUN : Satellite image classification using sparse codes of multiple features. In *Proc. IEEE Intl Conf. Signal Process. (ICSP'10)*, pages 952–955, Oct. 2010.
- [TA63] A.N. TIKHONOV et V.Y. ARSENIN : Solution of incorrectly formulated problems and the regularization method. *Soviet Math Dokl*, 4:1035–1038, 1963.
- [TAJ77] A.N. TIKHONOV, V.I.A. ARSENIN et F. JOHN : *Solutions of ill posed problems*. Winston, Washington, DC, 1977.
- [TALDM10] M. TELLO ALONSO, P. LOPEZ-DEKKER et J.J. MALLORQUI : A novel strategy for radar imaging based on compressive sensing. *IEEE Trans. Geosci. Remote Sens.*, 48(12):4285–4295, Dec. 2010.
- [TB03] M.E. TIPPING et C.M. BISHOP : Bayesian image super-resolution. In *Advances in Neural Information Processing Systems*, pages 1303–1310. MIT Press, 2003.
- [TCYS12] S.T. TU, J.Y. CHEN, W. YANG et H. SUN : Laplacian eigenmaps-based polarimetric dimensionality reduction for sar image classification. *IEEE Trans. Geosci. Remote Sens.*, 50(1):170–179, Jan. 2012.
- [TG60] G. TURIN et L. GEORGE : An introduction to matched filters. *IRE Trans. Inf. Theory*, 6(3):311–329, Jun. 1960.
- [TGS06] J.A. TROPP, A.C. GILBERT et M.J. STRAUSS : Algorithms for simultaneous sparse approximation. Part I: Greedy pursuit. *Signal Process.*, 86(3):572–588, Mar. 2006.
- [Tip01] M.E. TIPPING : Sparse Bayesian learning and the relevance vector machine. *J. Mach. Learning Research*, 1:211–244, 2001.
- [Tro06] J.A. TROPP : Just relax: convex programming methods for identifying sparse signals in noise. *IEEE Trans. Inf. Theory*, 52(3):1030–1051, Mar. 2006.
- [TSQ⁺10] T. THAYAPARAN, P. SURESH, S. QIAN, K. VENKATARAMANIAH, S. SIVASANKARASAI et K.S. SRIDHARAN : Micro-Doppler analysis of a rotating target in Synthetic Aperture Radar. *IET Signal Process.*, 4(3):245–255, Jun. 2010.
- [UHS03] L.M.H. ULANDER, H. HELLSTEN et G. STENSTROM : Synthetic-Aperture Radar processing using fast factorized back-projection. *IEEE Trans. Aerosp. Electron. Syst.*, 39(3):760–776, Jul. 2003.
- [VcFW08] K.R. VARSHNEY, M. ÇETIN, J.W. FISHER et A.S. WILLSKY : Sparse signal representation in structured dictionaries with application to Synthetic Aperture Radar. *IEEE Trans. Geosci. Remote Sens.*, 56(8):3548–3561, Aug. 2008.
- [VGS96] V. VAPNIK, S.E. GOLOWICH et A. J. SMOLA : Support vector method for function approximation, regression estimation, and signal processing. In *Proc. Advances in Neural Information Processing Systems (NIPS'96)*, pages 281–287. MIT Press, 1996.

BIBLIOGRAPHY

- [VV09] S. VILLENA et M. VEGA : Bayesian super-resolution image reconstruction using an l_1 prior. In *Proc. 6th Intl Symp. Image Signal Process. Anal.*, volume 4, pages 152–157, Sept. 2009.
- [Wan07] Y.F. WANG : *Computation methods of Inverse problems and applications*. High Educ. Press, Beijing, 2007. (In Chinese).
- [Weh87] Donald R WEHNER : High resolution radar. *Norwood, MA, Artech House, Inc., 1987, 484 p.*, 1, 1987.
- [WG91] N.J. WILLIS et H.D. GRIFFITHS : *Bistatic Radar*. Artech House, Norwood, MA, 1991.
- [WG07] N.J. WILLIS et H.D. GRIFFITHS : *Advances in Bistatic Radar*. Scitech Pub Inc, Raleigh, NC, 2007.
- [WHB06] M.C. WICKS, B. HIMED et H. BASCOM : Tomography of moving targets (TMT) for security and surveillance. *Advances in Sensing with Security Applications*, 2:323–339, 2006.
- [Whi05] J.C. WHITAKER : *The Electronics Handbook, Second Edition*. CRC Press, New York, 2005.
- [Wil95] P.M. WILLIAMS : Bayesian regularization and pruning using a Laplace prior. *Neural Comput.*, 7(1):117–143, 1995.
- [WLJW11] J. WU, F. LIU, L.C. JIAO et X.D. WANG : Compressive sensing SAR image reconstruction based on Bayesian framework and evaluation computation. *IEEE Trans. Image Process.*, 20(7):1904–1911, Jul. 2011.
- [Wu01] Z. WU : Tomographic imaging of isolated ground surfaces using radio ground waves and conjugate gradient methods. *IET Radar Sonar Navig.*, 148(1):27–34, Feb. 2001.
- [WW09] Z.M. WANG et W.W. WANG : Fast and adaptive method for SAR superresolution imaging based on point scattering model and optimal basis selection. *IEEE Trans. Image Process.*, 18(7):1477–1486, Jul. 2009.
- [XPC12] J. XU, Y. PI et Z. CAO : Bayesian compressive sensing in Synthetic Aperture Radar imaging. *IET Radar Sonar Navig.*, 6(1):2–8, Jan. 2012.
- [XPX04] J. XU, Y. N. PENG et X.G. XIA : Parametric autofocus of SAR imaging-coherent accuracy limitations and realization. *IEEE Trans. Geosci. Remote Sens.*, 42(11):2397–2411, Nov. 2004.
- [XWB05] M. XING, R. WU et Z. BAO : High resolution ISAR imaging of high speed moving targets. In *Proc. IEE Radar, Sonar, Navig.*, volume 152(2), pages 58–67, Feb. 2005.
- [XXZ⁺11] G. XU, M.D. XING, L. ZHANG, Y.B. LIU et Y.C. LI : Bayesian inverse Synthetic Aperture Radar imaging. *IEEE Geosci. Remote Sens. Lett.*, 8(6):1150–1154, Nov. 2011.
- [YBZS10] L. YU, J.P. BARBOT, G. ZHENG et H. SUN : Compressive sensing with chaotic sequence. *IEEE Signal Process. Lett.*, 17(8):731–734, Aug. 2010.
- [Yeg99] A.F. YEGULALP : Fast backprojection algorithm for Synthetic Aperture Radar. In *Proc. IEEE Radar Conf., Waltham, MA*, pages 60–65, 1999.
- [YMTP12] Y.J. YAN, G. MAURIS, E. TROUVE et V. PINEL : Fuzzy uncertainty representations of coseismic displacement measurements issued from sar imagery. *IEEE Trans. Instrum. Meas.*, 61(5):1278–1286, May 2012.

- [YSBZ11] L. YU, H. SUN, J.P. BARBOT et G. ZHENG : Bayesian compressive sensing for clustered sparse signals. *In Proc. IEEE Intl Conf. Acoustics, Speech, Signal Process. (ICASSP'11)*, pages 3948–3951, May 2011.
- [YYSH09] L. YU, Y. YANG, H. SUN et C. HE : Turbo-like iterative thresholding for sar image recovery from compressed measurements. *In Proc. Asian-Pacific Conf. SAR (APSAR'09)*, pages 664–667, Oct. 2009.
- [ZBXH07] Z.H. ZHANG, Z. BAO, M.D. XING et J.Y. HUANG : The analysis of SNR in passive distributed microsatellites SAR system. *J. Electron. Inform. Technol.*, 29(10):15–18, 2007.
- [Zha04] Y. ZHANG : Understanding image fusion. *Photogramm Eng. Rem. Sens.*, 70(6):657–661, 2004.
- [Zha10] Jixian ZHANG : Multi-source remote sensing data fusion: status and trends. *International Journal of Image and Data Fusion*, 1(1):5–24, 2010.
- [ZMD10] S. ZHU et A. MOHAMMAD-DJAFARI : A Bayesian approach to Fourier Synthesis inverse problem with application in SAR imaging. *In Proc. 30th Bayesian Inference and Maximum Entropy Methods in Science and Engineering*, volume 1305(1), pages 258–265, Jul. 2010.
- [ZMDLM11] S. ZHU, A. MOHAMMAD-DJAFARI, X. LI et J.J. MAO : Inverse problems arise in different Synthetic Aperture Radar imaging systems and a general Bayesian approach for them. *In Proc. SPIE Computational Imaging IX*, volume 7873(6), page 787306, Jan. 2011.
- [ZMDW⁺12] S. ZHU, A. MOHAMMAD-DJAFARI, H.Q. WANG, B. DENG, X. LI et J.J. MAO : Parameter estimation for SAR micromotion based on sparse signal representation. *EURASIP J. Adv. Signal Process.*, 2012(1):1–13, 2012.
- [ZMLW12] S. ZHU, A. MOHAMMAD-DJAFARI, X. LI et H.Q. WANG : A novel hierarchical bayesian method for SAR image reconstruction. *In AIP Conf. Proc. 31th Int. Workshop on Bayesian Inference and Maximum Entropy Methods in Science and Engineering (Maxent2011)*, Waterloo, Canada, volume 1443, pages 222–229, May. 2012.
- [ZR11] Z. ZHANG et B. RAO : Sparse signal recovery with temporally correlated source vectors using sparse bayesian learning. *IEEE J. Sel. Topics Signal Process.*, 5:912–926, Sept. 2011.
- [ZWL08] S. ZHU, H.Q. WANG et X. LI : A new method for parameter estimation of multicomponent LFM signal based on sparse signal representation. *In Proc. IEEE Intl Conf. Inf. Autom., Zhangjiajie, China*, pages 15–19, Jun. 2008.
- [ZXQ⁺10] L. ZHANG, M.D. XING, C.W. QIU, J. LI, J.L. SHENG, Y. LI et B. ZHENG : Resolution enhancement for Inversed Synthetic Aperture Radar imaging under low SNR via improved compressive sensing. *IEEE Trans. Geosci. Remote Sens.*, 48(10):3824–3838, Oct. 2010.
- [ZXT05] B. ZHENG, M.D. XING et W. TONG : *Radar imaging technology*. Electric Industrial Press, Beijing, 2005.